Friction

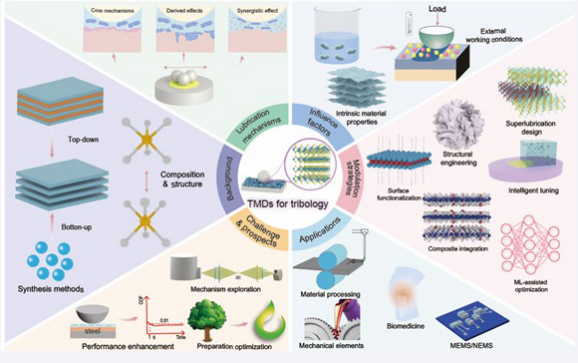
Review

Recent progress in transition metal dichalcogenides as advanced lubricants: Mechanisms, modulation strategies, and applications

Hongjie Li[1,2], Qingwen Dai[3], Derong Yan[4], Frank Hollmann[5], Zhen Zhao[1], Chengliang Hu[1,2,✉]

Cite this article: Li HJ, Dai QW, Yan DR, et al. *Friction* 2026, **14**: 9441231. https://doi.org/10.26599/FRICT.2026.9441231

ABSTRACT: The persistent economic and environmental challenges arising from friction-induced energy losses underscore the critical need for innovative lubrication technologies. Two-dimensional transition metal dichalcogenides (2D TMDs), characterized by their layered architecture and weak interlayer van der Waals (vdW) interactions, have emerged as promising nanolubricants due to their well-documented shear properties and ability to form low-friction tribofilms. However, practical applications of TMDs are hindered by inherent limitations, including insufficient load-bearing capacity and high sensitivity to environmental conditions. Accordingly, extensive research efforts have been directed toward the rational design and structural modification of TMD-based lubricants. This review outlines recent advances in TMD-based tribological systems, beginning with their structural characteristics and synthesis routes, followed by an in-depth discussion of lubrication mechanisms and key performance-influencing factors. Moreover, this review explores modulation strategies for TMD-based lubricants, from conventional methods to emerging approaches, along with their applications in diverse environments. Finally, this review identifies prevailing challenges and suggests promising research directions to guide the development of next-generation high-performance TMD-based lubricants.



KEYWORDS: transition metal dichalcogenide (TMD)-based lubricants; tribology; lubrication mechanisms; modulation strategies; applications

1 Introduction

Tribology, the science and technology of friction, wear, and lubrication between surfaces in relative motion, serves as the cornerstone for the performance and reliability of engineering systems [1]. However, friction and wear lead to surface degradation, energy dissipation, and mechanical failures, ultimately impairing industrial efficiency and sustainability [2, 3]. Studies indicate that friction accounts for approximately 30%–50% of global primary energy consumption, while wear is responsible for nearly 80% of mechanical equipment failures, resulting in annual economic losses amounting to hundreds of billions of dollars [4, 5]. These statistics highlight an urgent need for efficient lubrication strategies [6]. Research shows that a 20% reduction in friction could yield substantial energy savings and lower emissions [7]. Such evidence underscores the crucial role of tribological modulation in advancing green manufacturing, energy conservation, and sustainable development [8].

In recent years, the rapid growth of key industrial sectors has imposed increasingly demanding performance requirements on machinery, thereby intensifying the need to address tribological challenges [9]. Conventional lubrication methods, which rely on oils or greases to form protective tribofilms, are still widely used but face inherent limitations. For instance, low-viscosity greases may fail to maintain stable tribofilms under high shear or elevated temperatures, leading to increased asperity contact and accelerated wear [10]. Additionally, traditional additives such as zinc dialkyldithiophosphate (ZDDP) raise environmental and regulatory concerns [11]. Collectively, these shortcomings drive the development of advanced lubrication technologies.

The introduction of nanomaterials provides a promising solution to the issues outlined above, offering transformative

[1] National Engineering Research Center of Die & Mold CAD, State Key Laboratory of Metal Matrix Composites, School of Materials Science and Engineering, Shanghai Jiao Tong University, Shanghai 200240, China. [2] Inner Mongolia Research Institute, Shanghai Jiao Tong University, Hohhot 010010, China. [3] College of Mechanical and Electrical Engineering, Nanjing University of Aeronautics and Astronautics, Nanjing 210016, China. [4] Shanghai Chemical Chemicals Co., Ltd., Shanghai 201108, China. [5] Chemetall GmbH, Frankfurt am Main 60487, Germany.

✉ Corresponding author. E-mail: clhu@sjtu.edu.cn

Received: August 13, 2025; Revised: December 23, 2025; Accepted: February 4, 2026

© The Author(s) 2026. This is an open access article under the terms of the Creative Commons Attribution 4.0 International License (CC BY 4.0, http://creativecommons.org/licenses/by/4.0/).

potential for tribological systems by serving as solid coatings, reinforcement phases, or lubricant additives to enhance performance [12]. Well-designed nanolubricants effectively modify the frictional interface, leading to a lower coefficient of friction (COF) and reduced wear [13]. Since the 1970s, various nanomaterials have been explored for tribological applications, among which transition metal dichalcogenides (TMDs) stand out for their unique two-dimensional (2D) layered structure and micron-scale lateral dimensions [14]. The versatile physicochemical properties of TMDs, including large specific surface area (SSA), tunable electronic characteristics, favorable thermal conductivity, and excellent chemical stability, not only underpin diverse roles in electronics and energy systems but also render them highly promising for tribological applications, which are the core focus of this review [15, 16]. The lubricity of TMDs originates from their layered structure, in which weak interlayer van der Waals (vdW) interactions enable facile interplane sliding under shear stress. Moreover, the high polarizability of chalcogen atoms strengthens the adhesion of TMD layers to metallic surfaces, promoting the formation of low-shear-strength tribofilms, thereby reducing friction [17]. MoS_2 exemplifies this behavior with its exceptional performance in vacuum and dry environments, earning it the title "king of solid lubrication" [18].

As shown in Fig. 1, publications on TMD-based tribology have steadily increased over the past two decades, reflecting growing interest in TMDs as promising lubricants. Previous reviews have provided important insights into their tribological behavior, and Table 1 summarizes representative studies along with their key limitations in recent years [3, 19–24]. Most reviews organize their articles according to the physical forms of TMD-based lubricants (e.g., additives, coatings, or composite fillers) or specific application scenarios. Despite its simplicity, this approach may lead to a fragmented understanding. By obscuring the fundamental mechanisms shared across tribological systems, it hinders the development and deployment of high-performance TMD-based lubricants.

To fill this gap, this review proposes an integrated framework driven by performance optimization (Fig. 2). The framework systematically links material synthesis, lubrication mechanisms, performance determinants, modulation strategies, and application outcomes in a coherent sequence, explicitly relating material design to tribological performance. This approach provides a clear guideline for the rational development of high-performance TMD-based lubricants, a perspective that has rarely been emphasized in previous reviews. Specifically, the framework first summarizes the structural characteristics and synthesis routes of TMDs and then elucidates fundamental lubrication mechanisms and key factors governing tribological performance. It then covers performance modulation strategies, including established approaches and emerging strategies, as well as applications of TMD-based lubricants. Finally, the review identifies key scientific challenges and potential opportunities, providing a coherent roadmap for the optimized design of advanced TMD lubricating materials.

2 Background and fundamentals of TMDs

2.1 Composition and structure

TMDs, denoted by the general formula MX_2 (where M = Mo, W, V, Ti; X = S, Se, Te), are 2D layered materials composed of covalently bonded X–M–X monolayers stacked via weak vdW forces (Fig. 3(a)) [14]. The classification of TMD phases, including trigonal prismatic (1H), octahedral (1T), or distorted octahedral

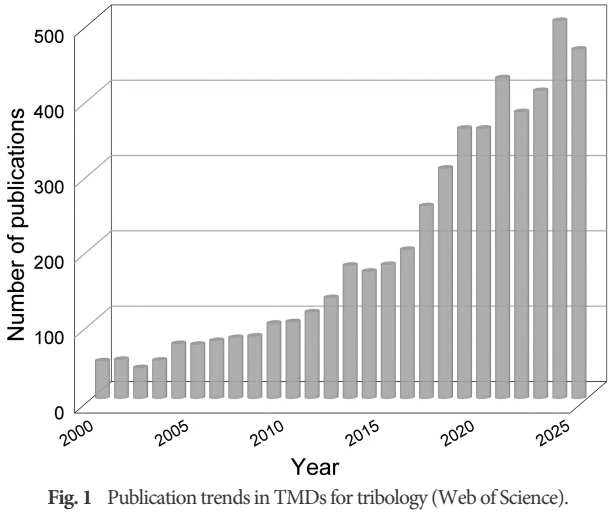


Fig. 1 Publication trends in TMDs for tribology (Web of Science).

Table 1 Comparison of representative reviews on TMD-based tribology

Ref.	Main content	Overlooked aspect
[19]	Summarizes the tribological applications of inorganic nanoadditives as lubricating additives.	Fails to collate other lubrication applications of TMDs and summarize their lubrication mechanisms and influencing factors.
[20]	Reviews the progress of 2D nanomaterials in tribology, including their roles as lubricant additives, coatings, reinforcement phases, and in superlubrication systems.	Lacks a summary of their lubrication mechanisms, influencing factors, and performance regulation strategies.
[3]	Summarizes the lubrication mechanisms and basic performance regulation methods of 2D materials.	Lacks summaries of their tribological influencing factors and application scenarios, and has research gaps in emerging modulation strategies.
[21]	Focuses on space applications, examining MoS_2 coating preparation and the effects of doping and nanocompositing on performance.	Lacks a summary of tribological applications of other TMD subclasses.
[22]	Focuses on TMD preparation methods, explores their applications in high-temperature self-lubricating coatings.	Lacks systematic collation of lubrication mechanisms, influencing factors, and modulation strategies.
[23]	Explores WS_2 preparation and applications as lubricant additives, highlighting how synthesis methods influence lubrication mechanisms.	Lacks discussion of other TMD subclasses and analysis of tribological factors.
[24]	Summarizes the tribological applications of MoS_2 as lubricating additives.	Neglects the MXenes' tribological applications, including lubricant coatings and composite fillers.
This work	Summarizes TMDs' synthesis, lubrication mechanisms, influencing factors, and modulation strategies, covers multidimensional applications, and discusses existing issues.	Fills the gaps of previous reviews regarding insufficient TMD subdivision and incomplete collation of mechanisms and applications, constructing a systematic framework for TMD tribology.

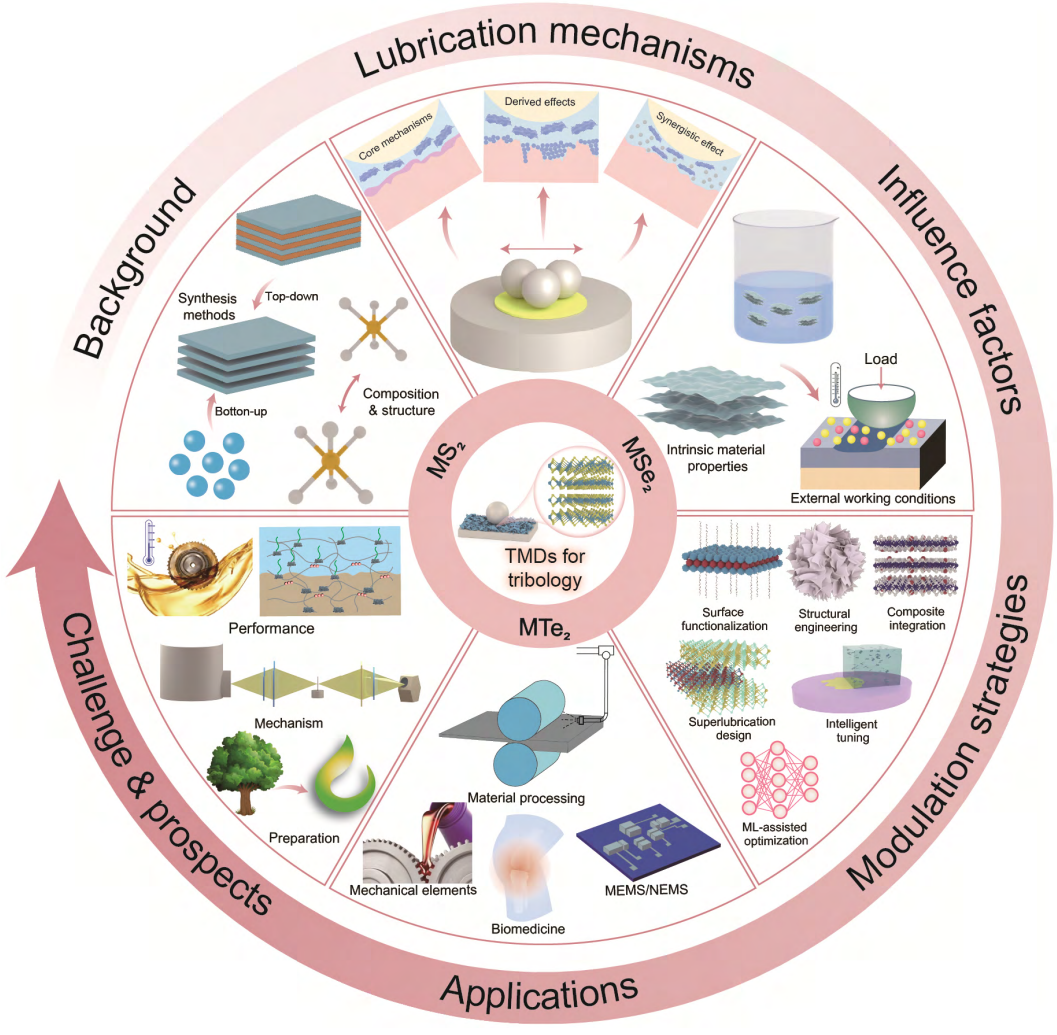


Fig. 2 Schematic illustration of TMD-based lubricants from synthesis and lubrication mechanisms to performance modulation, applications, and future perspectives.

variants, is determined by the metal–chalcogen coordination geometry and interlayer stacking (Fig. 3(b)) [25]. The numeric prefix in the phase notation denotes the number of X–M–X layers within the unit cell, and in the 1H phase, it corresponds to a monolayer derived from the 2H TMD phase [26]. Typically, the 1T phase tends to transform into various distorted structures (e.g., 1T', T_d, and 1T'') via intralayer distortion due to its higher energy than the 1H phase [27]. In addition to intralayer configurations, interlayer stacking sequences also give rise to distinct polymorphs. For example, 1H layers can stack into hexagonal 2H or rhombohedral 3R phases, while rearrangements of 1T' layers yield two distinct structures: 1T' and T_d [26, 28]. Such structural variations play a decisive role in determining the physicochemical properties of TMDs. Specifically, the 2H phase shows semiconducting behavior, the 1T phase manifests metallic properties, and the 1T' phase presents semimetallic characteristics [29].

2.2 Synthesis methods

The synthesis methods of TMDs, categorized into top–down and bottom–up approaches, largely determine their structural and surface properties, thus affecting tribological performance. Top–down methods exfoliate bulk crystals to yield monolayer or few-layer nanosheets with preserved intrinsic properties, while the bottom-up approach grows thin layers from molecular precursors, allowing precise control over thickness and surface functionality [30] (Fig. 4). The distinct controllability and applicability of these strategies lead to different tribological behaviors.

2.2.1 *Top–down approaches*

As a representative top–down strategy, exfoliation enables the direct preparation of monolayer or few-layer TMDs from bulk crystals [40]. Mechanical exfoliation, the pioneering technique, uses adhesive tape to peel atomic layers, yielding defect-free TMDs [41]. For instance, Zhao et al. [42] successfully obtained millimeter-sized monolayer 2H-$MoTe_2$ and bilayer $MoTe_2$ for electronic structure analysis, confirming the feasibility of this method (Figs. 5(a) and 5(b)). Although simple and suitable for research, this method offers limited control over thickness, lateral size, and morphology and is not easily scalable [14, 43].

To overcome these issues, scalable liquid-phase exfoliation techniques have been developed using ultrasound or shear forces to synthesize few- and multilayer TMDs with lateral sizes of tens to hundreds of nanometers [44]. Bai et al. [45] introduced a novel exfoliation strategy based on liquid gallium (Ga) intercalation at room temperature. With ultrasonic assistance, Ga intercalation expands the interlayer spacing and weakens vdW interactions, promoting effective exfoliation into 2D nanosheets (Fig. 5(c)). Structural analysis through scanning transmission electron microscopy (STEM) and electron energy loss spectroscopy (EELS) verified Ga incorporation into MoS_2 lattices and slight interlayer expansion (Fig. 5(d)). Despite being simple and low-cost, this

method yields a low proportion of monolayers, limits lateral size, and raises environmental issues due to toxic solvents [46].

Ion intercalation, especially using organolithium reagents, has become an effective strategy for improving exfoliation efficiency.

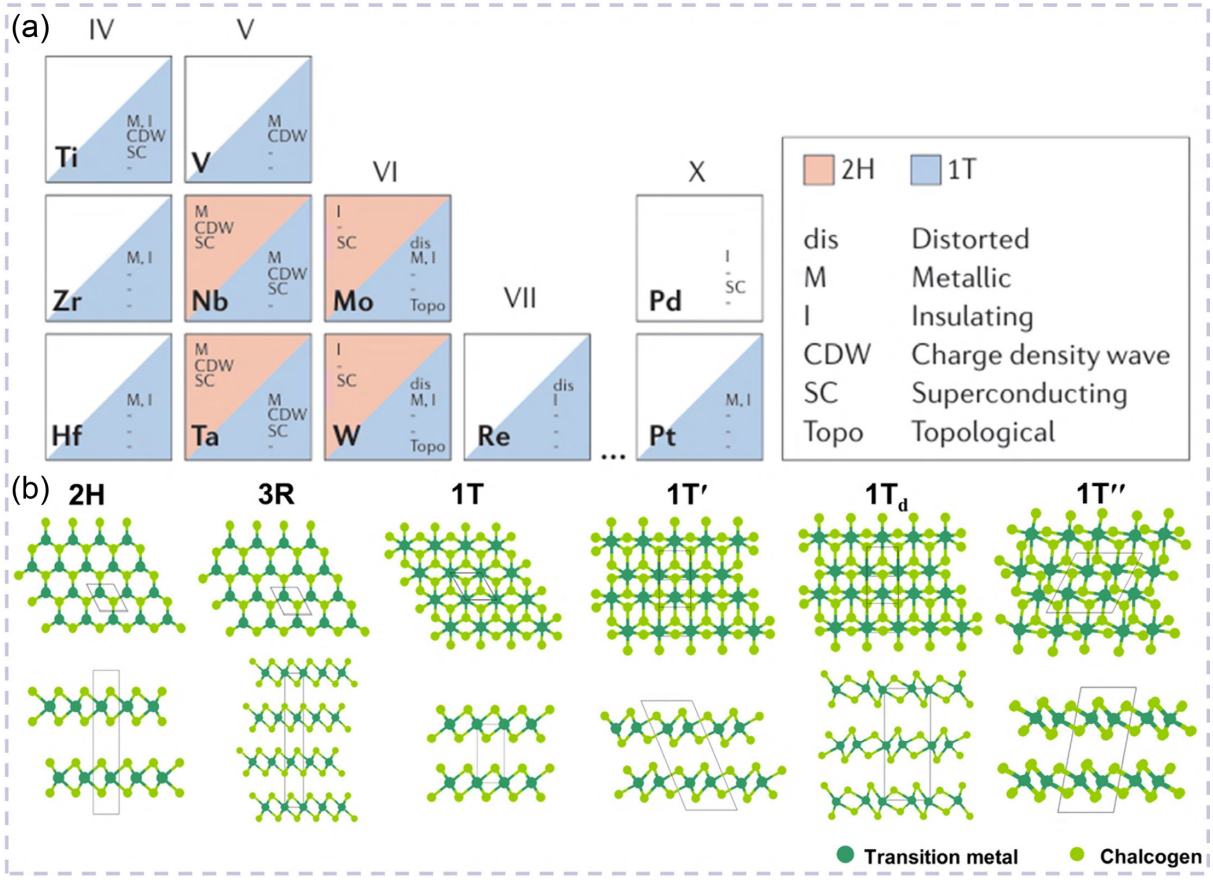


Fig. 3 (a) Elemental composition of TMDs. (b) Schematic models of structural phase of TMDs. Reproduced with permission from Ref. [14] for (a), © Macmillan Publishers Limited, part of Springer Nature 2017; from Ref. [25] for (b), © American Chemical Society 2024.

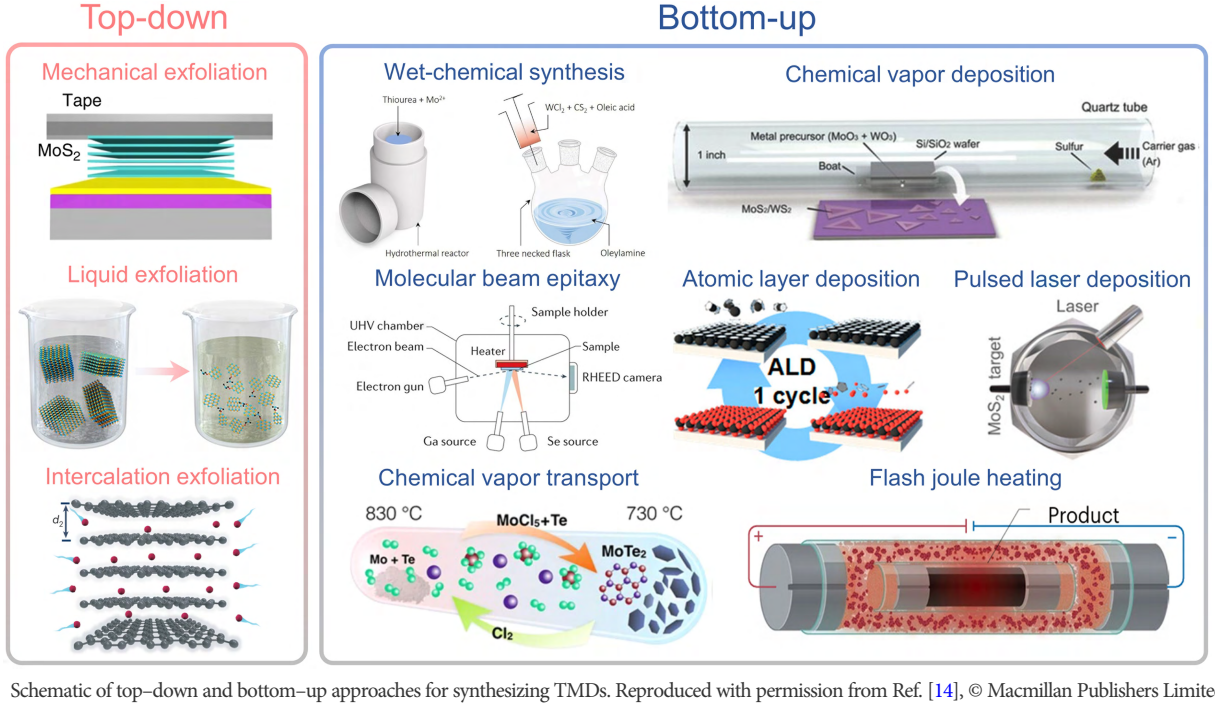


Fig. 4 Schematic of top–down and bottom–up approaches for synthesizing TMDs. Reproduced with permission from Ref. [14], © Macmillan Publishers Limited, part of Springer Nature 2017; from Ref. [31], © The Author(s) 2020; from Ref. [32], © The Author(s) 2019; from Ref. [33], © Springer Nature Limited 2023; from Ref. [34], © Wiley-VCH GmbH 2023; from Ref. [35], © WILEY-VCH Verlag GmbH & Co. KGaA, Weinheim 2018; from Ref. [36], © American Chemical Society 2013; from Ref. [37], © The Author(s) 2024; from Ref. [38], © The Author(s) 2016; from Ref. [39], © The Author(s) 2024.

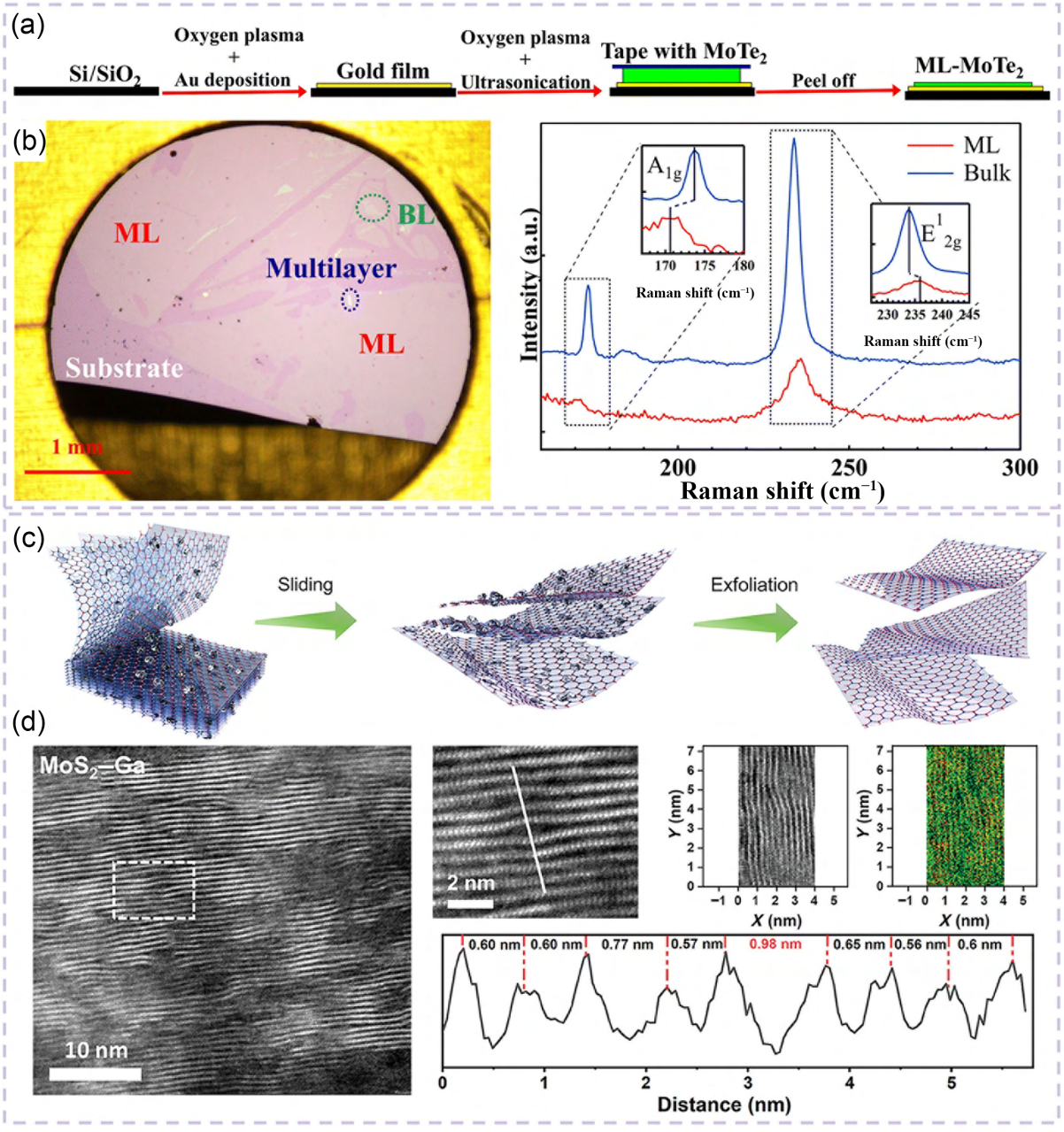


Fig. 5 (a) Fabrication process; (b) optical image and Raman spectra of 2H-$MoTe_2$ with mechanical exfoliation. (c, d) Ga-assisted exfoliation workflow and cross-sectional STEM/EELS analysis of MoS_2–Ga composite. Reproduced with permission from Ref. [42] for (a, b), © The Royal Society of Chemistry 2025; from Ref. [45] for (c, d), © Wiley-VCH GmbH 2024.

Lithium ion (Li^+) intercalation expands the interlayer spacing and weakens vdW forces, facilitating exfoliation into monolayer or few-layer TMDs [47]. However, the method is limited by slow intercalation kinetics, typically requiring over 48 h [48]. Faster methods have been developed, such as the ultrasound-assisted n-butyllithium (n-BuLi) technique reported by Yuwen et al. [49], which reduced the reaction time to less than 3 h while maintaining a high monolayer yield. Alternatively, electrochemical Li intercalation offers a high-throughput route to efficient layer separation [50]. Although monolayer yields can surpass 90%, the complexity of electrochemical setups hinders scaling, and residual Li^+ poses contamination risks.

2.2.2 Bottom–up approaches

Hydrothermal synthesis is a scalable and economical bottom–up approach for producing TMDs. The phase, morphology, and crystallinity of the products can be tuned by adjusting reaction parameters such as temperature, pressure, and precursor composition [51]. In this process, precursor dispersions are heated in sealed environments to trigger nucleation and growth of TMDs, typically yielding well-dispersed products. For example, Huang et al. [52] applied multiwalled carbon nanotubes (MWCNTs) as carriers and successfully prepared MoS_2 nanoflowers and nanotubes by controlling the raw materials, reaction temperature, and time, as shown in Figs. 6(a) and 6(b). Despite these advances, achieving consistently high crystallinity and precise thickness control is still challenging.

The hot-injection technique is a wet-chemical method that synthesizes colloidal TMDs by rapidly injecting precursors into a hot surfactant solution [53]. The resulting TMDs exhibit high

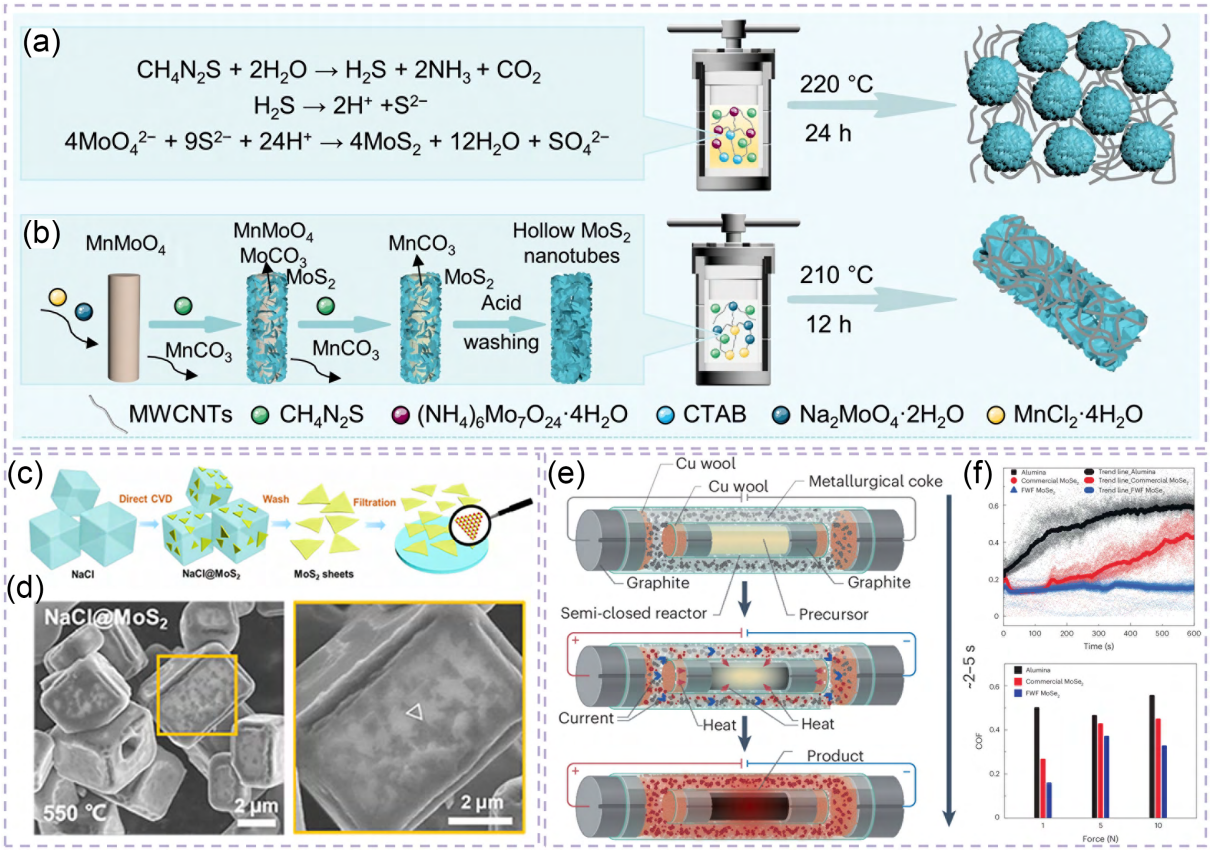


Fig. 6 (a, b) Schematic of synthesis of MoS_2 nanoflower (nanotube)/MWCNT heterojunction nanocomposites. (c) Schematic of CVD growth of 2D MoS_2 directly on NaCl crystals; (d) SEM images of NaCl@MoS_2 composites. (e) Schematic of FWF device, (f) COF comparison between commercial $MoSe_2$ and FWF $MoSe_2$. Reproduced with permission from Ref. [52] for (a, b), © Elsevier B.V. 2025; from Ref. [58] for (c, d), © Tsinghua University Press and Springer-Verlag GmbH Germany, part of Springer Nature 2020; from Ref. [39] for (e, f), © The Author(s) 2024.

purity, uniform size, and excellent dispersibility. However, residual surfactants and the need for precise injection control hinder scalability.

Chemical vapor deposition (CVD) enables the synthesis of large-area, high-crystallinity TMD films with precise thickness control and strong substrate adhesion [54]. In this process, vaporized metal and chalcogen precursors react on substrates to form MX_2 domains ranging from 1 to 100 μm [55]. However, achieving uniform coverage and precise thickness control is challenging due to vapor flux and thermal gradient limitations [37]. To address this, two-step approaches involving metal deposition followed by chalcogen annealing have been developed [56]. Following this approach, Lin et al. [57] combined physical vapor deposition (PVD) with CVD to fabricate $NbSe_2$ films with controlled thickness and grain morphology, demonstrating excellent room-temperature stability.

Furthermore, scalable synthesis of TMDs via CVD still presents substantial technical challenges. In a strategy to address this problem, Zhu et al. [58] developed a low-pressure CVD (LPCVD) method employing sodium chloride (NaCl) crystals as sacrificial templates, enabling efficient production of high-quality MoS_2 nanosheets (Fig. 6(c)). This method leverages the interaction between precursor materials (MoO_3 and sulfur powder) and the NaCl surface, enabling the formation of well-crystallized MoS_2 within minutes of reaction (Fig. 6(d)). Despite two decades of research, scalable and controllable CVD growth of TMDs remains a major bottleneck. Achieving uniform, high-quality films suitable for tribological applications requires careful optimization of reaction parameters [59].

Beyond conventional synthetic routes, advanced techniques, including molecular beam epitaxy (MBE), atomic layer deposition (ALD), pulsed laser deposition (PLD), and chemical vapor transport (CVT), enable precise fabrication of TMDs with atomic-scale control over their composition, crystallinity, and microstructure [14, 36, 38, 60]. Recently, flash Joule heating (FJH) has emerged as an ultrafast synthesis method capable of subsecond reactions. Choi et al. [39] developed a flash-within-flash Joule heating (FWF) strategy to synthesize ten TMDs (Fig. 6(e)). Of these, FWF-derived $MoSe_2$ exhibited superior tribological performance versus commercial benchmarks, highlighting the exceptional quality of this approach (Fig. 6(f)).

Overall, the preparation of TMDs necessitates balancing cost, material quality, and scalability, with a comparative summary provided in Table 2. Solution-based methods (e.g., hydrothermal, liquid exfoliation) offer low cost and straightforward operation. However, limited control over the layer number, defect density, and uniformity often compromises their tribological reliability. In contrast, vapor-phase methods (e.g., CVD, CVT, and MBE) produce highly crystalline, continuous films exhibiting superior tribological properties, yet demand complex equipment and precise growth conditions. ALD enables atomic-level thickness control but suffers from low deposition rates, limiting its large-scale application. PLD allows precise stoichiometric control yet frequently faces issues of film quality nonuniformity. Notably, different preparation methods can lead to variations in sample structure and quality, which in turn directly affect tribological performance and may result in the discrepancies observed among different studies. Furthermore, due to current limitations in fabrication techniques, low-cost, scalable production of TMDs beyond MoS_2 and WS_2 remains a significant challenge. Looking

Table 2 Summary of synthesis methods for TMDs

Category	Method	Key feature	Advantage	Limitation
Top–down	Mechanical exfoliation	Peeling of atomic layers from bulk crystals	High crystallinity and purity; minimal surface defects; and suitable for fundamental studies	Poor control over thickness and lateral size; low scalability; and not suitable for industrial production
	Liquid-phase exfoliation	Solvent-assisted delamination using mechanical energy	Scalable; low cost; and relatively simple	Low monolayer yield; small lateral size; and solvent toxicity issues
	Ion intercalation	Insertion of ions between layers to weaken the vdW forces	Enhanced exfoliation efficiency and monolayer yield; high-quality 2D layers	Slow kinetics (except ultrasound-assisted); complex electrochemical setups; potential residual ions; and challenging scale-up
Bottom–up	Hydro/solvothermal	Crystal growth from molecular precursors under high temperature and pressure	Economical; tunable morphology, phase, and crystallinity; and scalable	Limited crystallinity; difficult thickness control; and longer reaction times
	Hot-injection	Rapid injection of precursors into a hot solvent to form uniform nanocrystals	Uniform size and shape; high purity; and good dispersion	Residual surfactants; precise parameter control needed; and limited large-scale production
	CVD	Vapor-phase reaction of metal and chalcogen precursors on substrates	Large-area, high-quality films; layer and stoichiometry control; and low defect density	Thickness and uniformity control challenging; complex growth parameters; and limited scalability
	MBE, ALD, PLD, CVT	Atomic/nanoscale control via precise deposition or transport	Atomic-to-nanoscale control; high-quality, defect-controlled layers; and uniformity on complex substrates	Expensive; complex equipment; and limited throughput
	FJH	Ultrafast heating for subsecond synthesis	Ultrafast synthesis; high-quality TMDs; and superior tribological performance	Scalability and reproducibility need further validation

forward, hybrid strategies that integrate the advantages of multiple methods are expected to reconcile scalable production with enhanced tribological performance and to expand the application potential of other TMD subclasses.

3 Lubrication mechanisms of TMDs

TMDs, owing to their unique layered structures and exceptional physicochemical properties, exhibit distinct advantages in reducing friction and wear in mixed and boundary lubrication regimes. Their lubrication mechanisms are primarily governed by two core processes: (i) facilitating interlayer sliding as 2D nanomaterials and (ii) forming stable tribofilms at the tribointerfaces [61]. Building upon these processes, TMDs also demonstrate various derived effects and can work synergistically with other lubricant components or phases, thereby further enhancing their overall lubrication performance [62]. As illustrated in Fig. 7, these mechanisms can be systematically categorized into core mechanisms, derived effects, and synergistic mechanisms. Sections 3.1–3.3 will discuss how these mechanisms manifest and function in practical lubrication applications.

3.1 Core mechanisms

3.1.1 Interlayer sliding

The superior tribological properties of TMDs are attributed to the weak vdW forces connecting adjacent layers, which facilitate interlayer sliding. Under shear stress, the sliding mechanism allows TMDs to penetrate the tribointerfaces and form a protective layer that separates the contact surfaces, thereby achieving low friction and long-lasting lubrication [63]. Liu et al. [64] provided direct experimental evidence for this mechanism. Using atomic force microscopy (AFM) probes coated with two-dimensional nanosheets (e.g., TaS_2, MoS_2, and ReS_2), they measured ultralow COFs down to 10^{-4} between the nanosheets and bulk layered materials, clearly demonstrating superlubricity and confirming the interlayer sliding model (Figs. 8(a) and 8(b)). Moreover, interlayer sliding can effectively buffer contact stresses, improving the wear resistance of the frictional interface and extending the service life of the lubrication system [65].

3.1.2 Tribofilm formation

The formation of TMD-based tribofilms can be divided into two stages: initial physical adsorption followed by tribochemical reactions [66]. The initial physically adsorbed layer acts as a barrier, preventing direct asperity contact [67]. With continued sliding, frictional heat and shear stress induce tribochemical reactions, leading to the *in situ* formation of a robust tribofilm partially bonded to the substrate. Compared with purely physical films, this chemically bonded tribofilm exhibits higher load-bearing capacity and longer durability [68]. Kohlhauser et al. [69] reported the *in situ* formation of WS_2 tribofilms from WN coatings and sulfur in poly α-olefin (PAO)-8 lubricant containing 40 at% sulfur (Fig. 8(c)), which provided direct experimental evidence for the efficacy of tribofilms. The resulting interface maintained a low COF of 0.05 for 100 h and showed no measurable wear at the interface (Figs. 8(d) and 8(e)).

3.2 Derived effects

3.2.1 Ball-bearing effect

The ball-bearing behavior arising from interlayer sliding of TMD nanoparticles represents a promising approach to enhance lubrication efficiency. Spherical or quasi-spherical TMD nanoparticles can serve as nanoscale ball bearings, transforming sliding friction into rolling motion and thus reducing friction and wear [70]. The effectiveness of this mechanism relies on precise control of the particle size to ensure successful entry into the contact region [71]. Using a hydrothermal method, Liu et al. [17] synthesized monodisperse MoS_2 quantum dots (QDs; 4–7 nm) and maintained a stable dispersion in polyethylene glycol (PEG 200) for over 100 d (Figs. 9(a) and 9(b)). At 0.08 wt% additive concentration and 392 N load, this lubricant decreased the COF and wear volume by 10.5% and 86.8%, respectively, relative to pure PEG 200 (Fig. 9(c)). The enhanced performance is primarily due to the MoS_2 QDs functioning as nanoscale ball bearings,

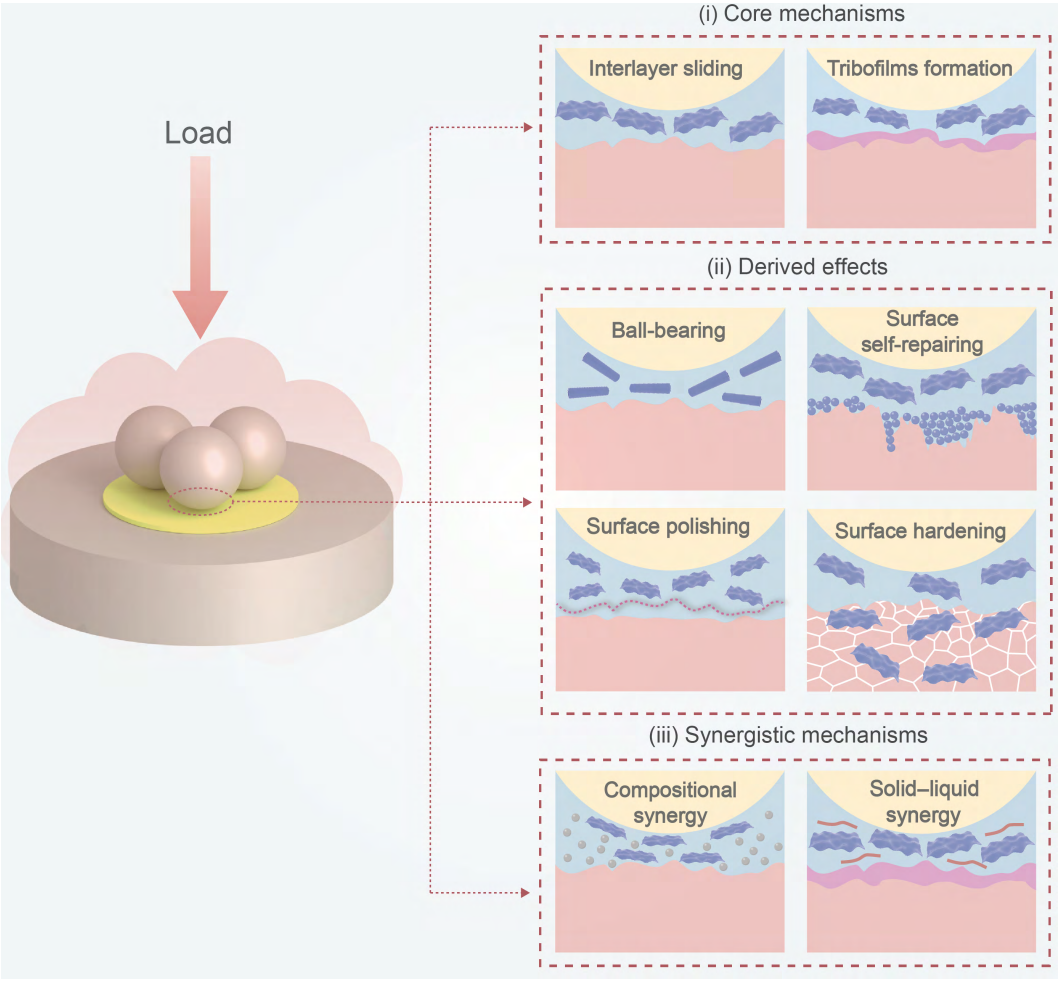


Fig. 7 Schematic diagram of lubrication mechanisms of TMDs.

whose appropriate size enables penetration into the contact region, surface repair, and promotion of tribofilm formation, thereby reducing friction and wear.

3.2.2 Surface self-repairing

The durability of solid TMDs is enhanced by a self-repair mechanism that operates in tandem with their primary lubricating functions [12]. This process is initiated as TMD nanoparticles occupy and seal surface pits, thereby alleviating localized contact pressure and suppressing plastic deformation [72]. Under transient high temperatures induced by sliding, the particles undergo partial melting, infiltration, and effective sealing of microcracks [73]. The molten material subsequently interacts with tribochemical products to form a protective film over damaged regions such as grooves. This film effectively restores the original surface topography and prevents direct contact between sliding surfaces [13]. Cao et al. [74] demonstrated that predesigned notches in WS_2/amorphous carbon (a-C) coatings could close under sliding, with the healed region acting as a lubricant microreservoir that achieved an ultralow COF of 0.02 (Fig. 9(d)). Real-time friction monitoring further confirms that stress excitation during sliding drives the restoration of surface defects in these coatings (Fig. 9(e)) [75].

3.2.3 Surface polishing

Surface polishing in TMD-based lubricants arises from nanoparticle-induced abrasive wear, where hard particles interact with rough interfaces during sliding [66]. Through combined micro-cutting and rolling actions, these particles progressively remove surface asperities, resulting in a smoother tribological interface with reduced roughness [76]. The polishing outcome is mainly dependent on the mechanical properties of the nanoparticles, especially their hardness relative to the friction surface [77]. However, surface polishing is highly sensitive to operating parameters; excessive load or inappropriate frequency can transform beneficial polishing into detrimental abrasive wear, leading to friction escalation and severe surface damage [67]. Ying et al. [78] demonstrated this load-dependent transition in WS_2 coatings prepared by high-power impulse magnetron sputtering (HiPIMS), where a load of 15 N promoted friction reduction with minimal polishing, while increasing to 20 N caused an abrupt friction rise and dominant abrasive wear.

3.2.4 Surface hardening

It is well established that under boundary lubrication conditions, the embedding of hard nanomaterials into soft surfaces leads to a tribological transformation layer (TTL) with distinct properties [62]. The TTL, consisting of refined grains and metastable phases, reinforces the surface through two primary mechanisms: improving hardness and yield strength by obstructing dislocation motion and enhancing wear resistance by deflecting cracks and inhibiting their propagation. Based on this mechanistic understanding, Yan et al. [79] developed a lubricant formulation employing MoS_2 and BN-doped Li grease (Fig. 9(f)). This

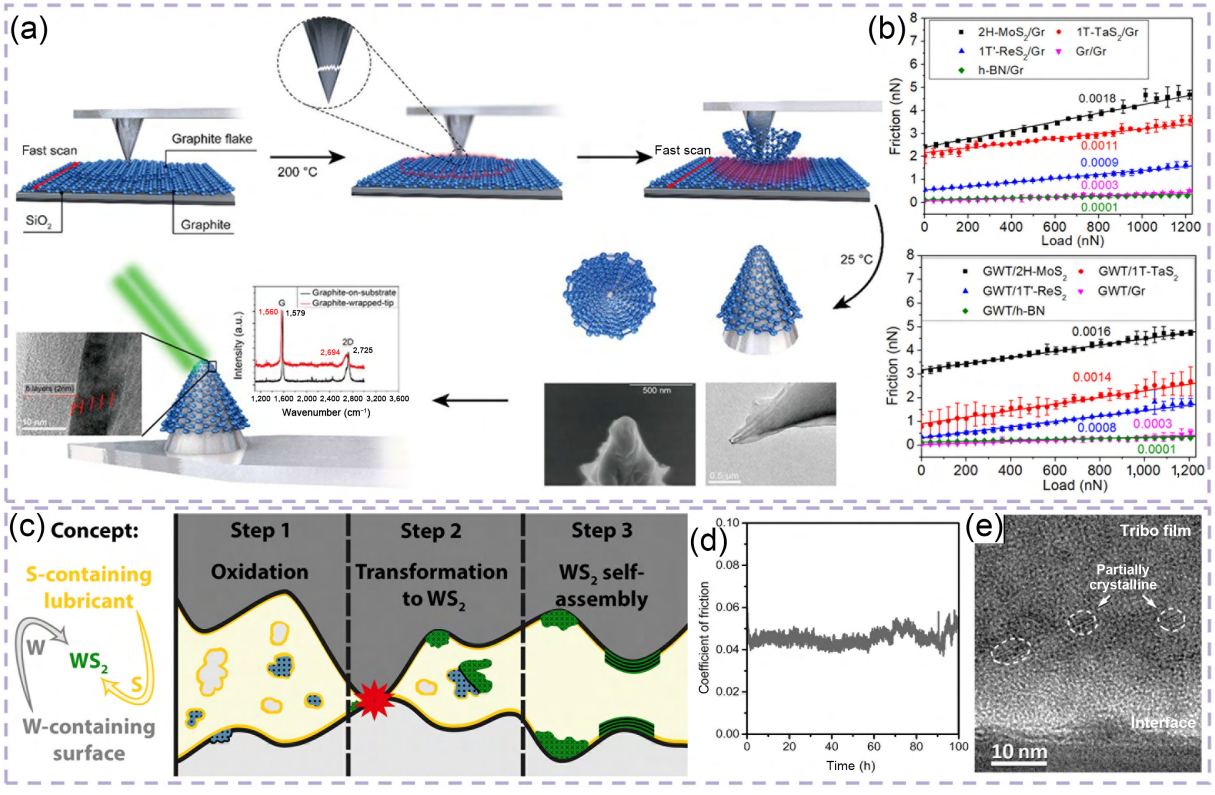


Fig. 8 (a) Schematic of 2D flake-wrapped AFM tip preparation; (b) friction performance of 2D sheet-wrapped tips on graphite versus graphite-coated tips (GWT) on layered materials. (c) *In situ* formation of WS_2 tribofilm; (d) COF of system remaining 0.05 in 100 h; and (e) TEM image of crystalline WS_2 nanoparticles embedded in tribofilm on Si_3N_4 ball surface. Reproduced with permission from Ref. [64] for (a, b), © American Chemical Society 2018; from Ref. [69] for (c–e), © The Authors 2020.

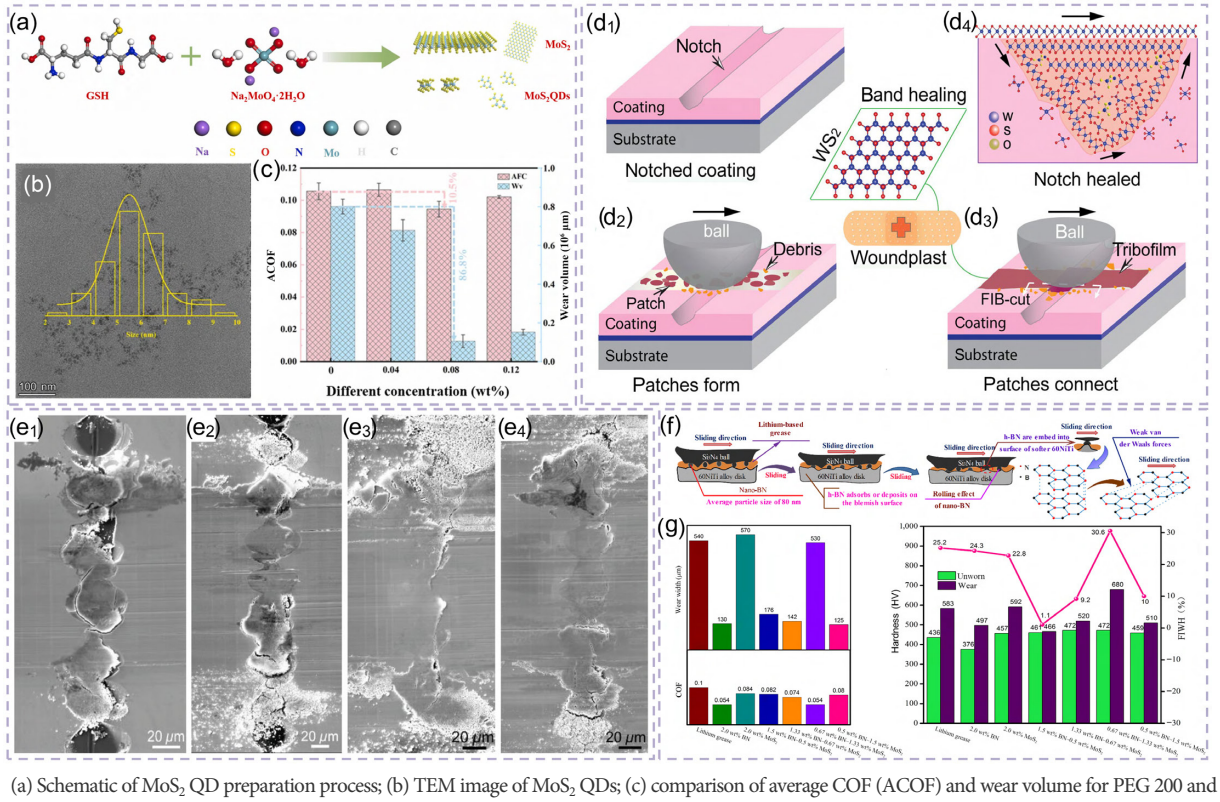


Fig. 9 (a) Schematic of MoS_2 QD preparation process; (b) TEM image of MoS_2 QDs; (c) comparison of average COF (ACOF) and wear volume for PEG 200 and MoS_2 QD/PEG lubricants at various concentrations. (d) Self-repairing process of WS_2/a-C tribofilms. (e) SEM image of damage self-healing process after multiple slides. (f) Friction-reduction, anti-wear, and surface-hardening mechanisms of lubricants; (g) wear track width, COF, and friction-induced work-hardening rate of 60NiTi under different lubrication conditions. Reproduced with permission from Ref. [17] for (a–c), © Elsevier Ltd. 2025; from Ref. [74] for (d), © The Author(s) 2019; from Ref. [75] for (e), © The Authors 2019; from Ref. [79] for (f, g), © Society of Tribologists and Lubrication Engineers 2019.

清華大学出版社 Tsinghua University Press | SciOpen

approach suppressed cracking in 60NiTi alloy while concurrently improving its tribological performance and enhancing the surface hardening effect (Fig. 9(g)).

3.3 Synergistic mechanisms

The integration of TMDs with other materials or their application in hybrid solid/liquid systems can unlock synergistic lubrication performance that surpasses the contribution of any single mechanism. This integrated approach constitutes a key strategy for performance optimization, which represents the current frontier in tribological research and will be detailed in Section 5.3.

Current research on the lubrication mechanisms of TMDs primarily depends on macroscopic observations, which provide valuable insights but fail to quantitatively uncover the underlying microscopic processes. The formation of tribofilms is generally regarded as the dominant mechanism, yet its dynamic evolution and structural changes under real operating conditions are still not well understood. In addition, derived effects such as self-repair and surface polishing are mostly verified under ideal or short-term conditions, and their long-term stability and controllability remain unclear. Future studies should integrate advanced *in situ* characterization with multiscale simulations to elucidate the coupling among structural evolution, interfacial chemistry, and evolution of tribological performance.

4 Key factors governing the tribological performance of TMDs

Building on the lubrication mechanisms summarized in Section 3, this section focuses on analyzing the key controlling factors that determine whether these mechanisms can be realized in actual tribological systems. These factors can be classified into two main categories: intrinsic material properties and external operating conditions. The former includes crystal structure, elemental composition, layer number, morphology, and dispersion, while the latter encompasses parameters such as load, sliding speed, and environmental atmosphere. Through interfacial processes, these factors directly influence the COF and wear parameters, thereby determining the practical effectiveness of the lubrication mechanisms. A systematic analysis of the coupling effects among these factors is key to evaluating and optimizing the lubrication performance of TMDs.

4.1 Intrinsic material properties

4.1.1 Elemental composition

As outlined in Section 2.1, the composition of transition metals and chalcogen elements in TMDs fundamentally determines their crystal structure, electronic properties, and consequent tribological behavior. A comparison between WS_2 and MoS_2 illustrates this point: WS_2 exhibits superior oxidation resistance, maintaining integrity up to 425 °C, whereas MoS_2 degrades above 350 °C [22]. Moreover, the oxidation product WO_3 has a lower COF than MoO_3, although the high cost of WS_2 limits its practical application. Similarly, chalcogen elements also play a critical role in tribological properties, as confirmed by Vazirisereshk et al. [80]. Their research, combining AFM experiments and molecular dynamics (MD) simulations, demonstrated an inverse correlation between friction and the atomic radius of chalcogen elements, following the trend of MoS_2 > $MoSe_2$ > $MoTe_2$ (Figs. 10(a) and 10(b)). This friction contrast arises from the combined effects of the lattice constant and energy barrier. Given the diversity of TMD nanomaterials, the relationship between elemental composition and tribological performance still requires systematic clarification.

4.1.2 Crystal phases

The lubricity of TMDs is closely linked to their crystal structure, with the 2H phase generally exhibiting superior tribological performance compared with the 1T/1T' phases, primarily due to its better thermodynamic stability [20]. Lee et al. [81] conducted an in-depth exploration of this mechanism, and their experimental evidence revealed that the COF of 1T'-MoS_2 ($MoSe_2$) is approximately an order of magnitude higher than that of the 2H phase. Further density functional theory (DFT) calculations attributed this difference to the stronger interfacial electronic excitation, the more efficient phonon dissipation, and the higher surface potential barrier of the metastable 1T' phase. In parallel, Liu et al. [82] confirmed the tribological advantage of 2H-MoS_2 over the 1T phase (Figs. 10(c)–10(e)). By tuning the annealing temperature to control the phase composition, they found that 2H-dominant samples achieved a lower COF and longer wear life. Mechanistic insights from DFT calculations revealed that this is due to the greater hydrophobicity of the 2H phase, which effectively protects the active sulfur-edge sites from water molecule adsorption in humid environments, thereby maintaining easy-shear characteristics at the interface. The combination of inherent electronic stability and environmental resistance renders the 2H phase an ideal structure for low-friction applications.

4.1.3 Layer number and interlayer spacing

The influence of the TMD layer number on the tribological properties remains a debated topic. One view holds that fewer layers weaken vdW forces, enabling sliding and tribofilm formation [83]. For instance, Yu et al. [84] demonstrated that monolayer $NbSe_2$ prepared by CVD achieved an ultralow COF (μ = 0.0085) at 60% relative humidity (RH) and remained stable for 50 d, with 30% lower friction than few-layer $NbSe_2$ and superior wear resistance to it (Figs. 10(f) and 10(g)). DFT analysis indicates that this improvement is due to enhanced interfacial adhesion and accelerated interlayer charge transfer, which together facilitate tribofilm formation (Figs. 10(h) and 10(i)). In contrast, multilayer TMDs are less sensitive to defects and wrinkles, allowing progressive friction reduction and improved wear resistance during continuous sliding [61]. These findings suggest that the optimal layer number of TMDs should balance interfacial adhesion, structural stability, and friction-induced structural evolution.

Expanding the interlayer spacing similarly reduces vdW, π–π, and electrostatic interactions, enhancing sliding [85]. For example, Liu et al. [86] synthesized Cu-modified 1T/2H-MoS_2 (CTHM) with a spacing enlarged to 0.99 nm versus 0.63 nm in 2H-MoS_2, leading to 45% lower friction and 77% higher wear resistance in PAO lubricants.

4.1.4 Morphology

The morphology of TMDs critically influences their tribological behavior through mechanisms including tribofilm formation and interlayer sliding [24]. For instance, Zhang et al. [87] reported that WS_2 nanoflower-based lubricants exhibited lower friction than those containing hexagonal nanosheets, owing to the *in situ* fragmentation of nanoflowers into ultrathin nanosheets (< 2 nm) that adsorb on the surface to form a dense tribofilm. As described in Section 2.2, various TMD morphologies can be synthesized by appropriate methods, and their tribological properties exhibit clear

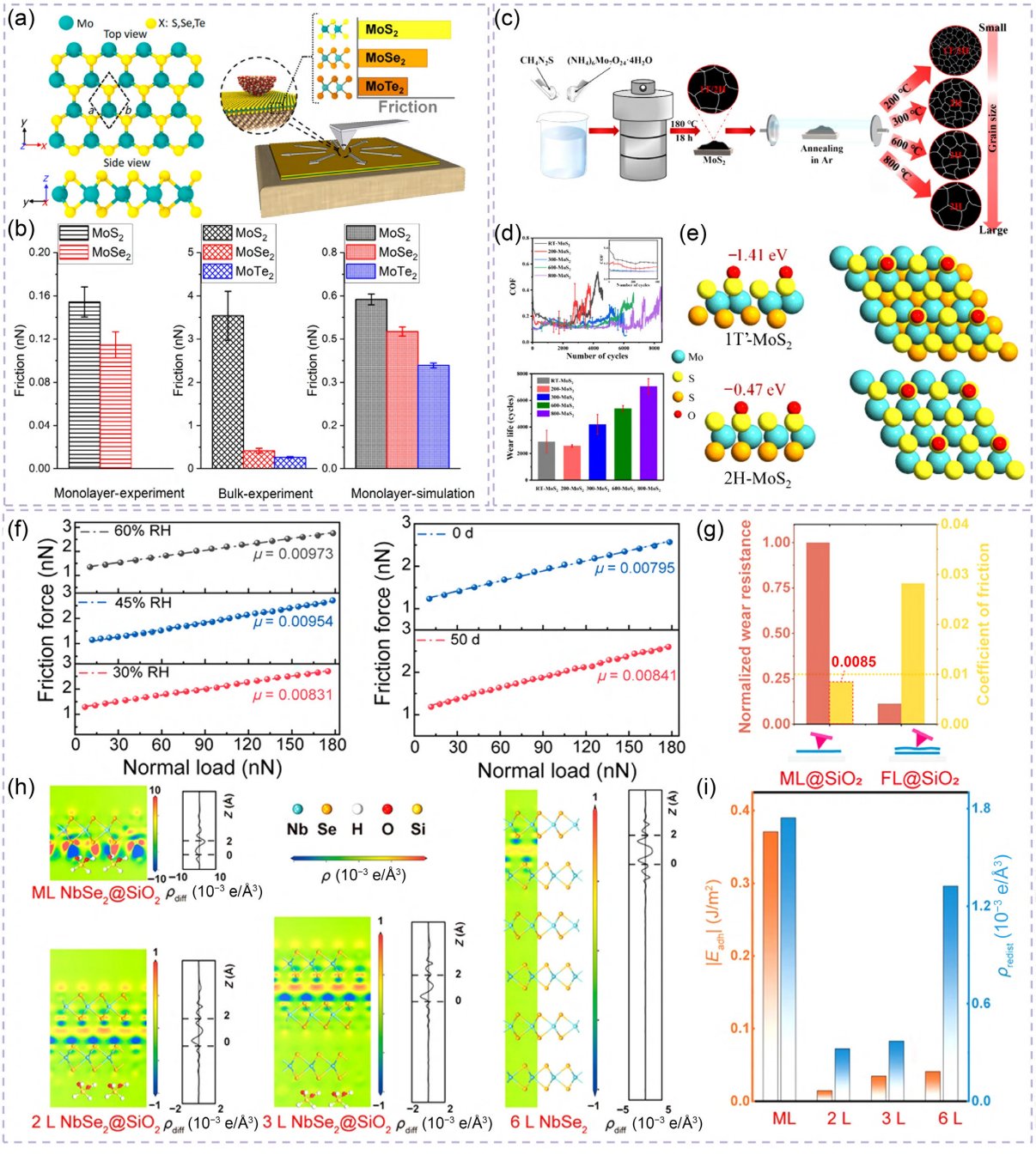


Fig. 10 (a) MoX_2 structural models and measurement setup; (b) friction forces on MoX_2 bulk/monolayer surfaces. (c) Schematic of synthesis strategy for phase-controlled MoS_2; (d) COF and wear life of MoS_2 versus temperature; (e) oxygen adsorption on 1T'/2H-MoS_2. (f) COF of $NbSe_2$ monolayers under varying humidity and aging; (g) comparison of friction and wear resistance in mono/few-layer $NbSe_2$; (h) interfacial charge redistribution in mono/few-layer $NbSe_2$@SiO_2; (i) adhesion energy ($|E_{adh}|$) and overall degree of charge redistribution (ρ_{redis}). Reproduced with permission from Ref. [80] for (a, b), © American Chemical Society 2020; from Ref. [82] for (c–e), © Elsevier B.V. 2024; from Ref. [84] for (f–i), © American Chemical Society 2023.

dimension-dependent characteristics. Generally, zero-dimensional (0D) and one-dimensional (1D) structures can achieve excellent lubrication through the ball-bearing effect but are prone to sedimentation and oxidation. 2D nanosheets can form efficient tribofilms due to their interlayer shear characteristics, while three-dimensional (3D) assemblies enhance tribofilm retention and load-bearing capacity but face challenges in dispersion. There is no consensus on the optimal TMD morphology, as it depends on synthesis routes and test conditions. Future research should focus on the targeted design and controllable synthesis of morphologies tailored for specific environments to optimize tribological performance.

4.1.5 *Dispersion stability*

In liquid lubrication, poor dispersion of TMDs leads to agglomeration and sedimentation, reducing lubrication efficiency and accelerating wear [88]. Current strategies to improve dispersion include ultrasonic treatment, chemical dispersants, and surface functionalization, which enhance particle adsorption and tribofilm formation. For example, Li et al. [89] used ultrasonic dispersion to produce smaller $MoSe_2$ nanoparticles with higher SSA ($MoSe_2$ T-NPs). Tests in white oil showed that the treated nanoparticles lowered friction by 43% and wear rate by 87% at a concentration of 0.75 wt% compared with untreated $MoSe_2$ NPs.

清華大学出版社 Tsinghua University Press | SciOpen

This improvement is attributed to the smaller particle size and higher SSA of $MoSe_2$ T-NPs, promoting tribofilm formation.

Overall, the above intrinsic properties of the material modulate the activation and effectiveness of lubrication mechanisms to varying degrees by governing interfacial interactions and the evolution of tribofilms. Therefore, tailoring these intrinsic material properties enables the optimization of the tribological performance of TMD-based lubricants and the realization of more stable macroscopic lubrication behavior.

4.2 External working conditions

4.2.1 Testing environments

The tribological behavior of TMDs is strongly influenced by environmental factors, particularly the surrounding atmosphere, temperature, and humidity [90]. The atmosphere dictates frictional response mainly through surface adsorption and oxidation reactions. Under inert or vacuum atmospheres, the lack of oxygen and moisture facilitates smooth interlayer sliding and favors the formation of stable transfer films. In contrast, oxygen-rich environments promote selective adsorption on defect sites, triggering oxidation and generating abrasive "hard spots" that accelerate wear [91]. Temperature exerts a pronounced effect on the frictional response of TMDs. In the low-temperature regime (≤ 100 °C), the majority of TMDs sustain a relatively low COF. As the temperature increases to the intermediate range (100–500 °C), accelerated oxidation and phase transitions hinder interlayer shearing, causing friction and wear to rise markedly [92]. At high temperatures (> 500 °C), the pure TMDs ultimately lose their lubricating functionality. Humidity is a key adverse factor influencing the tribological behavior of TMDs, mainly through structure-dependent mechanisms [93]. In general, a higher RH typically leads to an increase in the COF. This is primarily because water molecules adsorb at edge defects, forming hydrogen bonds that enhance interlayer adhesion [21]. Simultaneously, they synergize with oxygen to accelerate oxidation, thereby generating byproducts that contribute to wear.

Among various environmental influences, oxidation serves as the dominant pathway governing TMD tribology. Using MoS_2 as an example, lattice defects facilitate oxygen dissociation and adsorption by lowering the activation energy barrier, thereby accelerating oxidation kinetics (Fig. 11(a)) [94]. When oxygen and water coadsorb on these sites, O and OH radicals substitute S atoms, leading to Mo–S bond cleavage and the formation of stronger Mo–O bonds [95]. The resulting products, such as MoO_3 and H_2SO_4, perpetuate a self-propagating degradation cycle that destroys the lamellar structure (Fig. 11(b)) [96]. Moderate oxidation may generate a protective tribofilm that enhances wear resistance, whereas excessive oxidation destabilizes this film, damages the layered framework, and accelerates wear [97].

In summary, environmental factors fundamentally determine the stability and lifespan of TMD lubricating films through competitive adsorption and the initiation of irreversible oxidative degradation cycles.

4.2.2 Tribological pairs

The choice of tribological pairs is regarded as a key factor in tribological system design, as they serve not only as "testing conditions" but also as "active participants in interfacial reactions". For example, Grützmacher et al. [98] synthesized transition metal carbo–chalcogenides (TMCCs; e.g., Ta_2S_2C and Nb_2S_2C) via solid-state methods and evaluated their tribological performance on different counterbodies. The results showed that identical TMCC materials exhibited different COF values on

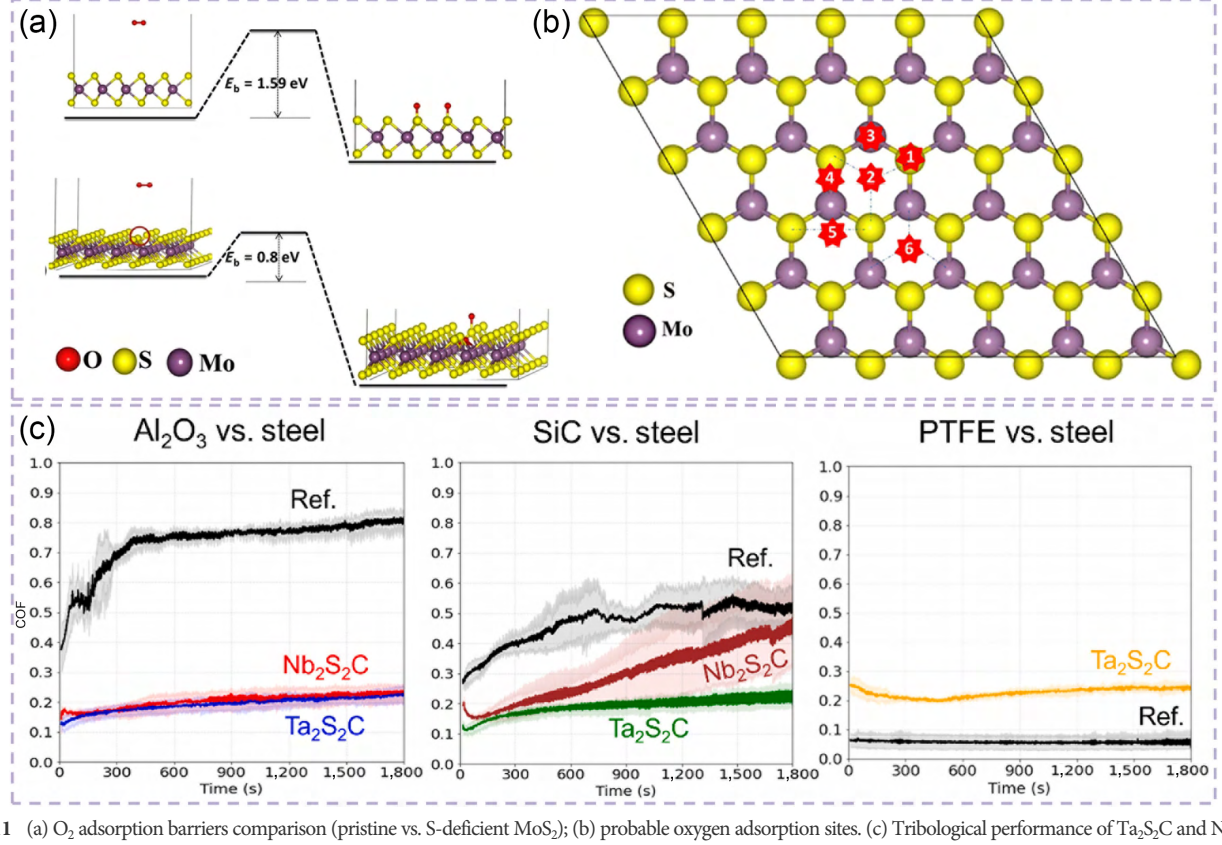


Fig. 11 (a) O_2 adsorption barriers comparison (pristine vs. S-deficient MoS_2); (b) probable oxygen adsorption sites. (c) Tribological performance of Ta_2S_2C and Nb_2S_2C powder against various counterbodies. Reproduced with permission from Ref. [94] for (a, b), © AIP Publishing LLC. 2015; from Ref. [98] for (c), © The Authors 2024.

Al_2O_3, SiC, and polytetrafluoroethylene (PTFE) (Fig. 11(c)). Notably, the combination of PTFE against steel displayed a lower COF, primarily due to the friction-reducing effect of PTFE, indicating that the counterbody plays a critical role in regulating the formation and properties of the tribofilm. Therefore, rational selection of tribological pairs can facilitate interfacial reactions to enhance tribological performance.

4.2.3 *Testing parameters*

In tribological evaluations of TMD-based lubricants, the COF, together with wear parameters, including wear rate, wear volume, and wear scar diameter (WSD), not only reflects tribological performance but also indicates the extent to which external load and shear stress influence the stability of the layered structure [99]. An excessive load leads to damage of the lubricating film, while an optimal load range allows orderly interlayer sliding and results in low friction. Sliding speed affects frictional heat accumulation and tribofilm formation. Moderate speeds can promote film reconstruction, but excessively high speeds may destabilize the lubricating layer due to thermal effects [100]. These observations suggest that the nonlinear variations in the COF and wear mainly arise from the balance between interlayer sliding and structural degradation [101]. Overall, operating parameters govern the stability and evolution of TMD-based tribofilms, ultimately determining their tribological performance.

In summary, the tribological performance of TMDs is governed by the complex interplay between intrinsic material properties and external operating conditions, which presents considerable challenges for reliable prediction and analysis. This coupling often results in inconsistent findings, particularly regarding structural parameters such as layer number, crystal phase, and morphology. Therefore, integrated strategies combining high-throughput experimentation, multiscale simulations, and *in situ* characterization are required to identify key factors and to guide the rational design of high-performance TMD-based lubricants.

5 Strategies to modulate TMD tribology

Conventional MoS_2 and WS_2 lubricants suffer from inherent drawbacks in harsh operating environments, such as oxidation sensitivity and rapid performance degradation [21]. To address these issues, researchers have developed TMD-based lubricants with customized properties through various modification strategies. This section reviews strategies for enhancing the tribological performance of TMDs, which can be categorized into two groups: conventional methods, such as surface modification, structural engineering, and composite integration, and emerging paradigms, including superlubricity design, intelligent tuning, and machine learning (ML)-assisted optimization (Fig. 12). Collectively, these strategies synergistically improve the versatility and durability of TMDs, enabling their deployment as high-performance nanolubricants under extreme operating conditions.

5.1 Surface functionalization

The poor dispersion stability and weak surface affinity of

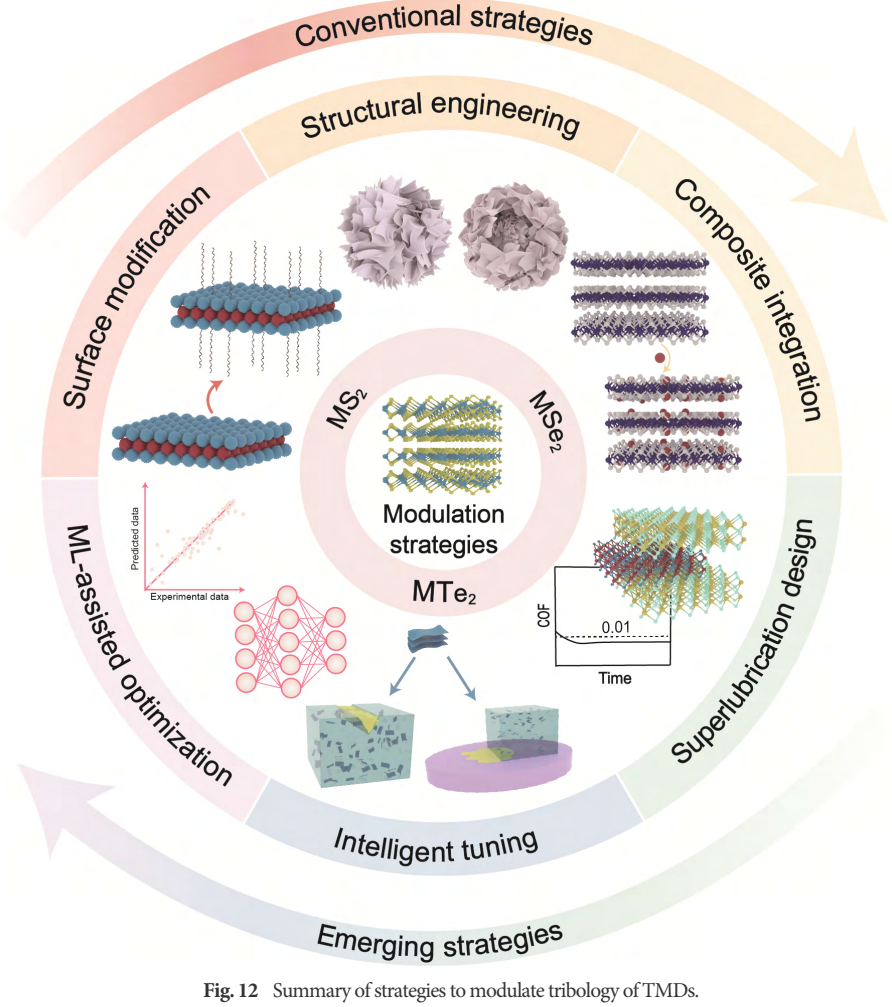


Fig. 12 Summary of strategies to modulate tribology of TMDs.

清華大学出版社 Tsinghua University Press | SciOpen

chemically inert TMDs limit their effectiveness as lubricant additives [102]. Surface functionalization, typically classified into noncovalent or covalent approaches, has emerged as a key strategy to address these limitations [103]. Among noncovalent strategies, mussel-inspired chemistry methods use polydopamine (PDA), polyphenols, or catechol derivatives to form intermediate layers on TMD surfaces that serve as platforms for grafting functional groups [104, 105]. For example, Wu et al. [106] combined mussel-inspired chemistry with Michael addition to prepare n-octadecyl mercaptan-functionalized MoS_2 (MoS_2–NOM), which was dispersed stably in PAO-10 (Fig. 13(a)). The addition of 1 wt% MoS_2–NOM resulted in marked reductions of 53% in the COF and 92% in the wear volume (Fig. 13(b)). This enhancement was ascribed to the formation of a robust tribofilm, as confirmed by X-ray photoelectron spectroscopy (XPS), composed of a complex mixture of chemical compounds on the steel surface (Fig. 13(c)).

Despite their versatility, noncovalent approaches produce weaker interfacial connections, limiting their long-term stability in harsh environments. Covalent functionalization forms stronger chemical bonds, such as reactions with organosilanes, alkylamines, or diazonium salts, and can improve dispersion stability while altering interfacial charge distribution and vdW interactions to reduce friction [107, 108]. Kumari et al. [109] grafted long-chain alkyl organosilanes onto WS_2–O to obtain WS_2–O–OCS (OCS = octadecyltrichlorosilane) and WS_2–O–OES (OES = octadecyl-triethoxysilane) hybrids dispersed in mineral lube oil (SN-150) (Fig. 13(d)). At a concentration of 200 ppm, the additives reduced the COF and wear volume by up to 52% and 79%, respectively (Fig. 13(e)). The authors attributed the effective lubrication to the formation of a tribo-induced WS_2-based film on steel counterparts, as evidenced by SEM, energy dispersive spectroscopy (EDS), and Raman analyses, which facilitates sliding and protects the contact interface (Figs. 13(f) and 13(g)). Ren et al. [110] applied ultraviolet-driven self-initiated photografting and photopolymerization to attach poly (3-sulfopropyl methacrylate potassium salt) (PSPMA) brushes to MoS_2, producing composites with improved aqueous dispersion stability and enhanced performance as water-based additives.

Although extensive research has investigated the surface functionalization of TMDs through noncovalent and covalent strategies, complex procedures have limited their large-scale application. To overcome this limitation, mechanochemical approaches have been introduced as environmentally benign methods for the low-waste synthesis of surface-functionalized nanoparticles via ball milling or ultrasonication [111]. In a representative study, Wang et al. [103] synthesized dextran-modified MoS_2 nanoparticles (MoS_2–dex NPs) by ball milling in a nitrogen atmosphere (Fig. 13(h)). The nanoparticles dispersed stably in a glycerol–water mixture and reduced friction and wear, with further improvement upon incorporation of graphene oxide (GO), as shown in Fig. 13(i). Mechanistic analysis indicated that GO-filled surface asperities and a composite tribofilm containing MoS_2, GO, and iron species formed at the interface, contributing to reduced friction and improved wear resistance (Fig. 13(j)).

5.2 Structural engineering

5.2.1 *Intrinsic structure assembly*

As discussed in Section 4.1, the tribological performance of lubricants is closely correlated with the structural parameters of the incorporated 2D nanomaterials, highlighting the importance of rational nanostructure design for achieving high lubrication efficiency [112, 113]. For instance, core–shell architectures enable synergistic integration of functional components to optimize tribological behaviors [114]. Liu et al. [115] prepared a core–shell structured WS_2/MoS_2 micro- and nano- composite, in which preoxidized micro-WS_2 was coated with nano-MoS_2. The addition of only 0.5 wt% of composite to base oil improved wear resistance,

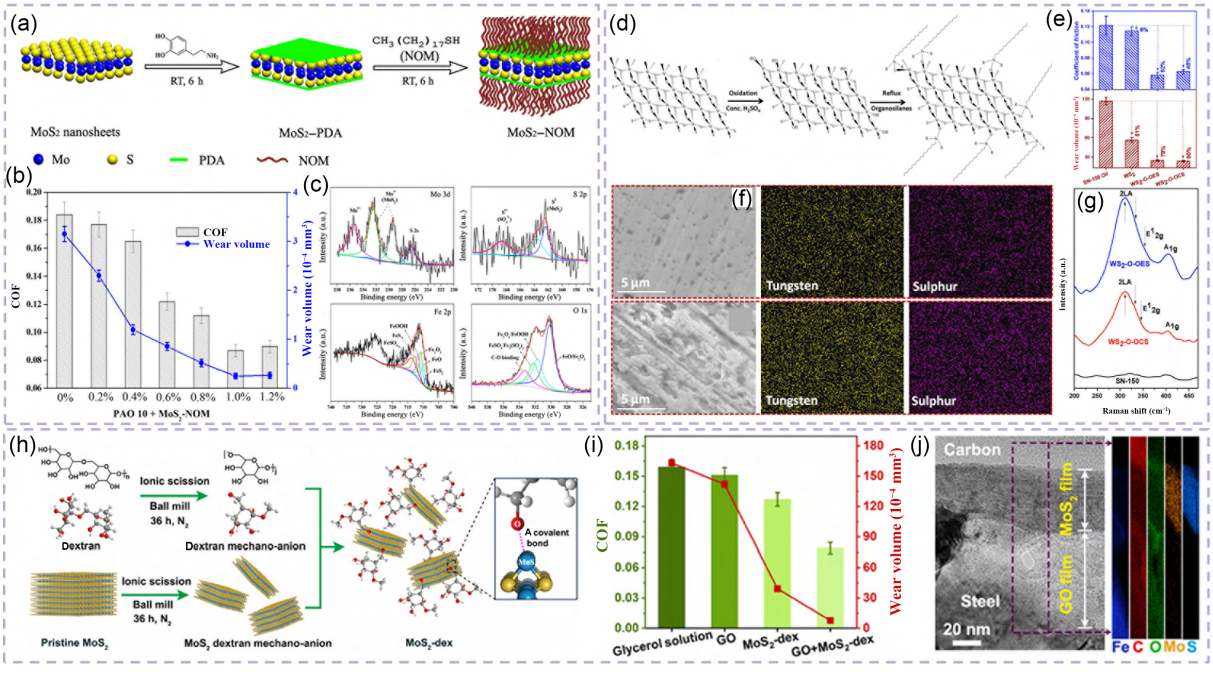


Fig. 13 (a) Synthesis of MoS_2–NOM; (b) COF and wear volume of steel disks lubricated by PAO-10 with varying MoS_2–NOM concentrations; (c) XPS analysis of wear scars under lubrication with PAO-10+1 wt% MoS_2–NOM. (d) Schematic of covalent organosilane grafting onto WS_2; (e) COF and wear volume: SN-150 oil vs. WS_2 dispersions; (f) wear scar microscopy and elemental mapping for WS_2–O-OES and WS_2–O-OCS lubrication; (g) Raman spectra of wear scars. (h) Ball-milling synthesis of dextran-functionalized MoS_2 nanoparticles; (i) lubricant performance: COF and wear volume comparison; (j) cross-sectional TEM and EDS mapping of wear track lubricated by MoS_2-dex/GO in glycerol. Reproduced with permission from Ref. [106] for (a–c), © American Chemical Society 2018; from Ref. [109] for (d–g), © American Chemical Society 2021; from Ref. [103] for (h–j), © American Chemical Society 2023.

reducing steel disk wear rates by up to 65.3% and WSDs by 33.7% compared with its individual components. The enhanced performance was attributed to a synergistic mechanism whereby micro-WS_2 served as a physical barrier and a tungsten-rich adsorption layer, while nano-MoS_2 sheets reacted with iron to generate a durable tribofilm.

Complementing core–shell structures, gradient multilayer architectures further improve tribological performance by optimizing the balance between hardness and toughness [116]. Gao et al. [117] developed a MoS_2/WB_2 multilayer system comprising a MoS_2 core and an ultrathin WB_2 interlayer (Fig. 14(a)). The WB_2 phase induces oriented growth of MoS_2 along the (002) plane, which concurrently enhances hardness, load-bearing capacity, and oxidation resistance while facilitating interfacial interdiffusion to inhibit delamination. As a result, the MoS_2/WB_2 nanolaminate exhibits low friction and minimal wear across a broad temperature range (25–400 °C), achieving a COF below 0.1 at 400 °C, which surpasses most conventional MoS_2-based coatings (Figs. 14(b) and 14(c)). TEM analysis further revealed that the highly ordered MoS_2 (002) nanosheets encapsulated oxide nanoparticles formed *in situ* during high-temperature sliding (Fig. 14(d)). This encapsulation suppressed oxide coarsening and reduced interparticle contact. Meanwhile, the embedded nanoparticles acted as nanoasperities to stabilize the sliding interface, thereby sustaining ultralow friction at elevated temperatures.

5.2.2 *In situ* tribofilm formation

Beyond intrinsic structural assembly, inducing tribochemical reactions to form TMD-based coatings *in situ* represents another promising strategy for enhancing lubrication. Grützmacher et al. [118] demonstrated this approach by depositing Se nanopowder on Mo- or W-coated steel surfaces sliding against Al_2O_3 balls under dry friction, which generated $MoSe_2$ or WSe_2 lubricating layers at the interface (Fig. 14(e)). The introduction of Se notably reduced the COF from 0.6 to 0.09 for $MoSe_2$, accompanied by a 75% decrease in wear rate, while WSe_2 exhibited a COF drop from 0.4 to 0.13 and a 26% wear rate reduction. Surface analysis confirmed the presence of 10–20 nm layered selenides in the contact region (Fig. 14(f)). MD simulations revealed that shear stress promotes bonding between metal fragments and Se nanoparticles, forming easily shearable 2D structures that underlie the low-friction behavior.

5.2.3 Defect modulation

Defect modulation through doping and vacancy engineering, as

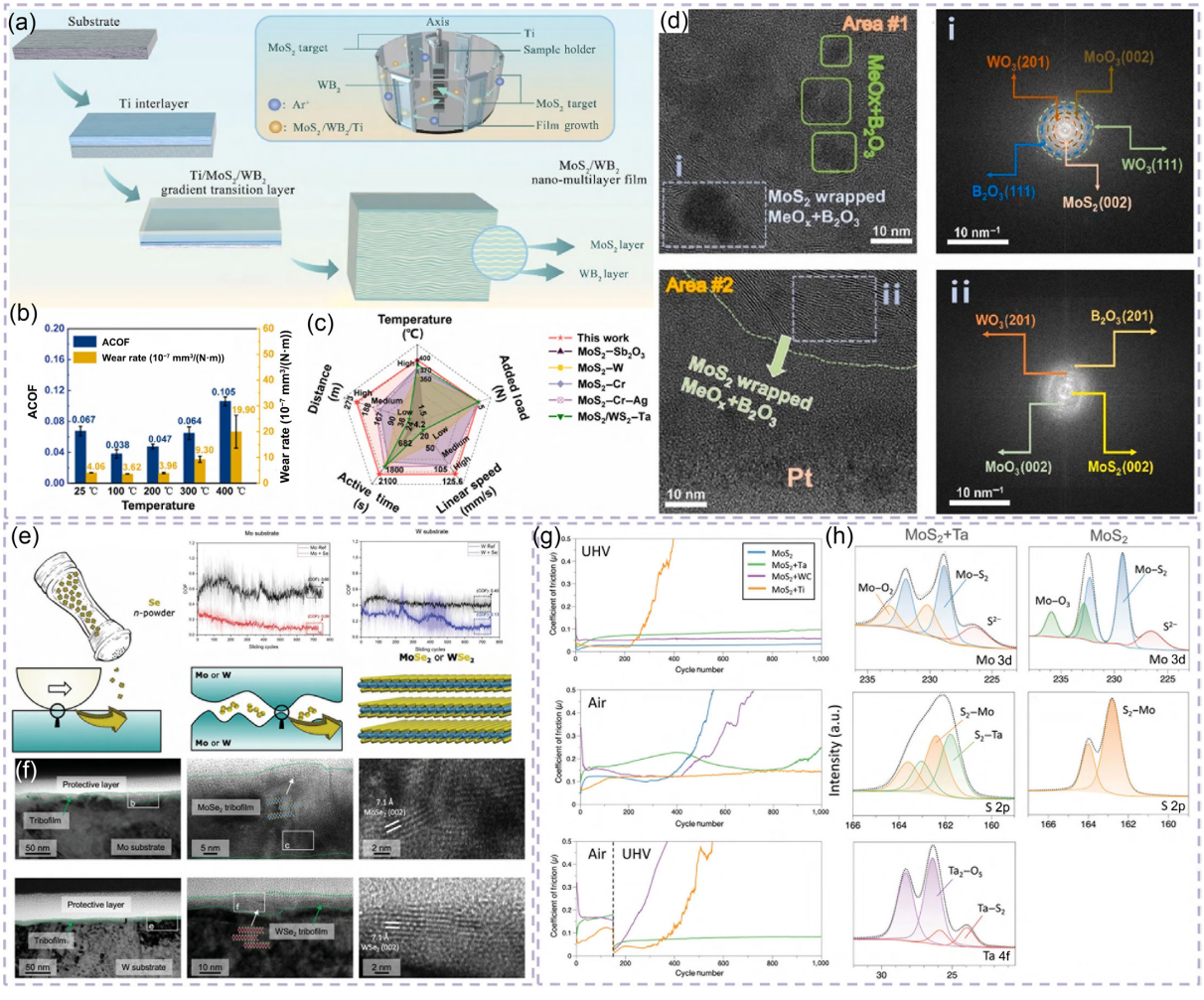


Fig. 14 (a) Scheme of MoS_2/WB_2 film formation; (b) ACOFs and wear rates across temperatures; (c) friction performance comparison of MoS_2/WB_2 with other MoS_2-based materials; and (d) high-resolution TEM (HRTEM) images and corresponding selected area electron diffraction (SAED) pattern of regions #1 and #2. (e) *In situ* friction-induced TMD lubricating layer (inset is Mo/W substrate friction curves); (f) TEM of tribofilms formed during sliding. (g) Tribological tests of pure and codeposited MoS_2 coatings under UHV, air, and UHV-to-air conditions; (h) XPS of MoS_2 and MoS_2+Ta coatings. Reproduced with permission from Ref. [117] for (a–d), © 2024 Elsevier Ltd. 2024; from Ref. [118] for (e, f), © The Authors 2023; from Ref. [121] for (g, h), © Wiley-VCH GmbH 2022.

清華大学出版社 Tsinghua University Press | SciOpen

an integral component of structural design strategies, enhances TMD tribological properties and environmental adaptability [119]. In terms of doping modulation, metal doping was initially employed to improve tribological performance. Metal dopants enhance the tribological performance of TMDs by preferentially oxidizing to form protective surface layers that mitigate oxidative damage and by promoting (0002)-oriented crystalline growth, which strengthens the material and improves wear resistance [120]. For instance, Serles et al. [121] developed Ta-doped MoS_2 coatings via codeposition, with comparison to three reference systems: pristine MoS_2, hard metal codeposition (MoS_2–Ti), and ceramic codeposition (MoS_2–WC) under ultrahigh vacuum (UHV), humid air, and transitional air-to-UHV conditions (Fig. 14(g)). The Ta-doped coatings demonstrated consistently superior lubricity across all environments. The authors attributed this performance to the sacrificial oxidation of Ta, which selectively forms Ta_2O_5, preventing the detrimental formation of MoO_3 (Fig. 14(h)). Furthermore, the TaS_2 phase exhibits inherent lubricity and environmental stability in both air and vacuum, providing persistent interfacial protection.

While metal doping offers notable benefits, it may also lead to the formation of abrasive oxides under certain conditions. As an optimized strategy, non-metal doping has gained attention for imparting oxidation resistance and enhancing film integrity. For example, Bin Yaqub et al. [122] reported that nitrogen-doped $MoSe_2$ (MoSeN) coatings exhibit improved compactness and hardness compared with pure $MoSe_2$. The authors assessed the tribological properties of MoSeN coatings under various environmental conditions and observed stable COFs ranging from 0.03 to 0.06 in most cases, except under dry nitrogen at 200 °C. Wear rates showed slight variation, with higher values recorded in dry nitrogen at 100 and 200 °C, while under other conditions, the rates remained within the range of $(1–7)\times10^{-7}$ mm^3/(N·m).

Alongside doping strategies, vacancy engineering has also emerged as a promising approach to modulating TMD tribological performance. Wang et al. [123] studied the tribological properties of substoichiometric WSe_{2-x} solid lubricating coatings deposited by magnetron sputtering in comparison with traditional MoS_2 coatings. The results showed that despite the lower selenium content (Se/W atomic ratio of 0.92) in the WSe_{2-x} coatings, their hardness and elastic modulus were higher than those of MoS_2, leading to a lower COF and reduced sensitivity to humidity.

5.3 Composite integration

5.3.1 Composite with nanomaterials

Among various modulation strategies, interface composite engineering has attracted increasing attention, as it enables multisynergistic lubrication mechanisms to overcome the intrinsic limitations of conventional TMD-based lubricants [112]. For example, the integration of 0D nanomaterials with 2D TMDs exemplifies this strategy, as it leverages complementary characteristics to reduce friction, minimize wear, and increase load-bearing capacity under boundary lubrication [124]. Shao et al. [125] integrated Bi_2O_3 nanoparticles into MoS_2, resulting in stable high-temperature lubrication, with a COF of 0.21–0.26 at 450–800 °C and a wear rate of 2.9×10^{-6} mm^3/(N·m) at 600 °C (Fig. 15(a)). The enhanced behavior resulted from stress–temperature coupling that induced tribochemical reactions and the formation of low-shear ternary oxides (Fig. 15(b)). Heterogeneous 2D interfaces arising from lattice mismatch have also been investigated as a route toward low friction [126]. Feng et al. [127] synthesized few-layer (FL) $Ti_3C_2T_x/MoS_2$ heterostructures and evaluated their performance as additives in mineral oil (150 N). Incorporating 0.3 wt% of the heterostructure reduced the COF by 39% and wear by 85% compared with the base oil. The hybrid outperformed individual components and their mixtures, owing to good dispersion, cooperative lubrication, and tribofilm formation.

Building upon binary composite systems, multicomponent nanocomposites offer greater tunability of structure and function, enabling more precise control over friction and wear. For instance, Bharti et al. [128] developed a ternary nanocomposite coating composed of multilayer graphene (MGr), MoS_2, and MWCNTs, achieving a marked reduction in the COF of 80%–85% across metals, ceramics, and semiconductors. The structural versatility of multicomponent systems enables further functional tuning. Yang et al. [116] designed a sandwich-like MoS_2/WC/Ag nanomultilayer film via magnetron sputtering (Fig. 15(c)). The structure exhibits a self-healing capability through Ag nanoparticle (Ag NP) migration along heterogeneous interfaces, enhancing corrosion resistance and retaining MoS_2 oxidation stability. After salt spray and atmospheric exposure, Ag NPs diffusion and aggregation within WC layers transform the multilayer into a composite structure, with an overall oxygen content below 2.5%, ensuring environmental durability (Fig. 15(d)). Furthermore, Ag NPs promote the formation of a dense tribofilm that encapsulates surface oxides and suppresses adhesive wear, leading to a consistently low COF and wear rate even after prolonged corrosion (Fig. 15(e)).

In addition to solid coating and additive systems, TMDs have also been incorporated as reinforcing phases in bulk self-lubricating composites to enhance mechanical robustness and tribological performance [129]. However, the weak interfacial interaction between fillers and matrices still limits the overall performance. To address this issue, Chen et al. [130] introduced hydroxyl-terminated hyperbranched polysiloxane (HBPSi–OH) as a "bridging agent" to strengthen the interfacial adhesion between MXene/WS_2 hybrids and epoxy (EP) resin (Fig. 15(f)). Benefiting from the reinforced interfacial bonding and the soft-hard synergistic effect, the resulting MXene/WS_2/HBPSi/EP (MWH/EP) composites exhibited superior overall properties. Compared with pure EP, the composite containing 0.6 wt% MXene/WS_2–1/4 wt% HBPSi showed 74.6% and 48.3% increases in impact and flexural strengths, respectively, while the average COF decreased to 0.30 and the wear rate was reduced by over 97% (Fig. 15(g)).

5.3.2 Composite lubricating systems

To overcome the limitations of traditional single-phase lubricants under severe conditions, multiphase composite systems have been developed to exploit synergistic effects, achieving tribological performance unattainable by any single phase [131–133]. Within this framework, solid-liquid hybrid systems have attracted particular attention, which combine structurally robust coatings as anti-wear and fatigue-resistant layers with high-performance liquid lubricants providing fluidic support and surface adaptability [134, 135]. For example, Hou et al. [131] fabricated a porous MoS_2 framework via hydrothermal synthesis, followed by infiltration with PAO-4, achieving stable liquid retention, delayed oxidation, and enhanced chemical resistance (Figs. 16(a) and 16(b)). The hybrid system reduced the COF to one-quarter that of bare MoS_2 and half that of pure PAO-4 while increasing the load-bearing capacity by over sixfold and extending the operating lifetime from 1,300 to over 16,000 cycles under 0.5 GPa contact pressure (Fig. 16(c)).

Furthermore, researchers have explored the integration of ionic

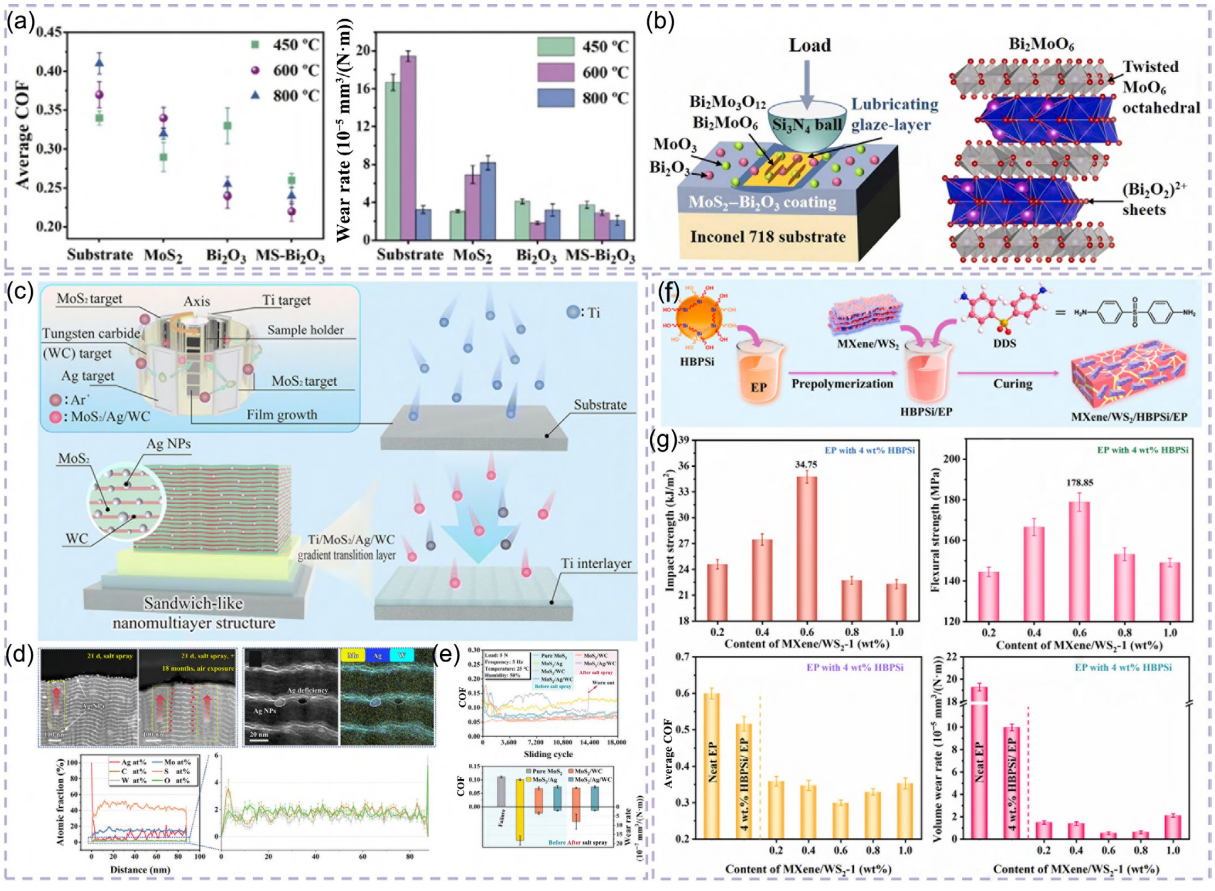


Fig. 15 (a) ACOF and wear rates of MoS_2–Bi_2O_3 lubricants at 450–800 °C; (b) high-temperature lubrication mechanism of lubricants. (c) Fabrication schematic of sandwich-like MoS_2/Ag/WC nanomultilayer film; (d) characterization of Ag diffusion path in MoS_2/Ag/WC nanomultilayer film; (e) tribological performance of MoS_2/Ag/WC multilayers before and after salt spray. (f) Preparation of MWH/EP composites; (g) mechanical strengths and tribological properties of 0.6 wt% MXene/WS_2–1/4 wt% HBPSi/EP composites. Reproduced with permission from Ref. [125] for (a, b), © Elsevier Ltd. 2025; from Ref. [116] for (c–e), © The Royal Society of Chemistry 2024; from Ref. [130] for (f, g), © Elsevier Ltd. 2025.

liquids (ILs) as the liquid component in solid–liquid lubrication systems. ILs, liquids at ambient temperature and composed of organic cations with tunable anions, offer high thermal stability, intrinsic polarity, and strong surface interactions, enabling protective boundary films, improved load-bearing capacity, and better dispersion of 2D nanomaterials [136, 137]. Leveraging these advantages, Quan et al. [138] evaluated the solid-liquid synergy in vacuum using a WS_2/MoS_2–Ag film coupled with ILs (IL1, IL2). The hybrid system surpassed the pure film, maintaining low wear rates below 7.9×10^{-8} mm^3/(N·m) and sustaining over 2.0×10^6 cycles. Notably, IL2 achieved a lower COF near 0.05 and smoother worn surfaces than IL1, attributed to its longer alkyl chains promoting stronger molecular interactions and enhanced adsorption onto the substrate.

Despite these advances, the inherent fluidity of liquid lubricants can cause leakage or creep under dynamic conditions. To address this, researchers have explored gels to achieve stable lubricant retention and continuous supply [139]. For instance, Yang et al. [140] developed a high-performance self-lubricating porous polyimide/oleogel composite (PPI-gel-TAM), in which porous polyimide was impregnated with tannic acid-functionalized MoS_2 (TA-MoS_2)-modified PAO-10 oleogel to achieve self-adaptive confined lubrication. This composite demonstrates macroscopic superlubricity, achieving an ultralow COF of 0.007 and a notably reduced wear rate of 2.81×10^{-8} mm^3/(N·m) (Fig. 16(d)). The exceptional tribological performance originates from a multilevel synergistic mechanism: continuous oil supply enabled by the porous structure, shear-thinning behavior of the lubricant, enhanced interfacial interactions provided by TA–MoS_2, and formation of a robust tribofilm (Fig. 16(e)).

Beyond phase hybridization, microstructural design offers a complementary route to enhance lubrication. Surface texturing enables controlled interactions between lubricants and substrate through engineered geometry [133]. Geometric parameters such as shape, size, and spacing play a crucial role in optimizing surface textures [141]. Sinha and Sharma [142] applied nanosecond lasers to fabricate circular (closed-pore) and S-shaped (open-pore) textures on Ti–3Al–2.5V substrates (Fig. 16(f)). Under lubrication with PAO-4 containing 1 wt% MoS_2, open-pore textures consistently achieved lower COFs and wear rates than closed-pore counterparts, which is attributed to achieving better lubricant retention (Fig. 16(g)).

Bioinspired texture designs have advanced composite lubrication systems by enabling multifunctionality within surface architecture [143]. Drawing inspiration from natural models such as pangolin scales and honeycombs, researchers have developed surface structures integrating lubricant reservoirs, fluid pathways, and mechanical buffering [144]. Nonetheless, precisely replicating complex biological templates remains challenging. Qin et al. [145] addressed this issue by applying curve fitting to extract shell surface profiles and embedding SnAgCu–WS_2 into wavy textures on TC4 alloy (Ti–6Al–4V). The synergy between bionic wave textures and SnAgCu–WS_2 coatings enhanced the tribological performance by promoting WS_2 nanosheet precipitation,

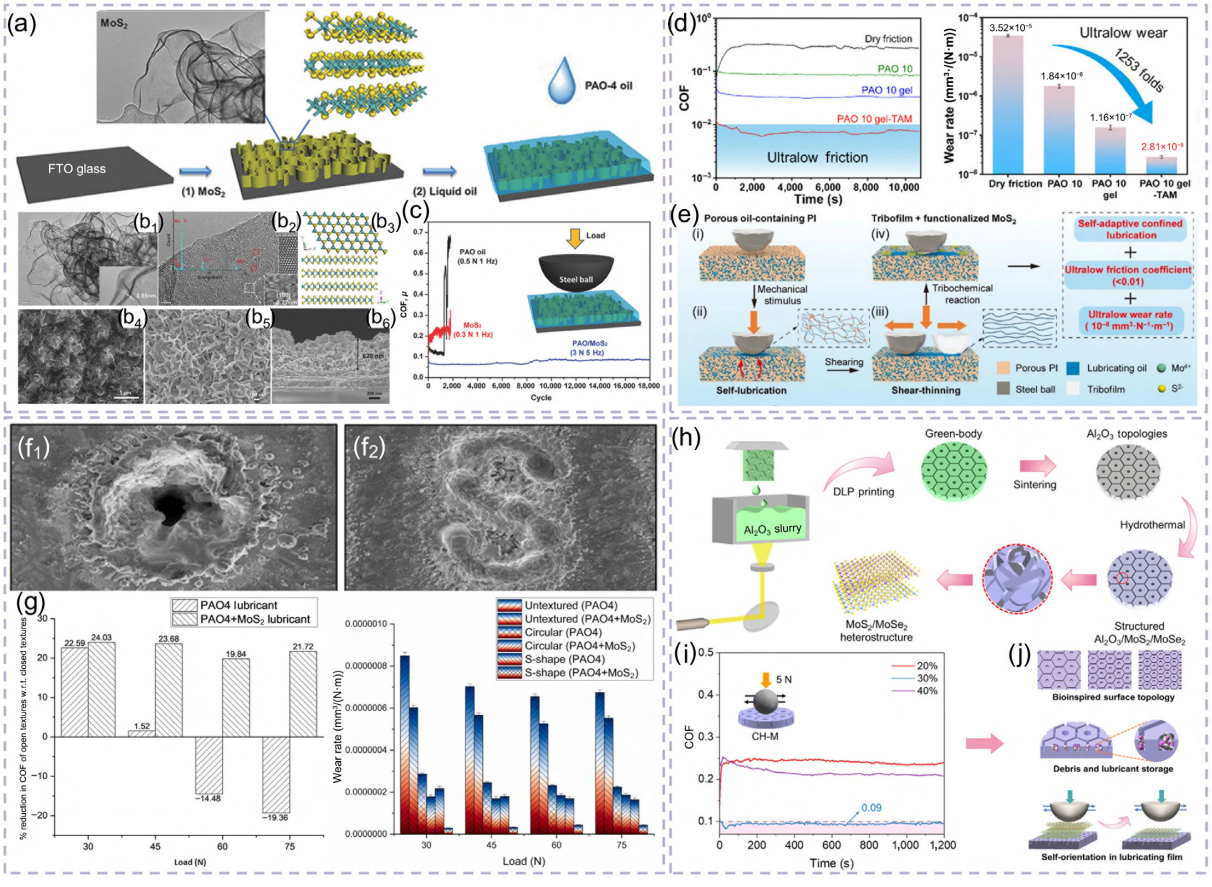


Fig. 16 (a) Preparation of PAO/MoS_2 coating; (b) TEM and field-emission SEM (FESEM) images of MoS_2 nanosheets and porous MoS_2 coatings; (c) comparison among solid, liquid, and complex lubrication. (d) COF and wear rate of PPI impregnated with different lubricants and without lubricants; (e) diagram of lubricating mechanisms for PPI-gel-TAM. (f) FESEM images of open and closed textured Ti–3Al–2.5V; (g) reduction in ACOF and wear rate of textures using PAO4 and PAO4/MoS_2. (h) Preparation route of bioinspired 3D-printed topological $Al_2O_3/MoS_2/MoSe_2$; (i) lubrication performance of CH–M composites with varying texture densities at 5 N; (j) schematic for ultralow friction mechanism of $Al_2O_3/MoS_2/MoSe_2$ under high load and dry sliding. Reproduced with permission from Ref. [131] for (a–c), © WILEY-VCH Verlag GmbH & Co. KGaA, Weinheim 2018; from Ref. [140] for (d, e), © Wiley-VCH GmbH 2025; from Ref. [142] for (f, g), © Elsevier Ltd. 2024; from Ref. [148] for (h–j), © American Chemical Society 2021.

alignment, and dynamic redistribution, achieving adaptive lubrication and *in situ* wear repair. In addition, additive manufacturing, presented by 3D printing technology, provides an effective strategy for fabricating complex surface architectures with high precision. Chen et al. [146] and Zhao et al. [147, 148] used 3D printing to design Al_2O_3 ceramic surfaces with bioinspired patterns, including petal-like, tree frog toe-like, and honeycomb units infused with lubricants. In the work by Zhao et al. [148], circular-core square and hexagonal honeycomb units fabricated with $MoS_2/MoSe_2$ heterostructures improved mechanical and tribological performance, achieving 16.23 GPa hardness, 227.62 MPa bending strength, and over 30% COF reduction (Fig. 16(h)). Among these, the hexagonal structure with 30% area density performed best under a 5 N load, with a COF of 0.09 and a wear rate of 2.5×10^{-5} mm³/(N·m) (Fig. 16(i)), which was attributed to minimized contact area, durable tribofilms, and a self-adjusting debris entrapment mechanism (Fig. 16(j)).

5.4 Superlubrication design

Superlubricity denotes a frictional regime with near-zero resistance between sliding interfaces, offering the potential to reduce energy loss and mechanical wear [149]. The exploration of this phenomenon has been historically linked to TMDs, beginning with early observations of ultralow friction in MoS_2 coatings, attributed to anisotropic sliding on sulfur-rich basal planes [150]. Subsequent research, including studies on fullerene-like MoS_2 nanoparticles and atomic-scale interlayer sliding measurements, has established TMDs as a principal material platform for structural superlubricity, achieving a COF as low as 10^{-4} [151, 152].

The current understanding identifies two prerequisites for structural superlubricity: the creation of asymmetric sliding interfaces and the reduction of contact area between tribo-pairs [153]. Constructing vdW heterojunctions has become a widely adopted strategy to achieve these requirements [154, 155]. Long et al. [156] demonstrated superlubricity in MoS_2/graphene heterostructures at elevated temperatures. Modeling using an edge multicontact approach revealed that localized thermal activation facilitates contact formation at fractured MoS_2 edges, enhancing interlayer sliding and reducing friction. In a more practical approach, Macknojia et al. [157] employed a spray-coating technique to deposit $Ti_3C_2T_x$–MoS_2 hybrid films on steel substrates, achieving an exceptionally low COF of 0.0034 under contact pressures exceeding 1.2 GPa, outperforming previously reported MoS_2 or MXene coatings (Figs. 17(a) and 17(b)). The superior tribological behavior arises from MoS_2 basal plane reorientation combined with MXene framework reinforcement, which collectively preserves crystallinity under severe sliding conditions (Fig. 17(c)).

In recent years, the pursuit of macroscale superlubricity has emerged as a critical objective [158]. However, this goal confronts persistent challenges from ambient environmental conditions, particularly humidity, a factor examined in detail in Section 4.2

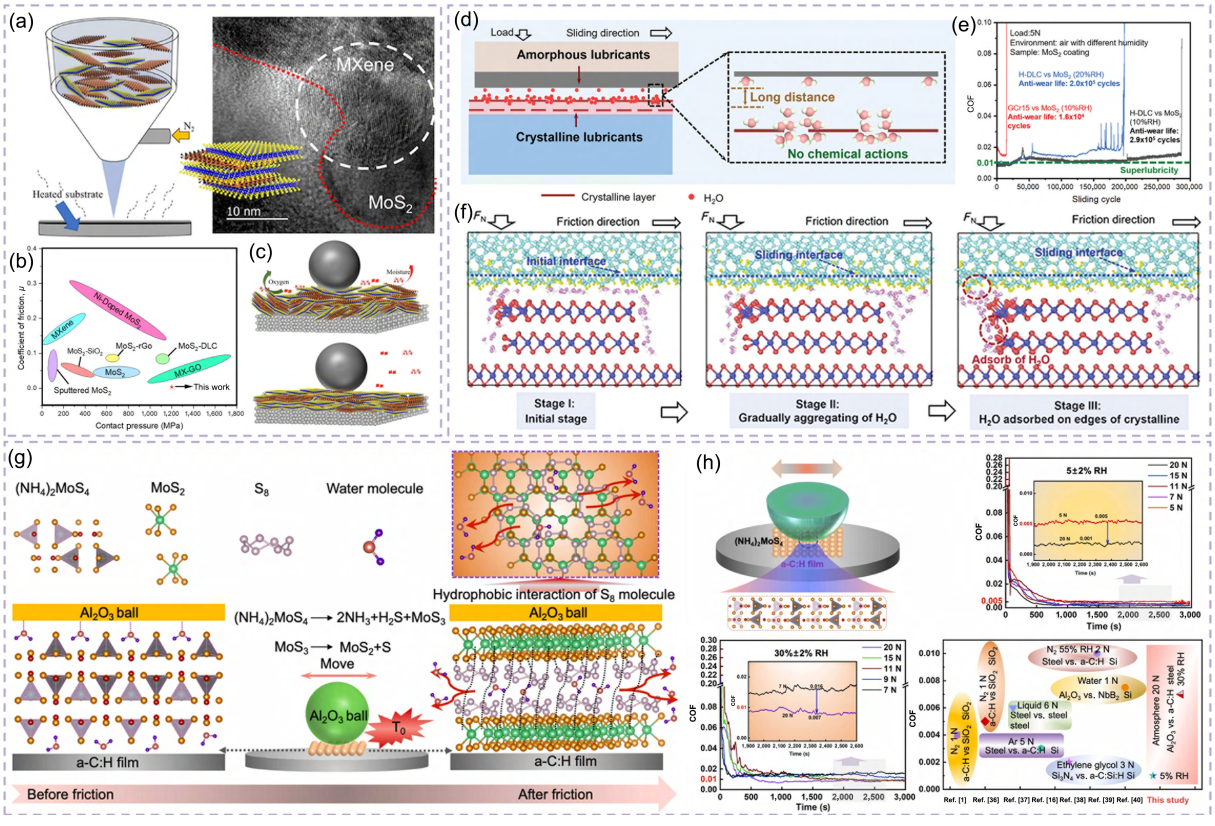


Fig. 17 (a) Fabrication and morphology of MXene/MoS_2 coating; (b) friction-pressure Ashby plot of pristine vs. doped MXene/MoS_2; (c) schematic of in operando densification and reorientation enabling superlubricity. (d) Design of macroscale superlubricity using DLC/TMD pair in humid air; (e) wear life of H-DLC/MoS_2 in air; (f) MD simulation of H-DLC/MoS_2 interfacial interactions. (g) Schematic for *in situ* formation of MoS_2/S_8/MoS_2 interlayers from $(NH_4)_2MoS_4$ on Al_2O_3 for superlubricity; (h) COF curves under varying humidity and load, compared with literature data. Reproduced with permission from Ref. [157] for (a–c), © American Chemical Society 2023; from Ref. [160] for (d–f), © Wiley-VCH GmbH 2024; from Ref. [161] for (g, h), © Elsevier Ltd. 2024.

[159]. To address this issue, researchers have developed various strategies to counteract interfacial destabilization induced by humidity-driven chemical reactions at defect sites. For example, Zhu et al. [160] designed tribo-pairs combining amorphous diamond-like carbon (DLC) with crystalline MoS_2 (Fig. 17(d)). The DLC–MoS_2 system exhibits weaker chemical bonding and lower sensitivity to wetting effects, maintaining stable superlubricity under 1.1 GPa contact pressure in air with RH below 25%, achieving a COF on the order of 10^{-3} and an anti-wear lifetime exceeding 2×10^5 cycles (Fig. 17(e)). Mechanistically, DLC–MoS_2 suppresses water accumulation at MoS_2 defect sites, preventing cross-linking within the friction layer (Fig. 17(f)). In an alternative strategy, Sun et al. [161] utilized friction-induced catalytic decomposition of $(NH_4)_2MoS_4$ (ATTM) to generate MoS_2 layers intercalated with S_8, forming a dual-function architecture that optimizes interlayer shear and acts as a hydrophobic barrier (Fig. 17(g)). This method achieved an ultralow COF below 0.01 under both dry and humid (30%±2% RH) conditions, reducing friction by over 75% compared with tribopairs lacking the formed MoS_2/S_8 interlayers (Fig. 17(h)). Despite the remarkable progress achieved under laboratory conditions, realizing macroscale superlubricity in practical environments remains constrained by environmental sensitivity, complex interfacial design, and long-term stability concerns.

5.5 Intelligent tuning

Intelligent tribology, as an emerging research direction, aims to integrate responsive, controllable, and self-adaptive components into material systems to achieve active regulation of interfacial frictional behavior [162]. Compared with traditional passive lubrication, this strategy allows real-time control of friction and wear, thereby enhancing the efficiency, reliability, and lifetime of the system [163]. TMDs offer a fertile platform for constructing intelligent lubrication systems, owing to their highly tunable electronic features and structural versatility [164]. For example, Shi et al. [165] exploited the semiconducting nature of MoS_2 to modulate friction via gate-voltage-induced changes in carrier concentration: A higher carrier concentration strengthens electron–phonon coupling and increases friction, whereas a lower concentration weakens coupling and reduces friction.

However, the intrinsic properties of TMDs alone are insufficient for precise, stimuli-responsive control under complex conditions, as their responsiveness to temperature, magnetic fields, or chemical environments is limited. To overcome these limitations, TMDs have been integrated with functional units capable of controllable structural transformations at the sliding interface, enabling lubrication to adapt dynamically to operating conditions [166]. For instance, Yang et al. [167] synthesized core–shell MoS_2@STAX (MoS_2@$C_{18}H_{37}N^+(CH_3)_3[XCl_3Br]^-$; X = Fe, Ce, Gd, Ho) through electrostatic self-assembly. In this system, layered MoS_2 nanosheets form the core, while magnetic surfactants constitute the shell, enabling magnetic responsiveness (Fig. 18(a)). Tests confirmed excellent surface adhesion and strong magnetic adsorption of the lubricant (Figs. 18(b) and 18(d)). Under a 0.792 T magnetic field and high shear, the MoS_2@STACe-based lubricant exhibited pronounced magnetorheological behavior (Fig. 18(c)). Furthermore, at 200 °C, the lubricant promoted the formation of a tribochemical film and a carbonaceous barrier layer at the contact interface, further enhancing the anti-friction and anti-wear performance (Fig. 18(e)).

清華大學出版社 Tsinghua University Press | SciOpen

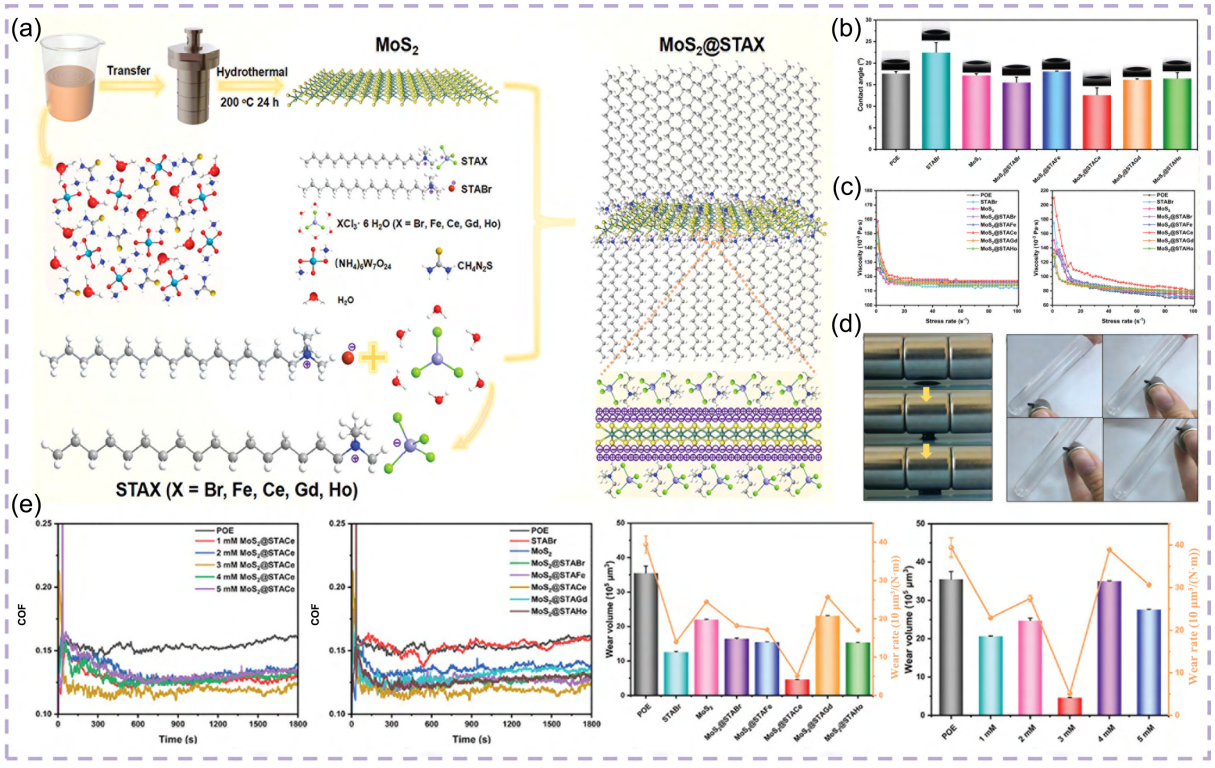


Fig. 18 (a) Synthesis of MoS_2@STAX via magnetic surfactant-assisted assembly; (b) contact angle of lubricants on steel; (c) frequency-dependent rheological and magnetorheological behavior; (d) magnetic response of lubricants under an external field; (e) COF, wear volume, and wear rate of steel lubricated with different formulations at 200 °C. Reproduced with permission from Ref. [167], © Wiley-VCH GmbH 2024.

Beyond magnetic responsiveness, TMD-based intelligent lubricants can respond to a variety of external stimuli, enabling active modulation of friction. For instance, temperature-driven phase transitions, such as the transformation from 1T to 2H, alter the interlayer structure and sliding behavior, thereby adjusting lubrication performance [81]. Similarly, light stimulation can control the physical state of the lubricant through photothermal or photoelectric effects, allowing adaptive regulation of interfacial friction [168]. These examples demonstrate that the inherently tunable structural characteristics of TMDs enable responses to multiple stimuli and precise control of friction [169]. Collectively, this multifunctionality highlights the potential of TMDs as a versatile platform for advanced intelligent lubrication systems capable of operating efficiently under dynamic and demanding conditions.

Despite these advances, intelligent lubrication remains in its infancy, facing limited mechanistic understanding, low functional integration, and poor adaptability to complex environments. A lack of real-time insight into trigger and feedback behaviors, along with challenges in scalable synthesis and long-term stability, continues to hinder practical implementation [163].

5.6 ML-assisted optimization

With the development of artificial intelligence (AI), ML has become an emerging approach to optimize the tribological performance of TMD-based lubricants through predictive modeling [170]. By identifying complex correlations among structural, compositional, and testing parameters, ML can predict friction and wear behaviors and thereby guide the optimization of material design and service conditions [171]. This predictive capability reduces the experimental workload and accelerates the development of high-performance lubricants. For instance, Wang et al. [172] integrated experimental measurements with ML algorithms to investigate and predict the tribological performance of WS_2 coatings under different loads, sliding speeds, and temperatures. The results showed that both the COF and wear rate increased with operating severity, with plastic deformation and adhesive wear dominating under heavy-load, high-speed, and high-temperature conditions. Among the models tested (Fig. 19), the extra trees (ET) model achieved the highest accuracy in COF prediction (0.899), while the gradient boosting regression tree (GBRT) model exhibited the best performance for wear rate prediction (0.948). Despite these advances, the application of ML in tribology remains immature. Challenges such as limited datasets and inconsistent experimental conditions still constrain model generalizability and reliability [173].

For modulating the tribological properties of TMDs, conventional approaches, while effective in enhancing lubrication, are limited by complex fabrication, high costs, and interfacial instability. Emerging strategies show promising results in laboratory settings, but their practical application remains constrained, facing persistent challenges in environmental adaptability, system integration, and data reliability. Current research has yet to establish reliable links between microscopic mechanisms and macroscopic performance, hindering progress in long-term durability, environmental stability, and scalable manufacturing. Achieving truly controllable friction remains a long-term challenge requiring sustained efforts.

6 Applications of TMD-based lubricants

The application scope of TMDs has expanded through novel architectures and innovative synthesis strategies. TMDs, initially applied in mechanical lubrication, currently show broad potential in diverse fields, such as material processing, mechanical components, biomedical systems, and micro-electromechanical

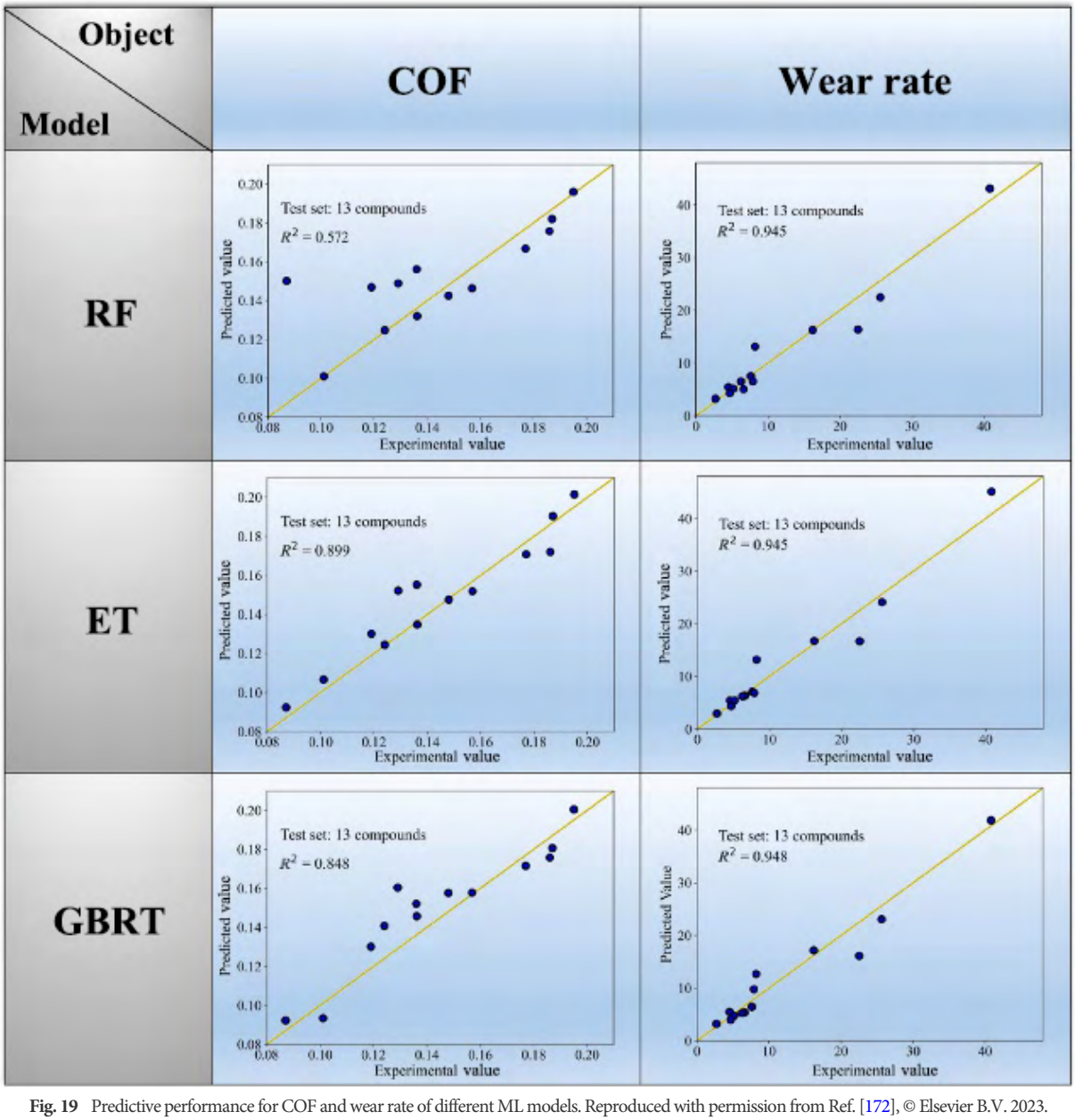


Fig. 19 Predictive performance for COF and wear rate of different ML models. Reproduced with permission from Ref. [172], © Elsevier B.V. 2023.

system (MEMS)/nanoelectromechanical system (NEMS) devices. This section outlines recent progress in these key areas, focusing on performance improvements and persistent challenges associated with stability and scalability.

6.1 Material processing

In processing operations, including rolling, turning, milling, and grinding, lubricants are indispensable for friction and wear reduction, temperature control, and surface quality improvement [174]. Conventional oil-based lubricants face challenges related to sustainability and operating safety, such as environmental risks and nozzle blockages [175]. Although water-based lubricants are environmentally benign, their intrinsic tribological performance remains limited. TMD nanoparticles, with high interfacial energy and low interlayer shear strength, enhance interfacial interactions and facilitate stable tribofilm formation on metal surfaces, resulting in pronounced reductions in friction and wear. Sethurajaperumal et al. [176] synthesized MoS_2 nanosheets using saponin-rich *Sapindus mukorossi* as a surfactant for exfoliation, achieving a stable aqueous dispersion. At a concentration of 0.1 wt%, the dispersion reduced the COF by 75% and WSD by 65% while also enhancing the surface quality during wire electrical discharge machining compared with conventional water–oil mixtures.

Despite these advances, the use of TMDs in high-temperature forming processes is still restricted due to their susceptibility to oxidation and inadequate hardness [177]. He et al. [178] addressed this challenge by designing a MoS_2–Al_2O_3 nanofluid that combined MoS_2 with ultrahard and thermally stable α-Al_2O_3 nanoparticles (Fig. 20(a)). Using a two-high roll mill, the nanofluid showed outstanding lubrication during hot rolling, lowering the rolling force by 26.9% and the oxide layer thickness by 54.2% compared with baseline lubricants (Figs. 20(b) and 20(c)). Due to the antioxidant effect of the nanofluid during lubrication, the proportion of Fe_2O_3 in the oxide scale was reduced, while MoS_2 underwent partial oxidation to MoO_3. The enhanced performance was attributed to a multicomponent tribofilm composed of MoS_2, Al_2O_3, and MoO_3, which collectively

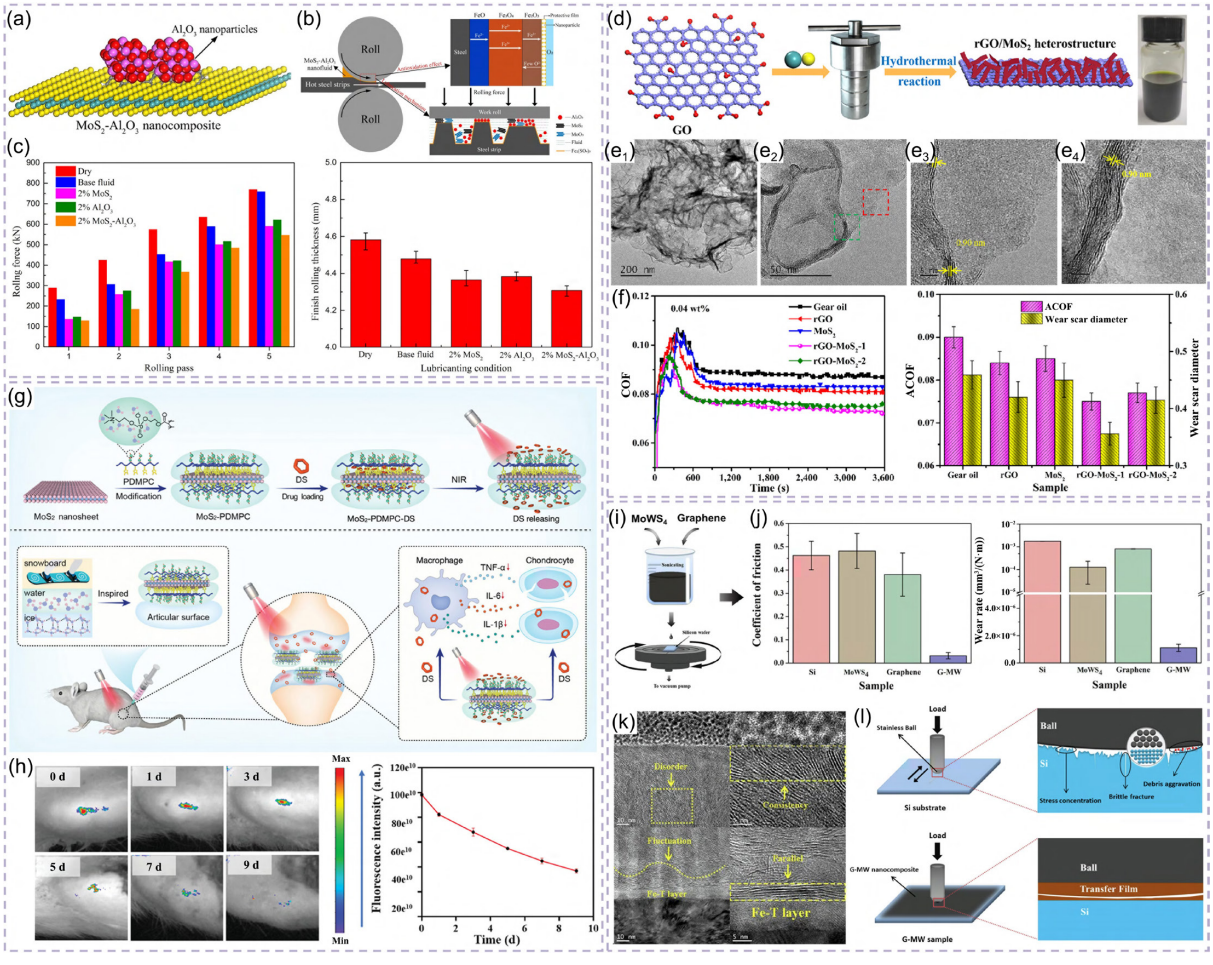


Fig. 20 (a) Schematic of MoS_2–Al_2O_3 nanocomposites; (b) two-high rolling mill lubrication by MoS_2–Al_2O_3 nanofluids; (c) rolling force and final strip thickness under varied lubrication. (d) Formation mechanism of rGO/MoS_2 nanocomposites; (e) TEM images of rGO–MoS_2 at varying magnifications; (f) COF and WSD of gear oil with additives. (g) Synthesis of MoS_2–PDMPC-DS and its near-infrared (NIR)-triggered drug release/lubrication; (h) fluorescence imaging/intensity in rat joint cavity post MoS_2–PDMPC injection. (i) Spin-coating process for G–MW samples on silicon substrates; (j) average COF and wear rate of samples; (k) HRTEM images of transfer film cross-section; (l) friction/wear mechanisms. Reproduced with permission from Ref. [178] for (a–c), © The Society of Manufacturing Engineers 2020; from Ref. [182] for (d–f), © Elsevier Ltd. 2022; from Ref. [187] for (g, h), © Wiley-VCH GmbH 2022; from Ref. [192] for (i–l), © Elsevier B.V. 2021.

improved the load-bearing capacity and thermal stability under extreme conditions.

6.2 Mechanical elements

Friction-induced wear limits the lifespan of mechanical systems, especially bearings, highlighting the need for advanced lubrication [66, 179]. For example, under water-lubricated conditions, the low viscosity of the lubricant often leads to inadequate tribofilm formation, particularly during demanding operating conditions such as start-stop cycles, low-speed motion, and high loads, thereby accelerating wear. To address these limitations, TMDs can be integrated as lubricant fillers due to their demonstrated efficacy in boundary and mixed lubrication regimes. In a representative study, Li et al. [180] developed ultrahigh molecular weight polyethylene (UHMWPE) composites incorporating GO, silica (SiO_2), and MoS_2 as reinforcing fillers. These composites showed remarkably improved performance in water-lubricated bearing tests, achieving an 84.4% reduction in wear rate and an ACOF of 0.031 compared with unreinforced UHMWPE.

Gear systems face harsher tribological challenges than bearings, requiring lubricants with high wear resistance, load-bearing capacity, and thermal stability, for which layered TMDs have shown promising potential as nanolubricants [181]. Fan et al. [182] demonstrated that rGO/MoS_2 heterojunctions with vertically aligned MoS_2 nanosheets on rGO scaffolds resulted in a 16.7% reduction in friction and an 80% decrease in wear in gear oils (Figs. 20(d)–20(f)). These enhancements arise from stable additive dispersion, formation of protective tribofilms, and reduced shear strength caused by lattice mismatch, collectively contributing to friction mitigation and improved wear resistance.

6.3 Biomedicine

Effective biological lubrication is essential for preserving the integrity of tissue-organ interfaces [183]. Insufficient lubrication leads to elevated shear stress and inflammatory responses, factors known to contribute to degenerative joint diseases such as osteoarthritis (OA) [184]. Owing to their intrinsic lubricity and anti-inflammatory characteristics, TMDs have shown promise as biolubricants [185]. However, in physiological environments, their layered structures are prone to oxidation, generating soluble MoS_4^{2-} species that undergo rapid metabolism and cause functional loss [186]. Thus, enhancing the physiological stability of TMD nanostructures is essential for sustained *in vivo* efficacy. Qiu et al. [187] engineered a multifunctional MoS_2-based composite comprising MoS_2 nanosheets, along with the biomimetic phospholipid copolymer poly(dopamine methacrylamide-co-2-

methacryloyloxyethyl phosphorylcholine) (PDMPC) and the anti-inflammatory drug diclofenac sodium (DS) (Fig. 20(g)). Within this hybrid system, MoS_2 functioned as both a lubricant and a drug carrier, while PDMPC improved oxidative stability, prolonged retention in the joint cavity, and maintained aqueous lubrication. The composite sustained its lubricating and therapeutic functions for more than one week in both *in vitro* and *in vivo* settings, concurrently mitigating wear and inflammation (Fig. 20(h)).

In advanced OA with joint necrosis, artificial joint replacement becomes necessary, emphasizing the need for implants with superior tribological performance. Although commonly used biomedical implant materials such as titanium alloys and polyethylene exhibit excellent biocompatibility, their insufficient friction and wear resistance under dry contact remains a critical limitation. To overcome these limitations, TMDs have been incorporated into polymer matrices or applied as surface coatings to enhance lubrication and durability [188, 189]. For example, Lv et al. [190] embedded MoS_2 nanosheets into polyetheretherketone (PEEK), producing composites with improved mechanical, tribological, and biocompatible properties for artificial joint applications. Similarly, Chen et al. [191] coated TC4 alloy with a MoS_2-based multilayer film, which effectively reduced friction. Moreover, the photothermal response of MoS_2 under near-infrared light allows dynamic regulation of the interfacial temperature and hydration, enabling reversible regulation of friction.

6.4 MEMS/NEMS

As electromechanical systems scale down to the micro- and nanoscale, their rapidly increasing surface-to-volume ratio renders surface interactions a dominant factor in device performance and longevity. For instance, in silicon-based MEMS/NEMS, reduced dimensions intensify adhesion, electrostatic forces, and vdW interactions at interfaces, leading to pronounced friction and accelerated wear that can ultimately cause system failure [192]. This challenge has underscored the urgent need for advanced nanolubrication strategies tailored to the stringent demands of MEMS/NEMS devices. Among various candidates, TMD-based lubricants have attracted increasing attention due to their outstanding interfacial lubricity and potential to enhance the reliability of miniaturized systems [193]. To demonstrate their practical applicability, Ren et al. [192] developed graphene/$MoWS_4$ heterostructure nanocomposites (G–MW) via a simple spin-coating method for lubricating silicon-based MEMS devices (Fig. 20(i)). Experiments revealed that the G–MW coatings achieved ultralow friction (~0.02) on silicon substrates in an argon (Ar) atmosphere, outperforming graphene (~0.3) and $MoWS_4$ (~0.7) while reducing the specific wear rate by three orders of magnitude (Fig. 20(j)). Surface analysis further indicated that the G–MW formed a stable, heterogeneous transfer film at the steel-composite interface during sliding. This film was key to the performance, as it prevented direct metal-material contact, thereby drastically reducing both friction and wear (Figs. 20(k) and 20(l)).

Even with their promising prospects, TMD-based lubricants face critical challenges that limit practical applications, including high production costs, limited durability in humid or physiological environments, and the lack of standardized manufacturing processes. These factors collectively constrain their commercialization, highlighting the gap between laboratory research and real-world deployment and underscoring key directions for future efforts.

7 Conclusions and prospects

In this review, we summarize recent progress in TMD-based lubricants, covering their applications as lubricant additives, solid coatings, and composite fillers (Tables 3–6). Through an in-depth analysis of the intrinsic properties and synthesis strategies of TMDs, this review elucidates their lubrication mechanisms, identifies key factors influencing tribological behavior, and evaluates the modulation strategies and application potential of TMDs as nanolubricants. Comparative analysis of representative systems reveals that rational structural regulation markedly enhances friction reduction and wear resistance, which highlights the central importance of structure-performance design in TMD-based tribological optimization (Fig. 21). Nevertheless, these modulation strategies still face several challenges in practical applications, including insufficient mechanistic understanding, immature scalable fabrication technologies, and incomplete functional integration. Future research should deepen the understanding of lubrication mechanisms, advance controllable material synthesis, and achieve coordinated optimization across multiple scales (Fig. 22). These efforts will establish a systematic roadmap toward engineering applications and support the sustainable development of TMD-based lubricants.

Scalable and green synthesis. Large-scale production of high-quality TMDs remains a key challenge limiting their industrial application. Current synthesis methods are constrained by high cost, high energy consumption, and batch-to-batch variability. These limitations hinder precise control over structural uniformity and reproducibility, which are critical for stable tribological performance. Future research should focus on developing continuous, low-energy, and industrially viable routes, such as mechanochemical or FJH methods, to achieve structurally uniform and reproducible TMDs. Additionally, green synthesis strategies using natural mineral precursors (e.g., molybdenite) offer a promising path to reduce production costs and improve sustainability, thereby facilitating scalable manufacturing of TMD-based lubricants.

Green solvent design. Eco-friendly solvents, including ILs, vegetable oils, and polyols, show favorable potential in green tribology. However, the stable dispersion of TMDs in liquid media remains a practical bottleneck. This issue primarily originates from the weak interfacial compatibility and aggregation tendencies of TMD nanosheets. Future efforts should systematically tune interfacial interactions between TMDs and base liquids through molecular design and surface modification, aiming to develop stable, recyclable, and high-performance green lubrication systems.

(ii) Mechanism exploration

***In situ* friction characterization.** Real-time observation of TMD dynamics during friction is highly challenging. Key processes, including tribofilm formation, lubrication failure, and material transfer, are not yet fully understood. The lack of direct experimental evidence limits a comprehensive understanding of structure–function relationships under realistic operating conditions. Future studies should develop integrated testing platforms combining tribological measurements with *in situ* spectroscopic and microscopic techniques, enabling real-time monitoring of interfacial chemical and structural evolution to provide direct evidence for lubrication mechanisms.

Multiscale quantitative modeling. Experiments alone cannot fully reveal the microscopic nature of TMD lubrication. Future research should establish a multiscale computational framework spanning DFT, MD, and finite element analyses integrated with ML-driven approaches to analyze large datasets and construct

Table 3 Summary of TMDs as lubricant additives

Material	Synthesis method	Base	Content (dispersion)	Operating condition[a]	Tribological property		lubrication mechanism	Ref.
					COF	Wear		
MoS_2 QDs	Hydrothermal exfoliation	PEG 200	0.08 wt% (8 months)	Four-ball tribometer (GCr15, 1,200 r/min, 392 N, 60 min, RT)	0.094	9×10^4 μm^3	Ball-bearing	[17]
BN/MoS_2	—	Li-based grease	1.33 wt%	Ball-on-disk (Si_3N_4, 60NiTi, 0.033 m/s, 10 N, 90 °C, 33 min, RT)	0.054	200 μm	Interlayer sliding; surface hardening	[79]
Cu-modified 1T/2H-MoS_2	Hydrothermal	PAO	0.5 wt% (21 d)	Ball-on-disk (GCr15, GCr15, 50 Hz, 7.84 N, 60 min, 1,200 μm, RT, 60% RH)	0.0603	33.3 μm^3/(N·m)	Interlayer sliding; tribofilm formation	[86]
WS_2	Solid-phase reaction	Paraffin oil	0.5 wt%	Ball-on-disk (GCr15, 45# steel, 100–400 r/min, 10–60 N, 30 min, RT)	0.08	—	Tribofilm formation	[87]
$MoSe_2$ T-NPs	Ultrasound refinement	White oil	0.075 wt% (4 h)	Ball-on-disk (GCr15, GCr15, 1–2.5 Hz, 5–30 N, 15 min, 6 mm, RT, 30% RH)	0.07	2.5×10^{-8} mm^3/(N·m)	Lamellar slip; tribo-film formation	[89]
MoS_2–NOM	Michael addition reaction	PAO-10	1 wt% (30 d)	Ball-on-disk (AISI 52100, AISI 52100, 25 Hz, 100 N, 30 min, 1 mm, 150 °C)	0.088	5×10^{-5} mm^3	Tribo-film formation	[106]
WS_2–O–OCS/OES	Oxidation; exfoliation; group grafting	SN-150	200 ppm (5 d)	Four-ball (AISI 52100, 1,200 r/min, 392 N, 60 min, 75°C)	0.058	1.5×10^{-3} mm^3	Tribo-induced WS_2-based thin film formation	[109]
MoS_2–PSPMA	Ultraviolet (UV) polymerization	Water	1 wt%	Ball-on-disk (316 L, stainless steel/pitted copper/coating, 2 Hz, 5 N, 15 min, RT)	0.075	—	Surface grafting-induced formation of tribofilms	[110]
MoS_2–dex NPs/GO	Ball milling	Glycerol/water	0.5/0.5 wt% MoS_2/GO (30 d)	Ball-on-disk (AISI 52100, AISI 52100, 25 Hz, 200 N, 30 min, 1 mm, 70 °C)	0.085	8×10^{-4} mm^3	Boundary protective film consisting of adsorbed film and tribofilm	[103]
Micro-WS_2/nano-MoS_2	Ultrasonic-assisted oxidation	Diisooctyl sebacate (DOS)	0.75 wt%	Ball-on-disk (GCr15, GC15, 50 Hz, 7.84 N, 60 min, 1.2 mm, 60 °C)	0.0822	89.0 μm^3/(N·m)	Layered structure; tribofilm formation	[115]
FL $Ti_3C_2T_x$/MoS_2	Hydrothermal	150 N	0.3 wt%	Ball-on-plate (GCr15, GCr15, 5 Hz, 20–140 N, 60 min, 1 mm)	0.0814	2.8×10^4 μm^3	Synergistic lubrication; formation of tribo-film	[127]
PPI-gel-TAM	Organic reaction; impregnation	PAO-10 gel	8 wt%	Ball-on-plate (steel, PPI, 1–5 Hz, 0–20 N, 11,000 s)	0.007	2.81×10^{-8} mm^3/(N·m)	Shear-thinning of lubricants; tribofilm formation	[140]
MoS_2 + texture	—	PAO-4	1 wt%	Ball-on-disk (ZrO_2, TC4, 10 Hz, 30–75 N, 2 mm)	0.03	4.2×10^{-8} mm^3/(N·m)	Synergistic lubrication	[142]
MoS_2@STACe	Hydrothermal; surface grafting	polyol esters (POE)	3 mM (STACe)	Ball-on-disc (AISI 52100, AISI 52100, 25 Hz, 50–200 N, 30 min, 1 mm, 150–200 °C)	0.089	40 μm^3/(N·m)	Interlayer sliding; tribofilm formation	[167]
MoS_2	SM-assisted exfoliation	Water-Sapindus mukorossi (SM)	0.1 wt%	Four-ball (SAE 52100, 400/800/1,200 r/min, 98.1–588.6 N, 60 min, RT)	0.15	300 μm	Ball bearing; tribo-film formation; self-healing	[176]
rGO/MoS_2	One-pot hydrothermal	Gear oil	0.04 wt% (15 d)	Four-ball (GCr15, 1,200 r/min, 392 N, 60 min, 75 °C)	0.075	0.356 mm	Stable dispersion; formation of tribofilms; interlayer sliding	[182]

[a] The parameters for the tribometer, such as ball, disc, frequency, linear velocity, applied load, time, stroke, temperature, humidity, and atmosphere, are obtained from the literature; however, not all of these parameters are included in every case.

quantitative models linking structure, interface, and performance. This framework will facilitate the inverse design and performance prediction of TMD lubrication systems, advancing the transition from empirical to data-driven design strategies.

(iii) Performance enhancement

Lubrication optimization. The continuous reduction of friction and wear remains a central goal in tribology. Currently, stable macroscopic superlubricity is regarded as the ideal limit for minimizing friction. While TMDs exhibit pronounced superlubricity at the nano- to microscale, achieving stable and rapid superlubricity at the macroscale remains a major challenge. Overcoming this bottleneck requires innovations in material synthesis and composite lubrication system design. In parallel, a systematic understanding of TMD failure mechanisms across diverse operating conditions is required to inform the design of material structures and interfacial properties. From the perspective of wear reduction, the key lies in shortening the running-in period. Techniques such as surface texturing or hardening can be employed to construct composite lubrication systems, thereby offering novel strategies for achieving efficient and durable lubrication.

Multifunctional integration. Expanding the application scope of TMDs requires functionalities beyond traditional lubrication. For example, the increasing demands of electric vehicles necessitate materials that can provide both lubrication and efficient heat dissipation. Future developments could focus on oil-

Table 4 Summary of TMDs as solid coatings

Coating	Synthesis method	Operating condition	Tribological property		Lubrication mechanism	Ref.
			COF	Wear		
$MoSe_2$	FWF; coating	Ball-on-disk (AISI 52100, Al_2O_3, 3 Hz, 1–10 N, 10 min, RT, 50% RH)	0.16	—	Interlayer sliding	[39]
TaS_2, MoS_2, ReS_2	Exfoliation	AFM (Si tips, RT, 56% RH)	10^{-4}	—	Interlayer sliding	[64]
WS_2	Tribo-chemical reaction	Ball-on-disk (Si_3N_4, AISI5200, 0.1 m/s, 0.5 GPa, 6,000 min, 90 °C, 40% RH)	0.05	No wear	*In situ* tribofilm formation	[69]
WS_2/a-C	Magnetron sputtering	Ball-on-disk (100Cr6, Si wafer, 0.1 m/s, 0.5 GPa, 5 N, 10,000 laps, RT, 5% RH)	0.02	2 μm	Tribofilm formation; self-repairing	[74, 75]
WS_2	HiPIMS	Ball-on-disk (GCr15, Si wafer/stainless steel, 1–20 Hz, 5–20 N, 60 min, 5 mm, RT, 60% RH)	0.07	7.86×10^{-7} $mm^3/(N\cdot m)$	Surface polishing	[78]
Monolayer $MoS_2/MoSe_2/MoTe_2$	CVD	AFM (7–20 nm UNCD, < 5×10^{-10} Torr)	0.11 nN	—	Interlayer sliding	[80]
1T'/2H-$MoS_2/MoTe_2$	Exfoliation	AFM (Si tips, 10 nN, RT, air)	0.12 (0.18)	—	Interlayer sliding	[81]
1T/2H-MoS_2	Drop-casting	Ball-on-disk (440C ball, 300 r/min, 4 mm, 3 N, 9,000 laps, RT, 40% RH)	0.1	7,045 cycles	Phase transformation; interlayer sliding	[82]
Mono/few-layer $NbSe_2$	CVD	AFM (25 nm Si probe, RT, 30%–60% RH)	0.0085	—	Interlayer sliding	[84]
Ta_2S_2C/Nb_2S_2C	Scraper-deposition	Ball-on-disk (Al_2O_3/SiC/100Cr6/PTFE, AISI 304 steel, 1 mm/s, 0.25 N, 1 mm, RT, 23%–46% RH)	0.15	0.5 μm	Tribofilm formation	[98]
MoS_2/WB_2	Magnetron sputtering	Ball-on-disk (GCr15, 316 L steel, 5 Hz, 5/12.56 cm/s, 5 N, 60 min, 1.2/8 mm, RT–400 °C, 45% RH)	0.047	1.88×10^{-7} $mm^3/(N\cdot m)$	Synergistic effect	[117]
$MoSe_2$, WSe_2	Tribo-chemical reaction	Ball-on-disk (Al_2O_3, AISI 52100, 5 Hz, 1,000 mm/min, 1 N, 7,000 cycles, 2 mm, RT, 45% RH)	0.09	—	*In situ* tribofilm formation	[118]
MoS_2 + Ta	Magnetron sputtering	Ball-on-disk (10 mm/s, 1 GPa, RT, 2×10^{-6}/1×10^{-5}Pa)	0.22	—	*In situ* lubricative TaS_2 phase formation	[121]
MoSeN	Magnetron sputtering	Ball-on-disk (100Cr6, AISI 52100 steel, 25 Hz, 0.1 m/s, 10 N, 20 min, 2 mm, RT, 25%–35% RH/dry N_2)	0.025	1×10^{-7} $mm^3/(N\cdot m)$	Nitrogen doping induces amorphous transformation	[122]
WSe_{2-x}	Magnetron sputtering	Ball-on-disk (AISI440C ball, WNr. 1.2379 steel disk, 1 Hz, 1–10 N, 1,000 s, 3 mm, RT, 40% RH)	0.054	1×10^{-6} $mm^3/(N\cdot m)$	Frictional heating of the surface	[123]
MoS_2/Bi_2O_3	Hydrothermal; spraying	Ball-on-plate (Si_3N_4 ball, Inconel 718 plate, 3 Hz, 10 N, 5 min, 5 mm, 450–800 °C)	0.21	2.9×10^{-6} $mm^3/(N\cdot m)$	Interlayer sliding; tribofilm formation	[125]
MGr/MoS_2/MWCNT	Spin coating	Ball-on-disc (Cr steel, metallic/ceramic/semiconducting, 100 r/min, 0.1 N, 60 min, RT, 40% RH)	0.13	—	Low shear tribofilm formation; synergistical lubrication	[128]
MoS_2/Ag/WC	Magnetron sputtering	Ball-on-disk (GCr15, 5 Hz, 5 N, 18,000 cycles, 5 mm, RT, 50% RH)	0.074	2×10^{-7} $mm^3/(N\cdot m)$	Nanomultilayer structure; Ag-inducing self-repairing	[116]
Porous MoS_2 + PAO-4	Hydrothermal	Ball-on-plate (steel, FTO glass, 1/5 Hz, 1–9 cm/s, 0.5–3 N, 18,000 cycles, 5 mm, RT, 50%–55% RH)	0.079	0.8 $\mu m^3/(N\cdot mm)$	Solid–liquid coordinated mechanism	[131]
WS_2/MoS_2–Ag/IL	Sputtering	Ball-on-disk (AISI 440C steel, AISI 440C/Si, 1,000 r/min, 3 N, 18,000 cycles, R5 mm, RT, 3.0×10^{-3} Pa)	0.05	7.9×10^{-8} $mm^3/(N\cdot m)$	Synergistic lubrication effect	[138]
$MoS_2/MoSe_2/Al_2O_3$	DLP printing; hydrothermal	Ball-on-disk (Al_2O_3, $MoS_2/MoSe_2/Al_2O_3$, 5 Hz, 2/5/10 N, 20 min, RT)	0.09	2.5×10^{-5} $mm^3/(N\cdot m)$	Coupling lubrication effect	[148]
MoS_2/graphene	Exfoliation; dry transfer	AFM (Si/SiO_x, dry N_2)	5.24×10^{-4} nN	—	Interlayer sliding	[156]
$Ti_3C_2T_x/MoS_2$	Spray coating	Ball-on-disk (AISI 52100, AISI 52100, 0.2 m/s, 1–20 N, 10 min, 120 m)	0.0034	—	Synergistic lubrication mechanism	[157]
DLC-MoS_2	Spraying; magnetron sputtering	Ball-on-disk (GCr15, Stainless steel, 6.36 Hz, 10 cm/s, 0.5/2/4/16 N, 10,000 cycles, 5 mm)	0.0010	—	Protective effect of amorphous DLC; interlayer sliding	[160]
a-C:H-ATTM	Magnetron sputtering; drop coating	Ball-on-disk (Al_2O_3, AISI 52100, 5 Hz, 5–20 N, 50 min, 5 mm, RT, 5%–70% RH)	0.007	—	Tribochemical reactions induce the formation of lubricating films	[161]
MoS_2	Mechanical exfoliation	AFM (Si tips, Si/SiO_2 wafer, 1.25μm/s, RT, 30% RH)	1.2 nN	—	Regulating the friction force through gate voltage	[165]
WS_2	Spray deposition	Ball-on-disk (Al_2O_3, phosphor bronze copper, 71/96/120/144 r/min, 6/9/12/15 N, 60 min, 250/300/350/400 K, RT, 25%–30% RH)	0.08	3.2×10^{-6} $mm^3/(N\cdot m)$	Interlayer sliding	[172]
MoS_2–PDMPC	Hydrothermal; surface grafting	AFM (PS microsphere, Si substrate, 2 Hz, 100–400 nN)	0.03	—	Interlayer shear; hydration layer protection	[187]

(Continued)

Coating	Synthesis method	Operating condition	Tribological property		Lubrication mechanism	Ref.
			COF	Wear		
PDA–MCN	PDA-assisted bonding	Ball-on-disk (PDMS, TC4, 1–3 Hz, 1/5/10 N, 5 mm, underwater)	0.15	—	Interface hydration effect	[191]
graphene/$MoWS_4$	Spin-coating	Ball-on-disk (GCr15, Si wafer, 7 Hz, 3.5 cm/s, 5 N, 600 cycles, 5 mm, RT, < 5% RH)	0.02	1.1×10^{-6} mm³/(N·m)	*In situ* formation of transfer film	[192]

Table 5 Summary of TMDs as composite fillers

Material	Synthesis method	Matrix	Content	Operating condition	Tribological property		lubrication mechanism	Ref.
					COF	Wear		
MoS_2/MWCNTs	Hydrothermal	PEEK	2 wt%	Ball-on-disk (GCr15 steel ball, 6 Hz, 8 mm, 80 N, 30 min, RT)	0.225	6.06×10^{-6} mm³/(N·m)	Tribofilm formation; ball-bearing; self-repairing	[52]
MXene/WS_2–HBPSi	Hydrothermal	EP	0.6 wt%/4 wt%	Pin-on-disk (200 r/min, 196 N, 120 min)	0.3	5.3×10^{-6} mm³/(N·m)	Synergistic interactions	[130]
SnAgCu–WS_2 + texture	Vacuum infiltration	SnAgCu	0.2 wt%	Ball-on-disk (AISI 52100, 1–4 Hz, 20 N, 30 min, 8 mm, RT, 50% RH)	0.169	8.4×10^{-3} mm³	Coupling effect of texture and solid lubricant	[145]
GO/SiO_2/MoS_2	Compression molding	UHMWPE	1 wt%	Ball-on-disk (Si_3N_4, 0.1 m/s, 15 N, 30 min, R5 mm, RT, water)	0.03	0.25×10^{-5} mm³/(N·m)	Coupling lubricative effect	[180]
MoS_2	Physical mixing; pressing; sintering	PEEK	4 wt%/8 wt%	Ring to ring (chrome steel, 200 r/min, 15 N, 120 min)	0.139	2.7 mm	—	[190]

Table 6 Overview of TMD-based lubricants: forms, mechanisms, and applications

Form	Lubrication mechanism	Key advantage	Key limitation	Typical application scenario
Lubricant additives	Interlayer sliding; tribofilm formation; ball-bearing effect; synergistic lubrication.	Design versatility and multifunctionality; easy integration into existing systems; improvement of the performance for base fluids; effective under boundary lubrication.	Dispersion stability issues; potential agglomeration and sedimentation.	Engine oils and gear oils; material processing fluids; anti-osteoarthritis drug carriers.
Solid coatings	Interlayer sliding; tribofilm formation; self-repairing effect; surface polishing; synergistic lubrication.	High load-bearing capacity; excellent performance in vacuum/dry conditions; long service life.	Sensitive to humidity & oxidation; performance degradation in harsh environments.	Mechanical elements (aerospace); MEMS/MENS.
Composite fillers	Synergistic lubrication.	Improved toughness & wear resistance.	Complex manufacturing processes; interfacial compatibility issues; high COF.	Self-lubricating mechanical elements; biomedical implants (e.g., artificial joints).

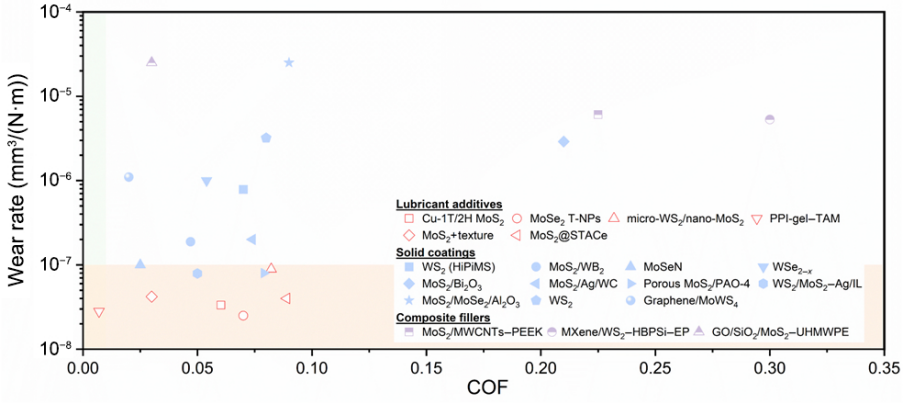


Fig. 21 Comparison of COF and wear rate among representative studies.

based systems that combine these dual functions. In addition, the concept of intelligent lubrication offers new opportunities for TMDs. By integrating sensing, responsiveness, and adaptive regulation, TMD-based systems can evolve from passive lubricants to active functional interfaces. Specifically, TMDs can be incorporated into sliding interfaces to sense key interfacial parameters, such as temperature and pressure, or be combined with functional molecules to form adaptive interfacial films with

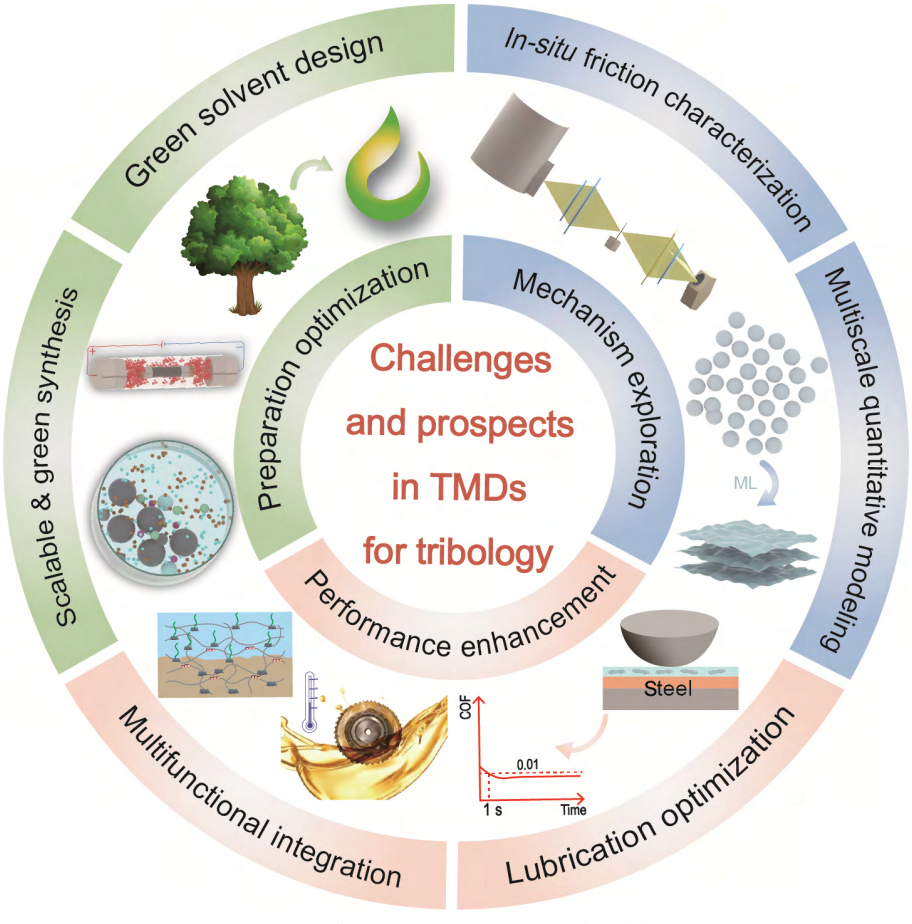


Fig. 22 Challenges and prospects in TMDs for tribology.

self-healing and corrosion resistance capabilities in response to mechanical stress or environmental changes.

Overall, future research on TMD-based lubricants should focus on a systematic closed loop of preparation optimization, mechanistic elucidation, and performance enhancement, progressively bridging the gap from experimental investigation to engineering implementation. By integrating fundamental understanding with engineering design, TMD-based lubricants are expected to play a pivotal role in green manufacturing, energy-efficient transportation, and advanced energy systems, providing a solid foundation for low-carbon and sustainable development.

Acknowledgements

This work was sponsored by the Shanghai Explorer Program (No. 24TS1413100), the National Natural Science Foundation of China (No. 52375353), and Inner Mongolia-SJTU Science and Technology Cooperation Special Project (China) (No. 2023XYJG0001-01-05).

Declaration of competing interest

The authors have no competing interests to declare that are relevant to the content of this article.

References

[1] Zhai W Z, Bai L C, Zhou R H, Fan X L, Kang G Z, Liu Y, Zhou K. Recent progress on wear-resistant materials: Designs, properties, and applications. *Adv Sci* **8**(11): 2003739 (2021)

[2] Qin C X, Yang H, Lu Y Q, Li B, Ma S H, Ma Y F, Zhou F. Tribology in nature: Inspirations for advanced lubrication materials. *Adv Mater* **37**(51): 2420626 (2025)

[3] Zhang X L, Ren T H, Li Z P. Recent advances of two-dimensional lubricating materials: From tunable tribological properties to applications. *J Mater Chem A* **11**(17): 9239–9269 (2023)

[4] Luo J B, Liu M, Ma L R. Origin of friction and the new frictionless technology—Superlubricity: Advancements and future outlook. *Nano Energy* **86**: 106092 (2021)

[5] Zhang Z Y, Du Y F, Huang S L, Meng F N, Chen L L, Xie W X, Chang K K, Zhang C H, Lu Y, Lin C T, et al. Macroscale superlubricity enabled by graphene-coated surfaces. *Adv Sci* **7**(4): 1903239 (2020)

[6] Zhang Z K, Shen C J, Zhang P P, Xu S L, Kong L C, Liang X B, Li C C, Qiu X Y, Huang J, Cui X. Fundamental, mechanism and development of hydration lubrication: From bio-inspiration to artificial manufacturing. *Adv Colloid Interfac* **327**: 103145 (2024)

[7] Berman D, Deshmukh S A, Sankaranarayanan S K R S, Erdemir A, Sumant A V. Macroscale superlubricity enabled by graphene nanoscroll formation. *Science* **348**(6239): 1118–1122 (2015)

[8] Katiyar J K, Rao T V V L N. Sustainable lubricants formulation for sustainable lubrication: A comprehensive review including machine learning predictions. *Tribol Int* **213**: 111075 (2026)

[9] Jiang Z Q, Wu J H, Yu L G, Bi J L, Wang Y D, Hu X Y, Zhang Y J, Li W H. Two-dimensional nanomaterials as lubricant additives: The state-of-the-art and future prospects. *J Mater Chem C* **13**(9): 4327–4373 (2025)

[10] Rosenkranz A, Righi M C, Sumant A V, Anasori B, Mochalin V N. Perspectives of 2D MXene tribology. *Adv Mater* **35**(5): 2207757 (2023)

[11] Song W, Zeng C Y, Ma X Y, Wong J S S, Ouyang C, Sun S Y, Zhang W W, Luo J B, Chen X, Li J J. *In-situ* catalysis of green lubricants into graphitic carbon by iron single atoms to reduce friction and wear. *Nat Commun* **16**: 2919 (2025)

[12] Liu L C, Zhou M, Jin L, Li L C, Mo Y T, Su G S, Li X, Zhu H W,

Tian Y. Recent advances in friction and lubrication of graphene and other 2D materials: Mechanisms and applications. *Friction* **7**(3): 199–216 (2019)

[13] Maji M, Kundu D, Chattopadhyay M K, Banerjee P. A paradigm shifts in the arena of nano lubricants from ICEVs to EVs: Present perspective and future directions. *J Mater Chem A* **13**(26): 20319–20354 (2025)

[14] Manzeli S, Ovchinnikov D, Pasquier D, Yazyev O V, Kis A. 2D transition metal dichalcogenides. *Nat Rev Mater* **2**(8): 17033 (2017)

[15] Belay Ibrahim K, Ahmed Shifa T, Zorzi S, Getaye Sendeku M, Moretti E, Vomiero A. Emerging 2D materials beyond mxenes and TMDs: Transition metal carbo-chalcogenides. *Prog Mater Sci* **144**: 101287 (2024)

[16] Chhowalla M, Shin H S, Eda G, Li L J, Loh K P, Zhang H. The chemistry of two-dimensional layered transition metal dichalcogenide nanosheets. *Nat Chem* **5**(4): 263–275 (2013)

[17] Liu H Y, Zhang Z P, Li X R, Zhang Y H, Fan X Q, Zhu M H. Ultra-high dispersion MoS_2 QDs hybrid polyethylene glycol: Multilayer heterostructure tribofilm. *Tribol Int* **210**: 110793 (2025)

[18] Chen Y J, Li H C, Su F H, Ma G Z, Li Q, Sun J F, Lin S S. Tribological behavior of MoS_2/a-C: Si composite films in high-temperature air and vacuum environments. *Tribol Int* **189**: 108988 (2023)

[19] Wang J H, Zhuang W P, Liang W F, Yan T T, Li T, Zhang L X, Li S. Inorganic nanomaterial lubricant additives for base fluids, to improve tribological performance: Recent developments. *Friction* **10**(5): 645–676 (2022)

[20] Wang R L, Zhang F Z, Yang K, Xiong Y H, Tang J, Chen H, Duan M C, Li Z J, Zhang H L, Xiong B Y. Review of two-dimensional nanomaterials in tribology: Recent developments, challenges and prospects. *Adv Colloid Interfac* **321**: 103004 (2023)

[21] Mukhtar S H, Gulzar A, Saleem S, Wani M F, Sehgal R, Yakovenko A A, Goryacheva I G, Sharma M D. Advances in development of solid lubricating MoS_2 coatings for space applications: A review of modeling and experimental approaches. *Tribol Int* **192**: 109194 (2024)

[22] Li M H, Zhou Q, Cao M M, Zhou Z, Liu X Y. High-temperature solid lubrication applications of Transition Metal Dichalcogenides (TMDCs) MX_2: A review. *Nano Mater Sci* **7**(4): 409–423 (2025)

[23] Jiang Z Q, Wang C X, Yu L G, Zhang S M, Kavaliova I N, Prozhega M V, Li W H. Tungsten disulfide nanomaterials as lubricant additives—An update. *Friction* **13**: 9441556 (2026)

[24] Jiang Z Q, Zhang Z H, Jiang A Y, Yang Z Z, Yu L G, Kavaliova I N, Prozhega M V, Hao Y X. MoS_2 nanoadditives for lubrication: Morphology, surface chemistry, and mechanisms. *Tribol Int* **214**: 111151 (2026)

[25] Zhai W, Li Z J, Wang Y J, Zhai L, Yao Y, Li S Y, Wang L X, Yang H, Chi B L, Liang J Z, et al. Phase engineering of nanomaterials: Transition metal dichalcogenides. *Chem Rev* **124**(7): 4479–4539 (2024)

[26] Voiry D, Mohite A, Chhowalla M. Phase engineering of transition metal dichalcogenides. *Chem Soc Rev* **44**(9): 2702–2712 (2015)

[27] Chen Y, Lai Z C, Zhang X, Fan Z X, He Q Y, Tan C L, Zhang H. Phase engineering of nanomaterials. *Nat Rev Chem* **4**(5): 243–256 (2020)

[28] Sokolikova M S, Mattevi C. Direct synthesis of metastable phases of 2D transition metal dichalcogenides. *Chem Soc Rev* **49**(12): 3952–3980 (2020)

[29] Hu H, Wang Z Y, Pan M L, Chen Y M, Han Y X, Wang J D. Interface effects in metal–2D TMDs systems: Advancing the design and development electrocatalysts. *Adv Sci* **12**(17): 2500226 (2025)

[30] Kumar R, Sarkar C, Bunekar N, Mishra Y K, Kaushik A. State-of-the-art transition metal dichalcogenides: Synthesis, functionalization, and biomedical applications. *Mater Today* **88**: 597–642 (2025)

[31] Huang Y, Pan Y H, Yang R, Bao L H, Meng L, Luo H L, Cai Y Q, Liu G D, Zhao W J, Zhou Z, et al. Universal mechanical exfoliation of large-area 2D crystals. *Nat Commun* **11**: 2453 (2020)

[32] Xu Y M, Yan L H, Li X Y, Xu H H. Fabrication of transition metal dichalcogenides quantum dots based on femtosecond laser ablation. *Sci Rep* **9**: 2931 (2019)

[33] Yang R J, Fan Y Y, Mei L, Shin H S, Voiry D, Lu Q Y, Li J, Zeng Z Y. Synthesis of atomically thin sheets by the intercalation-based exfoliation of layered materials. *Nat Synth* **2**(2): 101–118 (2023)

[34] Yang R J, Fan Y Y, Zhang Y F, Mei L, Zhu R S, Qin J Q, Hu J G, Chen Z X, Hau Ng Y, Voiry D, et al. 2D transition metal dichalcogenides for photocatalysis. *Angew Chem Int Edit* **62**(13): e202218016 (2023)

[35] Zhou J D, Tang B J, Lin J H, Lv D H, Shi J, Sun L F, Zeng Q S, Niu L, Liu F C, Wang X W, et al. Morphology engineering in monolayer MoS_2–WS_2 lateral heterostructures. *Adv Funct Mater* **28**(31): 1801568 (2018)

[36] Song J G, Park J, Lee W, Choi T, Jung H, Lee C W, Hwang S H, Myoung J M, Jung J H, Kim S H, et al. Layer-controlled, wafer-scale, and conformal synthesis of tungsten disulfide nanosheets using atomic layer deposition. *ACS Nano* **7**(12): 11333–11340 (2013)

[37] Panasci S E, Schilirò E, Roccaforte F, Giannazzo F. Gold-assisted exfoliation of large-area monolayer transition metal dichalcogenides: From interface properties to device applications. *Adv Funct Mater* **35**(5): 2414532 (2025)

[38] Goldstein T, Chen S Y, Tong J Y, Xiao D, Ramasubramaniam A, Yan J. Raman scattering and anomalous Stokes–anti-Stokes ratio in $MoTe_2$ atomic layers. *Sci Rep* **6**: 28024 (2016)

[39] Choi C H, Shin J, Eddy L, Granja V, Wyss K M, Damasceno B, Guo H, Gao G H, Zhao Y F, Higgs C F III, et al. Flash-within-flash synthesis of gram-scale solid-state materials. *Nat Chem* **16**(11): 1831–1837 (2024)

[40] Wang X, Wu J, Zhang Y W, Sun Y, Ma K K, Xie Y, Zheng W H, Tian Z, Kang Z, Zhang Y. Vacancy defects in 2D transition metal dichalcogenide electrocatalysts: From aggregated to atomic configuration. *Adv Mater* **35**(50): 2206576 (2023)

[41] Wang X, Wu J, Zhang Y W, Sun Y, Ma K K, Xie Y, Zheng W H, Tian Z, Kang Z, Zhang Y. Vacancy defects in 2D transition metal dichalcogenide electrocatalysts: From aggregated to atomic configuration. *Adv Mater* **35**(50): 2206575 (2023)

[42] Zhao W J, Zhou X Y, Yan D Y, Huang Y, Li C, Gao Q, Moras P, Sheverdyaeva P M, Rong H T, Cai Y Q, et al. Synthesis and electronic structure of atomically thin 2H-$MoTe_2$. *Nanoscale* **17**(17): 10901–10909 (2025)

[43] Thayil R, Parne S R, Ramana C V. 2D MoS_2 for next-generation electronics and optoelectronics: From material properties to manufacturing challenges and future prospects. *Small* **21**(14): 2412467 (2025)

[44] Burse S R, Tyagaraj H B, Safarkhani M, Marje S J, Gagankumar S K, Al Ghaferi A, Alhajri E, Chodankar N R, Huh Y S, Han Y K. Unleashing potential: Engineering advancements in two-dimensional MoS_2 for improved energy applications. *Adv Compos Hybrid Ma* **8**(2): 216 (2025)

[45] Bai Y C, Xu Y A, Sun L X, Ward Z, Wang H Z, Ratnayake G, Wang C, Zhao M C, He H Q, Gao J X, et al. Two-dimensional nanosheets by liquid metal exfoliation. *Adv Mater* **37**(8): 2416375 (2025)

[46] Backes C, Higgins T M, Kelly A, Boland C, Harvey A, Hanlon D, Coleman J N. Guidelines for exfoliation, characterization and processing of layered materials produced by liquid exfoliation. *Chem Mater* **29**(1): 243–255 (2017)

[47] Tedstone A A, Lewis D J, O'Brien P. Synthesis, properties, and applications of transition metal-doped layered transition metal dichalcogenides. *Chem Mater* **28**(7): 1965–1974 (2016)

[48] Chou S S, Huang Y K, Kim J, Kaehr B, Foley B M, Lu P, Dykstra C, Hopkins P E, Brinker C J, Huang J X, et al. Controlling the metal to semiconductor transition of MoS_2 and WS_2 in solution. *J Am Chem Soc* **137**(5): 1742–1745 (2015)

[49] Yuwen L H, Yu H, Yang X R, Zhou J J, Zhang Q, Zhang Y Q, Luo Z M, Su S, Wang L H. Rapid preparation of single-layer transition metal dichalcogenide nanosheets via ultrasonication enhanced lithium intercalation. *Chem Commun* **52**(3): 529–532 (2016)

[50] Tan C L, Cao X H, Wu X J, He Q Y, Yang J, Zhang X, Chen J Z, Zhao W, Han S K, Nam G H, et al. Recent advances in ultrathin two-dimensional nanomaterials. *Chem Rev* **117**(9): 6225–6331 (2017)
[51] Zhang X Y, Ma G Q, Wang J. Hydrothermal synthesis of two-dimensional MoS_2 and its applications. *Tungsten-Singapore* **1**(1): 59–79 (2019)
[52] Huang S L, Jia D, Hu W G, Zhan S P, Yang T, Zhang W L, Lu B W, Duan H T. Morphology-regulated molybdenum disulfide/multi-walled carbon nanotubes hybrids for enhanced tribological and mechanical performance of polyether ether ketone composites. *Chem Eng J* **521**: 166758 (2025)
[53] Hu Z Y, O'Neill R, Lesyuk R, Klinke C. Colloidal two-dimensional metal chalcogenides: Realization and application of the structural anisotropy. *Acc Chem Res* **54**(20): 3792–3803 (2021)
[54] Jiang J Z, Li N, Zou J, Zhou X, Eda G, Zhang Q F, Zhang H, Li L J, Zhai T Y, Wee A T S. Synergistic additive-mediated CVD growth and chemical modification of 2D materials. *Chem Soc Rev* **48**(17): 4639–4654 (2019)
[55] Fu W, John M, Maddumapatabandi T D, Bussolotti F, Yau Y S, Lin M, Johnson Goh K E. Toward edge engineering of two-dimensional layered transition-metal dichalcogenides by chemical vapor deposition. *ACS Nano* **17**(17): 16348–16368 (2023)
[56] Kim T S, Dhakal K P, Park E, Noh G, Chai H J, Kim Y, Oh S, Kang M, Park J, Kim J, et al. Gas-phase alkali metal-assisted MOCVD growth of 2D transition metal dichalcogenides for large-scale precise nucleation control. *Small* **18**(20): 2106368 (2022)
[57] Lin H H, Zhu Q, Shu D J, Lin D J, Xu J, Huang X L, Shi W, Xi X X, Wang J W, Gao L B. Growth of environmentally stable transition metal selenide films. *Nat Mater* **18**(6): 602–607 (2019)
[58] Zhu L J, Yang P F, Huan Y H, Pan S Y, Zhang Z Q, Cui F F, Shi Y P, Jiang S L, Xie C Y, Hong M, et al. Scalable salt-templated directed synthesis of high-quality MoS_2 nanosheets powders towards energetic and environmental applications. *Nano Res* **13**(11): 3098–3104 (2020)
[59] Turchanin A, George A. Tailored growth of transition metal dichalcogenides' monolayers by chemical vapor deposition. *Small* **21**(28): 2403089 (2025)
[60] Yu J, Han W, Suleiman A A, Han S Y, Miao N H, Ling F C. Recent advances on pulsed laser deposition of large-scale thin films. *Small Methods* **8**(7): 2301282 (2024)
[61] Yang C X, Wang G X, Guo S W, Sun J L. Potential and progress of two-dimensional nanomaterials in oil-based lubrication. *Chinese Chem Lett* **36**(9): 111178 (2025)
[62] Nyholm N, Espallargas N. Functionalized carbon nanostructures as lubricant additives—A review. *Carbon* **201**: 1200–1228 (2023)
[63] Berman D, Erdemir A, Sumant A V. Graphene: A new emerging lubricant. *Mater Today* **17**(1): 31–42 (2014)
[64] Liu Y M, Song A S, Xu Z, Zong R L, Zhang J, Yang W Y, Wang R, Hu Y Z, Luo J B, Ma T B. Interlayer friction and superlubricity in single-crystalline contact enabled by two-dimensional flake-wrapped atomic force microscope tips. *ACS Nano* **12**(8): 7638–7646 (2018)
[65] Wang G X, Yang C X, Li D, Guo S W. A boost lubrication performance of reduced graphene oxide synergizing with carbonized polymer dots via tribochemistry. *Carbon* **218**: 118694 (2024)
[66] Jiang Z Q, Sun Y K, Liu B K, Yu L G, Tong Y P, Yan M M, Yang Z Z, Hao Y X, Shangguan L J, Zhang S M, et al. Research progresses of nanomaterials as lubricant additives. *Friction* **12**(7): 1347–1391 (2024)
[67] Wang B X, Qiu F, Barber G C, Zou Q, Wang J, Guo S Y, Yuan Y F, Jiang Q C. Role of nano-sized materials as lubricant additives in friction and wear reduction: A review. *Wear* **490–491**: 204206 (2022)
[68] Yi S, Li J J, Liu Y F, Ge X Y, Zhang J, Luo J B. *In-situ* formation of tribofilm with $Ti_3C_2T_x$ MXene nanoflakes triggers macroscale superlubricity. *Tribol Int* **154**: 106695 (2021)
[69] Kohlhauser B, Ripoll M R, Riedl H, Koller C M, Koutna N, Amsüss A, Hutter H, Ramirez G, Gachot C, Erdemir A, et al. How to get noWear? —A new take on the design of *in-situ* formed high performing low-friction tribofilms. *Mater Design* **190**: 108519 (2020)
[70] Li P P, He W H, Ju P F, Ji L, Liu X H, Wu F, Lu Z B, Li H X, Chen L, Liu J Z, et al. Acquisition of molecular rolling lubrication by self-curling of graphite nanosheet at cryogenic temperature. *Nat Commun* **15**: 5747 (2024)
[71] Lu Z Y, Lin Q Q, Cao Z T, Li W Y, Gong J J, Wang Y, Hu K H, Hu X G. MoS_2 nanomaterials as lubricant additives: A review. *Lubricants* **11**(12): 527 (2023)
[72] Yi C L, Hu C Z, Shi L, Bai M L, Li Y B, Tang D W. Frictional properties of MoS_2 on a multi-level rough wall under starved lubrication. *Phys Chem Chem Phys* **25**(20): 14348–14358 (2023)
[73] Kong L H, Sun J L, Bao Y Y. Preparation, characterization and tribological mechanism of nanofluids. *RSC Adv* **7**(21): 12599–12609 (2017)
[74] Cao H T, De Hosson J T M, Pei Y T. Self-healing of a pre-notched WS_2/a-C coating. *Mater Res Lett* **7**(3): 103–109 (2019)
[75] Cao H T, Wen F, De Hosson J T M, Pei Y T. On the self-repair of WS_2/a-C tribocoating. *Adv Mater Interfaces* **7**: 1900938 (2020)
[76] Azman N F, Samion S. Dispersion stability and lubrication mechanism of nanolubricants: A review. *Int J Pr Eng Man-GT* **6**(2): 393–414 (2019)
[77] Mosleh M, Shirvani K A. *In-situ* nanopolishing by nanolubricants for enhanced elastohydrodynamic lubrication. *Wear* **301**(1–2): 137–143 (2013)
[78] Ying P Y, Sun H Y, Zhang P, Lin C H, Yang T, Wu J B, Huang M, Wang T L, Lian Z B, Levchenko V. Preparation and tribological properties of WS_2 solid lubricating coating with dense structure using HiPIMS. *J Mater Res Technol* **32**: 530–540 (2024)
[79] Yan C, Zeng Q F, Hao Y C, Xu Y T, Zhou M. Friction-induced hardening behaviors and tribological properties of 60NiTi alloy lubricated by lithium grease containing nano-BN and MoS_2. *Tribol T* **62**(5): 812–820 (2019)
[80] Vaziriserehk M R, Hasz K, Zhao M Q, Johnson A T C, Carpick R W, Martini A. Nanoscale friction behavior of transition-metal dichalcogenides: Role of the chalcogenide. *ACS Nano* **14**(11): 16013–16021 (2020)
[81] Lee D, Jeong H, Lee H, Kim Y H, Park J Y. Phase-dependent friction on exfoliated transition metal dichalcogenides atomic layers. *Small* **19**(47): 2302713 (2023)
[82] Liu X N, Le K, Yang W J, Liu Y Z, Luo Y, Zheng X W, Chen H, Xu S S, Liu W M. Tailoring the crystallinity and phase composition of MoS_2 nanosheets for better lubrication performance. *Appl Surf Sci* **673**: 160856 (2024)
[83] Huynh N P, Kim H J, Chung K H. Long-term wear characteristics of single-layer h-BN, MoS_2, and graphene. *Tribol Int* **213**: 111059 (2026)
[84] Yu T T, Shen R L, Wu Z S, Du C H, Shen X J, Jia N, Deng H Y, Zhao Y K, Zhang L Q, Feng Y G, et al. Monolayer $NbSe_2$ favors ultralow friction and super wear resistance. *Nano Lett* **23**(5): 1865–1871 (2023)
[85] Arole K, Pas S E, Thakur R M, Amiouny L A, Kabir M H, Dujovic M, Radovic M, Lutkenhaus J L, Green M J, Liang H. Effects of intercalation on ML-$Ti_3C_2T_z$ MXene properties and friction performance. *ACS Appl Mater Inter* **16**(46): 64156–64165 (2024)
[86] Liu H Y, Li W Y, Xu Y, Hu E Z, Qin G C, Hu K H. Tribological performance of Cu-modified large interlayer spacing 1T/2H-MoS_2 nanoparticles in soot-contaminated polyalphaolefin. *J Ind Eng Chem* **151**: 238–250 (2025)
[87] Zhang X H, Wang J T, Xu H X, Tan H, Ye X. Preparation and tribological properties of WS_2 hexagonal nanoplates and nanoflowers. *Nanomaterials* **9**(6): 840 (2019)
[88] Xiao H P, Liu S H. 2D nanomaterials as lubricant additive: A review. *Mater Design* **135**: 319–332 (2017)
[89] Li Y H, Lu H L, Liu Q, Qin L G, Dong G N. A facile method to enhance the tribological performances of $MoSe_2$ nanoparticles as oil additives. *Tribol Int* **137**: 22–29 (2019)

[90] Miao X N, Li Z P, Liu S W, Wang J Q, Yang S R. MXenes in tribology: Current status and perspectives. *Adv Powder Mater* **2**(2): 100092 (2023)
[91] Joseph A, Vijayan A S, Shebeeb C M, Akshay K S, John Mathew K P, Sajith V. A review on tailoring the corrosion and oxidation properties of MoS_2-based coatings. *J Mater Chem A* **11**(7): 3172–3209 (2023)
[92] Cairns E, Ayyagari A, McCoy C, Berkebile S, Berman D, Aouadi S M, Voevodin A A. Tribological behavior of molybdenum disulfide and tungsten disulfide sprayed coatings in low viscosity hydrocarbon environments. *Tribol Int* **179**: 108206 (2023)
[93] Huang Y Q, Gao H Y, Yu K H, Niu Z W, Yang Z X, Zhang B, Gao K X, Zhang J Y, Alpas A T. Friction mechanisms of WS_2 in humid environments: Investigating H_2O adsorption via DFT computations and sliding friction experiments. *Tribol Int* **203**: 110416 (2025)
[94] Santosh K C, Longo R C, Wallace R M, Cho K. Surface oxidation energetics and kinetics on MoS_2 monolayer. *J Appl Phys* **117**(13): 135301 (2015)
[95] He J, Wang D S, Hu M, Gao X M, Sun J Y, Li Z H, Lv H Y, Guo L B, Fu Y L, Liu Z L, et al. Unveiling the degradation mechanisms of MoS_2 lubricating films in authentic low earth orbit via China space station exposure experiment. *Adv Funct Mater* **36**(10): e23156 (2026)
[96] Ross S, Sussman A. Surface oxidation of molybdenum disulfide. *J Phys Chem* **59**(9): 889–892 (1955)
[97] Reidy K, Mortelmans W, Jo S S, Penn A N, Foucher A C, Liu Z J, Cai T, Wang B M, Ross F M, Jaramillo R. Atomic-scale mechanisms of MoS_2 oxidation for kinetic control of MoS_2/MoO_3 interfaces. *Nano Lett* **23**(13): 5894–5901 (2023)
[98] Grützmacher P G, Majed A, Marquis E, Sui X D, Righi M C, Sauer M, Foelske A, Naguib M, Gachot C. Transition metal carbo chalcogenides: A novel family of 2D solid lubricants. *Carbon* **231**: 119695 (2025)
[99] Lu X Y, Gu X L, Shi Y J. A review on the synthesis of MXenes and their lubrication performance and mechanisms. *Tribol Int* **179**: 108170 (2023)
[100] Ma F, Wang L Q, Zheng D Z, Wang W X, Wang T J, Wu L P, Gu L, Zhang C W. Frictional heat accumulation at cyclically rolling-sliding contacts with consideration to time-dependent contact pressure. *Tribol Int* **191**: 109144 (2024)
[101] Li C, Huang H B, Qu J H, Cao J, Huang F H, Wang Y G. Mechanism of wear and COF variation of vulcanized rubber under changing loads and sliding velocities: Interpretation at the atomic scale. *Tribol Int* **170**: 107505 (2022)
[102] Kabir M H, Dias D, Velhal M, Liang H. Effects of oxidation-assisted grafting of MoS_2 on tribological performance of steels. *Tribol Int* **211**: 110826 (2025)
[103] Wang X Z, Li C C, Gong K L, Wu X H. Surface-modified MoS_2 nanoparticles as tribological additives in a glycerol solution. *ACS Appl Nano Mater* **6**(8): 6662–6669 (2023)
[104] Zhang C, Wu B H, Zhou Y S, Zhou F, Liu W M, Wang Z K. Mussel-inspired hydrogels: From design principles to promising applications. *Chem Soc Rev* **49**(11): 3605–3637 (2020)
[105] Zhou X, Wang K L, Wu Y, Wang X B, Zhang X. Mussel-inspired interfacial modification for ultra-stable MoS_2 lubricating films with improved tribological behavior on nano-textured ZnO surfaces using the AACVD method. *ACS Appl Mater Inter* **14**(23): 27484–27494 (2022)
[106] Wu X H, Gong K L, Zhao G Q, Lou W J, Wang X B, Liu W M. Surface modification of MoS_2 nanosheets as effective lubricant additives for reducing friction and wear in poly-α-olefin. *Ind Eng Chem Res* **57**(23): 8105–8114 (2018)
[107] Garrido M, Naranjo A, Pérez E M. Characterization of emerging 2D materials after chemical functionalization. *Chem Sci* **15**(10): 3428–3445 (2024)
[108] Presolski S, Pumera M. Covalent functionalization of MoS_2. *Mater Today* **19**(3): 140–145 (2016)
[109] Kumari S, Chouhan A, Sharma O P, Tawfik S A, Tran K, Spencer M J S, Bhargava S K, Walia S, Ray A, Khatri O P. Surface functionalization of WS_2 nanosheets with alkyl chains for enhancement of dispersion stability and tribological properties. *ACS Appl Mater Inter* **14**(1): 1334–1346 (2022)
[110] Ren H H, Zeng H Y, Sun C F, Yang J H, Luo X P, Li J, Li B, Sheng W B. Polymer brush-functionalized MoS_2 as a water-based lubricant additive. *Macromol Rapid Comm* **46**(4): 2400793 (2025)
[111] Zhang Z X, E H J, Zhai B X, Gao Y, Huang Z, Chen J, et al. Review of recent advances in porous organic frameworks as additives for lubrication. *ACS Appl Mater Inter* **17**(35): 49119–49147 (2025)
[112] Yang K, Xiong Y H, Wu G J, Lin H B, Tang J, Wu C, Chen H L, Wang Y Q. Multi-dimensional nano-additives for their superlubricity: Tribological behaviors and lubrication mechanisms. *Adv Mater Interfaces* **12**(9): 2400796 (2025)
[113] Chen Z Y, Lan Z, Huang W, Yan H X, Jin Y L, Yang G F, Guo Z Z, Ren F, Sun Z F, Ren P G. Recent advances in state-of-the-art 2D MXenes: Synthesis, mechanical and tribological properties. *Coordin Chem Rev* **548**: 217175 (2026)
[114] Liu S, Li S, Wang Y X, Xue S H, Liu S J, Ye Q, Zhou F, Liu W M. Fabrication of vanadium oxide-encapsulated hybrid carbon nanospheres for enhanced tribological performance. *Small* **20**(52): 2406027 (2024)
[115] Liu H Y, Xu Y, Hu E Z, Hu K H. Synthesis and tribological properties of WS_2/MoS_2 micro-nano composite lubricant. *Tribol Int* **204**: 110506 (2025)
[116] Yang M, Fan X, Ren S M, Wang L P. Enhanced environmental adaptability of sandwich-like MoS_2/Ag/WC nanomultilayer films via Ag nanoparticle diffusion-dominated defect repair. *Mater Horiz* **11**(21): 5230–5243 (2024)
[117] Gao Z R, Nie W M, Wang H X, Ren S M, Du D L, Du S Y, Li J L. Enhancing mechanical performance and high-temperature lubrication enabled by MoS_2/WB_2 nanolayered films. *Compos Part B—Eng* **275**: 111350 (2024)
[118] Grützmacher P G, Cutini M, Marquis E, Rodríguez Ripoll M, Riedl H, Kutrowatz P, Bug S, Hsu C J, Bernardi J, Gachot C, et al. Se nanopowder conversion into lubricious 2D selenide layers by tribochemical reactions. *Adv Mater* **35**(42): 2302076 (2023)
[119] Colas G, Saulot A, Regis E, Berthier Y. Investigation of crystalline and amorphous MoS_2 based coatings: Towards developing new coatings for space applications. *Wear* **330**: 448–460 (2015)
[120] Lu Z X, Zhang C Z, Zeng C, Ren S M, Pu J B. A novel design by constructing MoS_2/WS_2 multilayer film doped with tantalum toward superior friction performance in multiple environment. *J Mater Sci* **56**(31): 17615–17631 (2021)
[121] Serles P, Nicholson E, Tam J, Barri N, Chemin J B, Wang G R, Michel Y, Singh C V, Choquet P, Saulot A, et al. High performance space lubrication of MoS_2 with tantalum. *Adv Funct Mater* **32**(20): 2110429 (2022)
[122] Bin Yaqub T, Nadeem I, Fernandes F, Yaqoob K, Kalin M, Cavaleiro A. Nitrogen alloyed $MoSe_2$ coatings—Role of optimized morphology, structure and mechanical properties on diverse environment sliding performance. *Tribol Int* **209**: 110716 (2025)
[123] Wang Y, Rai H, Polcar T. Load-dependent sliding behavior of WSe_{2-x} solid lubricant coating. *Wear* **580–581**: 206305 (2025)
[124] Tan X, Yu X Q, Huang W Y, Zhou Y F, Hu E Z, Ding X K, Li C, Hu K H. Influence of MoS_2–La/CQDs quantum dispersion on the tribological behaviors of PEG200. *Wear* **564**: 205685 (2025)
[125] Shao X B, Ren Y, Guo K, Du C F, Wang X Z, Chen J, Liu J X, Wang L, Yang J. Achieving high temperature lubrication of MoS_2–Bi_2O_3 nanoparticles composite: Through the formation of nanocrystalline ternary oxide and glaze layer. *Tribol Int* **206**: 110577 (2025)
[126] Ru G L, Qi W H, Sun S, Tang K W, Du C F, Liu W M. Interlayer friction and adhesion effects in penta-$PdSe_2$-based van der Waals heterostructures. *Adv Sci* **11**(34): 2400395 (2024)
[127] Feng P, Ren Y P, Li Y T, He J F, Zhao Z, Ma X L, Fan X Q, Zhu M H. Synergistic lubrication of few-layer $Ti_3C_2T_x/MoS_2$ heterojunction as a lubricant additive. *Friction* **10**(12): 2018–2032 (2022)

[128] Bharti P, Neogi A, Sharma R, Dhand C, Kumar R, Kumar P, Sankaranarayanan S K R S, Dwivedi N. Decision trees within 1D/2D material systems for enabling highly lubricious and wear resistant surfaces. *Carbon* **217**: 118603 (2024)
[129] Vo T D, Deng G Y, Tieu A K, Su L H, Wu X T, Nguyen C, Wexler D, Yang J. Excellent tribological performance at elevated temperatures and associated mechanisms of novel AlCoCrFeNi–MoS_2 solid self-lubricating composite. *Tribol Int* **189**: 109011 (2023)
[130] Chen Z Y, Lan Z, Huang W, Ren P G, Yan H X, Guo Z Z, Jin Y L, Sun Z F. Enhanced self-lubricating and wear-resistance of epoxy composites synergistically reinforced by HBPSi and MXene/WS_2 heterostructured filler. *Compos Sci Technol* **272**: 111397 (2025)
[131] Hou K M, Yang S R, Liu X H, Wang J Q. The self-ordered lamellar texture of MoS_2 transfer film formed in complex lubrication. *Adv Mater Interfaces* **5**(8): 1701682 (2018)
[132] Htwe Y Z N, Al-Janabi A S, Wadzer Y, Mamat H. Review of tribological properties of nanoparticle-based lubricants and their hybrids and composites. *Friction* **12**(4): 569–590 (2024)
[133] Rosenkranz A, Costa H L, Baykara M Z, Martini A. Synergetic effects of surface texturing and solid lubricants to tailor friction and wear—A review. *Tribol Int* **155**: 106792 (2021)
[134] Cao W H, Yan W H, Yang X, Li Z J, Geng J, Dong Y, Zhang Y, Qi X W. Multiscale study on the solid–liquid synergistic lubrication mechanism of graphite and liquid lubricant in polymer composites. *Carbon* **230**: 119605 (2024)
[135] Fan X Q, Xue Q J, Wang L P. Carbon-based solid–liquid lubricating coatings for space applications—A review. *Friction* **3**(3): 191–207 (2015)
[136] Zhou Y, Qu J. Ionic liquids as lubricant additives: A review. *ACS Appl Mater Inter* **9**(4): 3209–3222 (2017)
[137] Cai M R, Yu Q L, Liu W M, Zhou F. Ionic liquid lubricants: When chemistry meets tribology. *Chem Soc Rev* **49**(21): 7753–7818 (2020)
[138] Quan X, Zhang S W, Hu M, Gao X M, Jiang D, Sun J Y. Tribological properties of WS_2/MoS_2–Ag composite films lubricated with ionic liquids under vacuum conditions. *Tribol Int* **115**: 389–396 (2017)
[139] Zhang J Y, Jiang D, Wang D S, Yu Q L, Bai Y Y, Cai M R, Weng L J, Zhou F, Liu W M. MoS_2 lubricating film meets supramolecular gel: A novel composite lubricating system for space applications. *ACS Appl Mater Inter* **13**(48): 58036–58047 (2021)
[140] Yang D, Zhang L Q, Yu T T, Du C H, Wang L C, Wang W P, Feng Y G, Liu W M, Wang D A. Hierarchical MoS_2-oleogel in porous polyimides: A self-adaptive confined lubrication strategy for ultralow friction and wear. *Adv Funct Mater* **36**(6): e17029 (2026)
[141] Wang Z Q, Ye R H, Xiang J B. The performance of textured surface in friction reducing: A review. *Tribol Int* **177**: 108010 (2023)
[142] Sinha A K, Sharma M D. Tribological performance of open and closed textured Ti–3Al–2.5V under effect of MoS_2 as solid lubricant for aerospace applications. *Tribol Int* **201**: 110260 (2025)
[143] Xing Y Q, Zhu M Y, Wu Z, Li Z, Bai S W, Zhang K D, Liu L. High-temperature tribological properties of Si_3N_4/TiC ceramic with bionic surface textures and DLC coatings. *Tribol Int* **186**: 108648 (2023)
[144] Cui X B, Duan S Q, Guo J X, Ming P M. Bionic multifunctional surface microstructure for efficient improvement of tool performance in green interrupted hard cutting. *J Mater Process Tech* **305**: 117587 (2022)
[145] Qin S Q, Shi X L, Xue Y W, Zhang K P, Huang Q P, Wu C H, Ma J, Shu J P. Coupling effects of bionic textures with composite solid lubricants to improve tribological properties of TC4 alloy. *Tribol Int* **173**: 107691 (2022)
[146] Chen C, Zhao Y, Mei H, Kong Z Y, Mao M X, Cheng L F. Excellent lubrication properties of 3D printed ceramic bionic structures. *Ceram Int* **46**(15): 23463–23470 (2020)
[147] Zhao Y, Mei H, Chang P, Yang Y B, Cheng L F, Zhang L T. High-strength printed ceramic structures for higher temperature lubrication. *Compos Part B—Eng* **221**: 109013 (2021)
[148] Zhao Y, Mei H, Chang P, Yang Y B, Huang W F, Liu Y, Cheng L F, Zhang L T. 3D-printed topological MoS_2/$MoSe_2$ heterostructures for macroscale superlubricity. *ACS Appl Mater Inter* **13**(29): 34984–34995 (2021)
[149] Du C H, Yu T T, Sui X D, Zhang Z F, Cai R S, Zhang L Q, Feng Y G, Feng M, Zhou F, Wang D A. Macro-superlubricity induced by tribocatalysis of high-entropy ceramics. *Adv Mater* **37**(4): 2413781 (2025)
[150] Martin J M, Donnet C, Le Mogne T, Epicier T. Superlubricity of molybdenum disulphide. *Phys Rev B* **48**(14): 10583–10586 (1993)
[151] Chhowalla M, Amaratunga G A J. Thin films of fullerene-like MoS_2 nanoparticles with ultra-low friction and wear. *Nature* **407**(6801): 164–167 (2000)
[152] Li H, Wang J H, Gao S, Chen Q, Peng L M, Liu K H, Wei X L. Superlubricity between MoS_2 monolayers. *Adv Mater* **29**(27): 1701474 (2017)
[153] Peng D L, Wang Y, Li H, Wu Z H, Yang X Q, Huang X Y, Xiang X J, Nie J H, Qu C Y, Cao W, et al. Structural superlubric slidevices. *Device* **3**(6): 100745 (2025)
[154] Jiang B Z, Zhao Z C, Gong Z B, Wang D L, Yu G M, Zhang J Y. Superlubricity of metal-metal interface enabled by graphene and $MoWS_4$ nanosheets. *Appl Surf Sci* **520**: 146303 (2020)
[155] Ru G L, Qi W H, Tang K W, Wei Y R, Xue T W. Interlayer friction and superlubricity in bilayer graphene and MoS_2/$MoSe_2$ van der Waals heterostructures. *Tribol Int* **151**: 106483 (2020)
[156] Long Y Y, Wang X, Tan W, Li B W, Li J D, Deng W, Li X M, Guo W L, Yin J. High-temperature superlubricity in MoS_2/graphene van der Waals heterostructures. *Nano Lett* **24**(25): 7572–7577 (2024)
[157] Macknojia A, Ayyagari A, Zambrano D, Rosenkranz A, Shevchenko E V, Berman D. Macroscale superlubricity induced by MXene/MoS_2 nanocomposites on rough steel surfaces under high contact stresses. *ACS Nano* **17**(3): 2421–2430 (2023)
[158] Tang H J, Chen X C, Deng W L, Luo J B. Comprehensive review: Advances and critical mechanisms in liquid superlubricity. *Adv Colloid Interfac* **344**: 103585 (2025)
[159] Li R Y, Yang X, Li J C, Wang Y F, Ma M. Macroscale, humidity-insensitive, and stable structural superlubricity achieved with hydrogen-free graphene nanoflakes. *Nat Commun* **15**: 9197 (2024)
[160] Zhu D X, Zhang J, Li P P, Li Z, Li H X, Liu X H, Ma T B, Ji L, Zhou H D, Chen J M. Robust macroscale superlubricity in humid air via designing amorphous DLC/crystalline TMDs friction pair. *Adv Funct Mater* **34**(30): 2316036 (2024)
[161] Sun L, Yang Z X, Zhang B, Xing Z Y, Zhang J Y, Wang F G, Qiang L. Superlubricity via operando formation of MoS_2/S_8 heterojunctions on steel surface with amorphous carbon protection. *Nano Energy* **123**: 109404 (2024)
[162] Yin N, Yang P F, Liu S K, Pan S H, Zhang Z N. AI for tribology: Present and future. *Friction* **12**(6): 1060–1097 (2024)
[163] Gong H J, Yu C C, Zhang L, Xie G X, Guo D, Luo J B. Intelligent lubricating materials: A review. *Compos Part B—Eng* **202**: 108450 (2020)
[164] Cao H T, Bai M W, Inkson B J, Zhong X L, De Hosson J T M, Pei Y T, Xiao P. Self-healing WS_2 tribofilms: An *in-situ* appraisal of mechanisms. *Scripta Mater* **204**: 114124 (2021)
[165] Shi B, Gan X H, Yu K, Lang H J, Cao X A, Zou K, Peng Y T. Electronic friction and tuning on atomically thin MoS_2. *npj 2D Mater Appl* **6**: 39 (2022)
[166] Gong H J, Song Y, Li G L, Zhang L, Guo D, Xie G X. An intelligent polymer composite with self-lubricating and self-healing functionalities. *Compos Part B—Eng* **260**: 110776 (2023)
[167] Yang T, Wang X Z, Liu H C, Chen S W, Liu J M, Zhao Q, Gong K L, Li W M, Liang Y M, Wang X B. Electrostatically self-assembled magnetic nanoparticles for high-temperature resistant and friction-controlled lubrication system. *Small* **20**(48): 2405018 (2024)
[168] Zhang H T, Yuan S G, Zheng B Y, Wu P, Zheng K, Li Y, Chen Z H, He X M, Wang J, Yang X C, et al. Engineered nano-lubricant with photothermal-triggered drug release and acid-degradable ion

delivery for osteoarthritic microenvironment regulation. *Chem Eng J* **522**: 168085 (2025)
[169] Torres-Cavanillas R, Forment-Aliaga A. Design of stimuli-responsive transition metal dichalcogenides. *Commun Chem* **7**: 241 (2024)
[170] Yin N, Xing Z G, He K, Zhang Z N. Tribo-informatics approaches in tribology research: A review. *Friction* **11**(1): 1–22 (2023)
[171] Vogel D J, Babuska T F, Mings A, MacDonell P A, Curry J F, Larson S R, Dugger M T. Harnessing machine learning to predict MoS_2 solid lubricant performance. *Tribol Lett* **73**: 23 (2025)
[172] Wang G Q, Song J F, Zhao G, Ding Q J, Yin T Q, Wang H X. Tribological performance prediction of WS_2 coating under different conditions by machine learning. *Wear* **532**: 205092 (2023)
[173] Mishra N, Baradeswaran A. AA8086/TiB_2–MoS_2 hybrid nanocomposites: Ultrasonic synthesis and machine learning prediction of wear behaviour. *Wear* **584**: 206393 (2026)
[174] Huang S Q, Wu H, Jiang Z Y, Huang H. Water-based nanosuspensions: Formulation, tribological property, lubrication mechanism, and applications. *J Manuf Process* **71**: 625–644 (2021)
[175] Meng Y N, Sun J L, He J Q, Yang F L. Metallographic structure improvement of hot rolled strip induced by high temperature diffusion of MoS_2 nano-lubricant. *J Manuf Process* **81**: 1–13 (2022)
[176] Sethurajaperumal A, Srivastava S, Ganesh G, Sundara R, Varrla E. Natural surfactant stabilized aqueous MoS_2 nano-lubricants for reducing friction and wear. *Chem Eng J* **496**: 154080 (2024)
[177] Upadhyay R K, Kumar A. Effect of humidity on the synergy of friction and wear properties in ternary epoxy-graphene-MoS_2 composites. *Carbon* **146**: 717–727 (2019)
[178] He J Q, Sun J L, Meng Y N, Pei Y. Superior lubrication performance of MoS_2–Al_2O_3 composite nanofluid in strips hot rolling. *J Manuf Process* **57**: 312–323 (2020)
[179] Marian M, Berman D, Rota A, Jackson R L, Rosenkranz A. Layered 2D nanomaterials to tailor friction and wear in machine elements—A review. *Adv Mater Interfaces* **9**(3): 2101622 (2022)
[180] Li B B, Zhou X C, Huang J, Huang Q P, Guo X, Liu X S. Investigation of multi-scale fillers on tribological properties of UHMWPE composites for water-lubricated bearings. *Tribol Int* **212**: 110961 (2025)
[181] Liu H L, Liu H J, Zhu C C, Parker R G. Effects of lubrication on gear performance: A review. *Mech Mach Theory* **145**: 103701 (2020)
[182] Fan X Q, Li X P, Zhao Z, Yue Z F, Feng P, Ma X L, Li H, Ye X Y, Zhu M H. Heterostructured rGO/MoS_2 nanocomposites toward enhancing lubrication function of industrial gear oils. *Carbon* **191**: 84–97 (2022)
[183] Yang L M, Zhao X D, Ma Z F, Ma S H, Zhou F. An overview of functional biolubricants. *Friction* **11**(1): 23–47 (2023)
[184] Mao X W, Yang Y N, Qian Y P, Chen K X, Zhao Y L, Shang S M, Cao Y, Wang Y G, Li Y K, Zhang H Y. Hydration-lubricated, cartilage-targeted, and anti-inflammatory triple-functional nanospheres for the treatment of osteoarthritis. *Adv Funct Mater* **35**(48): e2501235 (2025)
[185] Yao Q, Chen X Y, Sheng H X, Zhang Y Z, Chen R J, Fan P, Kou L F. Lubricating nano/micro particles for osteoarthritis therapy. *Mater Horiz* **12**(22): 9476–9508 (2025)
[186] Guiney L M, Wang X, Xia T, Nel A E, Hersam M C. Assessing and mitigating the hazard potential of two-dimensional materials. *ACS Nano* **12**(7): 6360–6377 (2018)
[187] Qiu W J, Zhao W W, Zhang L D, Wang H M, Li N Y, Chen K X, Zhang H Y, Wang Y G. A solid–liquid composite lubricating "nano-snowboard" for long-acting treatment of osteoarthritis. *Adv Funct Mater* **32**(46): 2208189 (2022)
[188] Liu X Y, Chu P K, Ding C X. Surface modification of titanium, titanium alloys, and related materials for biomedical applications. *Mat Sci Eng R* **47**(3–4): 49–121 (2004)
[189] Naffakh M, Díez-Pascual A M. Nanocomposite biomaterials based on poly(ether-ether-ketone) (PEEK) and WS_2 inorganic nanotubes. *J Mater Chem B* **2**(28): 4509–4520 (2014)
[190] Lv X K, Wang X H, Tang S C, Wang D L, Yang L L, He A X, Tang T T, Wei J. Incorporation of molybdenum disulfide into polyetheretherketone creating biocomposites with improved mechanical, tribological performances and cytocompatibility for artificial joints applications. *Colloid Surface B* **189**: 110819 (2020)
[191] Chen Z, Liu Y N, Sun Y, Liu G Q, Zhou F, Liu W M. Mussel-inspired adhesive friction-controlled lubricating coating for titanium alloy used in artificial joint replacement. *Appl Surf Sci* **626**: 157265 (2023)
[192] Ren K X, Yu G M, Zhang Z X, Wu W C, Tian P, Chhattal M, Gong Z B, Li Y, Zhang J Y. Self-organized transfer film-induced ultralow friction of Graphene/$MoWS_4$ heterostructure nanocomposite. *Appl Surf Sci* **572**: 151443 (2022)
[193] Cao X A, Gan X H, Lang H J, Yu K, Ding S Y, Peng Y T, Yi W M. Anisotropic nanofriction on MoS_2 with different thicknesses. *Tribol Int* **134**: 308–316 (2019)



Hongjie Li is currently a Ph.D. candidate at the School of Materials Science & Engineering, Shanghai Jiao Tong University. His research centers on material processing tribology and high-temperature lubrication.



Chengliang Hu is a professor at the Institute of Forming Technology & Equipment, School of Materials Science and Engineering, Shanghai Jiao Tong University. He was an Alexander von Humboldt Research Fellow. His research focuses on precision forging technologies and tribology in metal forming. Over the past 10 years, he has led 20 research projects funded by the National Natural Science Foundation of China, the Ministry of Industry and Information Technology, and various industrial partners.